

ALMA MATER STUDIORUM · UNIVERSITÀ DI BOLOGNA

Scuola di Scienze
Corso di Laurea Magistrale in Fisica del Sistema Terra

THE ROUTES OF THE MEDITERRANEAN SEA CIRCULATION

Relatore:
Prof.ssa Nadia Pinardi

Presentata da:
Giulia Vecchioni

Correlatori:
Prof.ssa Paola Cessi
Dott.ssa Louise Rousselet
Dott. Francesco Trotta

Sessione III
Anno Accademico 2021/2022

Abstract

The Mediterranean Sea is a semi-enclosed basin connected to the Atlantic Ocean through the narrow and shallow Strait of Gibraltar and further subdivided in two different sub-basins, the Eastern Mediterranean and the Western Mediterranean. These two are connected through the Strait of Sicily which has a sill depth of 430 *m* and thus allowing only surface and intermediate water to be exchanged.

On annual basis, the heat loss during wintertime overwhelms the heat gained during summer resulting in a net heat budget of -7 W/m^2 which, combined with exceeding evaporation over precipitation and runoff together with wind stress, is responsible for the antiestuarine character of the zonal thermoaline circulation. As Wüst describes in his pioneer work, an inflow of Atlantic Water enters the Strait of Gibraltar and reaches the Eastern Mediterranean where it becomes the denser and colder Levantine Intermediate Water (LIW). After this transformation, the LIW spreads throughout the Mediterranean affecting the deep water formation processes which occur in the northern regions of both the Western and Eastern Mediterranean, and partially exiting the Strait of Gibraltar. The outflow is mainly composed of LIW and deep water masses formed in the Western Mediterranean Sea, thus it represents the first evidence of the connection between meridional overturning cells and the basin-wide zonal overturning cell.

The aim of this thesis is to validate and quantitatively assess the main routes of water masses composing the outflow at Gibraltar Strait, using for the first time in the Mediterranean Sea a lagrangian interpretation of the eulerian velocity field produced from an eddy-resolving reanalysis dataset, spanning from 2000 to 2012.

In the first part, an overview of the Mediterranean circulation from recent literature is presented focusing the attention on the vertical circulation and the sites where the dense and deep water formation processes occur along with their variability.

Then, a lagrangian model named Ariane is used to map out three-dimensional trajectories in order to describe the pathways of water mass transport from the Strait of Sicily, the Gulf of Lyon and the Northern Tyrrhenian Sea to the Gibraltar Strait. As shown for Blanke and Raynaud (1997) and Döös (1995), the lagrangian diagnostic provides useful qualitative and quantitative information on water mass movements. Thus, numerical experiments were carried out by seeding millions of particles in the Strait of Gibraltar and following them backwards in time to track the origins of water masses and transport exchanged between the different sections of the Mediterranean.

Finally, the main routes of the intermediate and deep water masses are reconstructed from virtual particles trajectories, which highlight the role of the Western Mediterranean Deep Water (WMDW) as the main contributor to the Gibraltar Strait outflow. For the first time, the quantitative description of the flow of water masses coming from the Eastern Mediterranean towards the Gibraltar Strait is provided and a new route that directly links the Northern Tyrrhenian Sea to Gibraltar Strait has been detected.

Sommario

Il mar Mediterraneo è un bacino semichiuso connesso all'Oceano Atlantico tramite il poco profondo Stretto di Gibilterra e ulteriormente diviso in due diversi sottobacini, il Mediterraneo orientale e il Mediterraneo occidentale. Questi ultimi sono connessi dallo Stretto di Sicilia, che ha una profondità massima di 430 m, e quindi permette lo scambio delle sole acque superficiali e intermedie.

Su base annuale, il calore perso durante il periodo invernale supera il calore assorbito nel periodo estivo portando ad un bilancio di calore netto pari a $-7 W/m^2$ che, combinato all'eccesso di evaporazione rispetto alla precipitazione e al runoff insieme allo stress del vento, è responsabile della dinamica antiestuarina della circolazione termoalina zonale. Come Wüst descrive nel suo pionieristico studio, il flusso di Acqua Atlantica entra dallo Stretto di Gibilterra e raggiunge il Mediterraneo orientale dove si trasforma nella più fredda e densa Acqua Levantina Intermedia (LIW). Dopo questa trasformazione, la LIW si diffonde in tutto il Mediterraneo influenzando i processi di formazione di acqua profonda che avvengono nelle regioni settentrionali sia del Mediterraneo occidentale che orientale e in parte uscendo dallo Stretto di Gibilterra. Il flusso uscente è principalmente composto da LIW e masse d'acqua profonda formate nel Mediterraneo occidentale, quindi rappresenta la prima evidenza della connessione tra le celle dell'overturning meridionale e la cella zonale del bacino.

Lo scopo di questa tesi è quello di convalidare e valutare quantitativamente le principali rotte delle masse d'acqua che compongono il flusso uscente allo Stretto di Gibilterra, usando per la prima volta nel mar Mediterraneo un'interpretazione lagrangiana del campo di velocità euleriano prodotto da un dataset di rianalisi che va dal 2000 al 2012 e capace di risolvere gli eddies.

Nella prima parte è esposta una panoramica della circolazione del Mediterraneo riportata dalla letteratura, focalizzando l'attenzione sulla circolazione verticale e le aree dove avvengono processi di formazione di acque dense e profonde insieme alla loro variabilità.

In seguito, il modello lagrangiano Ariane è stato utilizzato per mappare le traiettorie tridimensionali con il fine di descrivere i percorsi del trasporto delle masse d'acqua dallo Stretto di Sicilia, dal Golfo dei Leoni e dal Tirreno Settentrionale verso lo Stretto di Gibilterra. Come dimostrato per Blanke and Raynauld (1997) e Döös (1995), la diagnostica lagrangiana fornisce informazioni qualitative e quantitative utili sui movimenti delle masse d'acqua. Sono stati quindi svolti esperimenti numerici in cui milioni di particelle sono state inizializzate allo Stretto di Gibilterra e seguite indietro nel tempo per tracciare le origini delle masse d'acqua e il trasporto scambiato tra le differenti sezioni del Mediterraneo.

Infine, le principali rotte delle masse d'acqua intermedie e profonde sono ricostruite dalle traiettorie delle particelle virtuali, in cui si evidenzia il ruolo dell'Acqua Profonda del Mediterraneo Occidentale (WMDW) come principale contributore del flusso uscente a Gibilterra. Per la prima volta, viene presentata la descrizione quantitativa del flusso di masse d'acqua provenienti dal Mediterraneo Orientale verso lo Stretto di Gibilterra ed è stata individuata una nuova rotta che collega direttamente il Mar Tirreno Settentrionale allo Stretto di Gibilterra.

Contents

1	Introduction	1
1.1	An overview of the Mediterranean horizontal circulation	2
1.1.1	Variability of the Mediterranean circulation	6
1.2	The Mediterranean vertical circulation	7
1.2.1	Water mass analysis	9
1.3	Zonal and meridional streamfunction	11
1.3.1	Zonal overturning circulation	15
1.3.2	Western Meridional overturning circulation	15
1.3.3	Eastern Meridional overturning circulation	17
1.4	Water mass formation processes	17
1.4.1	Water mass formation variability	20
1.4.2	Theory of dense and deep water formation	26
1.4.3	Intermediate Water	31
1.4.4	Deep Water	33
1.5	Thesis objectives	36
2	Data and methods	39
2.1	Reanalysis data	39
2.1.1	Model system description	40
2.1.2	Data assimilation scheme	43
2.1.3	Data quality control	44
2.1.4	Vertical velocity computation	47
2.2	Lagrangian analysis	48
2.2.1	Lagrangian offline diagnostic tool	49
2.2.2	Experiments configuration	53

CONTENTS

3	The deep water routes	57
3.1	Qualitative analysis of the parcel trajectories	57
3.2	The deep routes transports	60
3.2.1	T-S diagrams	64
3.2.2	Transit times	66
4	The intermediate water routes	69
4.1	Qualitative analysis of the parcel trajectories	69
4.2	The intermediate routes transports	71
4.2.1	T-S diagrams	73
4.2.2	Transit times	74
5	Conclusions and outlooks	77
	Bibliography	81

Chapter 1

Introduction

The Mediterranean Sea is a semi-enclosed basin connected to the Atlantic Ocean through the narrow Strait of Gibraltar, which has a sill depth of ~ 300 m. It is further divided in two sub-basins, the Eastern Mediterranean (EMED) and the Western Mediterranean (WMED), separated by the Strait of Sicily which is 430 m deep. They differ in topography and can be further divided in smaller sub-basins. The WMED exhibits narrow continental shelves with the exception of the Gulf of Lyon where dense waters are formed and then reach greater depths by cascading. The easternmost and deepest part (about 3500 m) of the WMED is the Tyrrhenian Sea located between the Italian peninsula and the islands of Corsica and Sardinia, while the Algero-Provençal basin reaches the maximum depth of 2500 m and it is the wider, spanning from the Ligurian Sea towards the Alboran Sea.

On the other hand, the EMED appears more complicated with two semi-enclosed basins, the Aegean and Adriatic Sea. The Levantine Sea is the easternmost part of the EMED and it merges with the Ionian Sea through the Cretan Passage at a depth of about 1500 m between Crete and the Lybian coast (Zavatarelli and Mellor, 1995). The Aegean Sea communicates with the Levantine and Ionian Sea through straits between the Greek and Turkish coast and Crete and Rhodes islands. Finally, the Adriatic Sea features an extended continental shelf and to the south it ends in the Ionian Sea passing by the Strait of Otranto.

In the Mediterranean, the evaporation rate exceeds the precipitation and runoff, resulting in a maximum average evaporation of 0.7 m/yr (Legates and Willmott, 1990) and a net heat loss of 7 W/m² a year (Castellari et al., 1998). Although the net heat flux shows an interannual and seasonal variability, a steady-state can be achieved on a multidecadal timescale during which the net loss should be compensated by an advective flux of the same amplitude at Gibraltar (Garret et al., 1993).

As documented by Cessi et al. (2014), buoyancy loss within the basin along with wind stress give rise to an antiestuarine circulation with an inflow of Atlantic Water (15 °C and 36.2 psu) at the surface in the Strait of Gibraltar and outflow of saltier (38.4 psu),

colder ($13.5\text{ }^{\circ}\text{C}$) water at depth (Lascazatos and Nittis, 1998). The outflowing water mass is composed of two water types: the Western Mediterranean Deep Water and the Levantine Intermediate Water (LIW) (Bryden and Stommel, 1982).

1.1 An overview of the Mediterranean horizontal circulation

According to Pinardi and Navarra (1993), the general circulation of the Mediterranean Sea is driven by three main forcings:

- the inflow-outflow system at Gibraltar Strait is the controlling mechanism for the overall basin salt and mass budget on the timescale of several decades
- thermal and evaporative fluxes at the air-sea interface drive the overturning circulation, being one of the source-sink mechanism of water mass formation processes which occur seasonally
- wind stress forces the basin-wide circulation in sub-basin pattern with seasonal variability

Thus, it is possible that the thermal and wind forcing could be acting on the same time scales, the first inducing water transformation processes and the latter causing the transport and dispersal of such waters (Pinardi and Navarra, 1993).

Regarding the role of wind stress, the double-gyre structure of the general circulation is due to westerly winds crossing the basin from November to June (Castellari et al., 1998). Furthermore, low resolution simulations from Pinardi and Navarra (1993) and analyses of the barotropic flow field from Pinardi et al. (2015) have confirmed that northern areas are characterized by cyclonic circulations while the southern areas by anticyclonic gyres and eddies, due to the different wind curl sign. The northern cyclonic gyres are also forced by deep and intermediate water formation processes while the southern gyres store intermediate-mode waters which compose the permanent thermocline of the basin (Pinardi et al., 2015).

It has been shown that the mesoscale component of the Mediterranean circulation dominates the flow, especially in the Eastern Mediterranean (Ayoub et al., 1998). The Mediterranean eddy field is composed of eddies with a long persistency in time, hence addressed as gyres, probably due to nonlinear dynamical balances, specific atmospheric forcing and the bathymetry.

A recent overview of the horizontal circulation is offered by Pinardi et al. (2015) who described for the first time the large-scale time-mean circulation structure by using a part of a mesoscale permitting reanalysis dataset, from 1987 to 2007. A schematic of

1.1 – An overview of the Mediterranean horizontal circulation

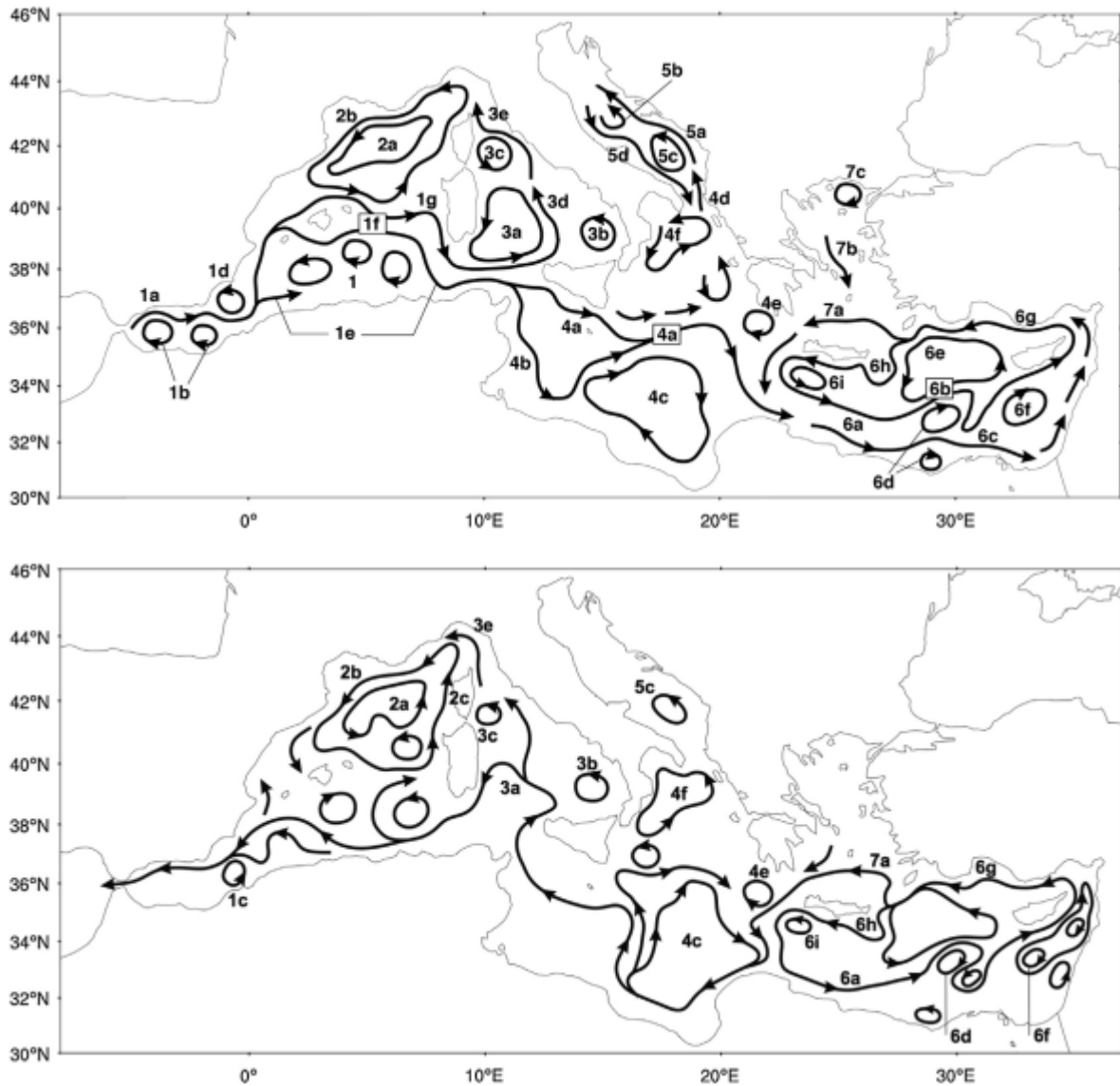


Figure 1.1: The schematic of the mean surface circulation structures as deduced from the 1987–2007 reanalysis mean flow field. Upper panel: surface circulation. Lower panel: 200–300 m average circulation. Names of the currents are reported in Tab. 1.1. Reproduced from Pinardi et al. (2015).

the surface and intermediate general circulation emerging from this study is presented in Fig. 1.1, whereas in Tab. 1.1 names of the main structures can be found.

As it has been demonstrated by previous analyses, the Mediterranean circulation is dominated by intense open ocean and boundary jet structures, semi-permanent large-scale

eddies and gyres.

At the surface, Atlantic Water current entering from Gibraltar meanders around the two Alboran gyres which may disappear from time to time (Vélez-Belch et al., 2005). Then, two intensified currents are defined, one going northward toward the Ibiza channel and contributing to open ocean eastward jet, while the other forming an intensified segment of the Algerian Current.

An open ocean jet, the Western Mid-Mediterranean Current as named in Tab. 1.1, partially merges with the cyclonic structure known in literature as Gulf of Lyon gyre. The rest turns southward along the western coasts of Sardinia forming the Southerly Sardinia Current and then it joins the Algerian Current, which branches in three parts: two entering the Sicily Strait and a third one flows northeastward in the Tyrrhenian Sea.

The Algerian Current, entering the Sicily Strait, branches along the southern coasts then converging into both the Syrte Gyre and the Atlantic Ionian Stream, which divides the Ionian Sea into northern and southern regions, and eventually it reaches the Levantine basin. In the Eastern Mediterranean, the two largest amplitude currents are the northern boundary intensified currents of the Rhodes Gyre and the currents passing through the Cretan Passage. In addition, the two eastern marginal seas, the Aegan and the Adriatic, show a cyclonic circulation.

Regarding the circulation at intermediate depth as average of currents between 200 and 300 metres, it can be representative of the main dispersal paths of the Levantine Intermediate Water which forms in the Levantine basin.

Looking at the lower panel of Fig. 1.1, in the Cretan Passage the surface pattern results more defined as shown by Western Cretan Cyclonic Gyre and Cretan Sea Westward Current, anyway the basin-scale cyclonic area of the Rhodes Gyre and the Cretan Passage is consistent with the surface flow. The reconstructed Mediterranean circulation indicates that the preferred path for the LIW is southward, along the Gulf of Sirte shelf break as part of the large scale transport of the anticyclonic Syrte Gyre (Pinardi et al., 2006). The well-known westward LIW current of the Sicily Strait emerges as a branching of the Syrte Gyre south-western intensified current.

From a centennial integration of general circulation model, Wu and Haines (1998) find another path of the LIW toward the Adriatic Sea, even though the reconstructed circulation from Pinardi et al. (2015) is unable to point out.

After passing through the Sicily Strait, the LIW path is characterized by two major branches starting approximately at 6° E one directed northward toward the Gulf of Lyon Gyre, and the second westward toward the Strait of Gibraltar. The latter is the residual of a complex eddy flow field that itself moves westward in the offshore areas of the Algerian basin and advects filaments of LIW at its borders (Puillat et al., 2006).

1.1 – An overview of the Mediterranean horizontal circulation

Current systems	Components
System 1	1a: Atlantic Water Current (AWC) 1b: Western and Eastern Alboran Gyres 1c: Almera-Oran front 1d: Almera-Oran cyclonic eddy 1e: Algerian Current segments 1f: Western Mid-Mediterranean Current (WMMC) 1g: Southern Sardinia Current (SCC)
System 2	2a: Gulf of Lyon Gyre (GLG) 2b: Liguro-Provenal-Catalan Current (LPCC) 2c: Western Corsica Current (WCC)
System 3	3a: South-Western Tyrrhenian Gyre (SWTG) 3b: South-Eastern Tyrrhenian Gyre (SETG) 3c: Northern Tyrrhenian Gyre (NTG) 3d: Middle Tyrrhenian Current 3e: Eastern Corsica Current (ECC)
System 4	4a: Atlantic-Ionian Stream (AIS) 4b: Sicily Strait Tunisian Current (SSTC) 4c: Syrte Gyre (SG) 4d: Eastern Ionian Current (EIC) 4e: Pelops Gyre (PG) 4f: Northern Ionian Cyclonic Gyre
System 5	5a: Eastern South-Adriatic Current (ESAC) 5b: Middle Adriatic Gyre 5c: South Adriatic Gyre 5d: Western Adriatic Coastal Current (WACC)
System 6	6a: Cretan Passage Southern Current (CPSC) 6b: Mid-Mediterranean Jet 6c: Southern Levantine Current (SLC) 6d: Mersa Matruh Gyre System (MMGS) 6e: Rhodes Gyre (RG) 6f: Shikmona Gyre System (SGS) 6g: Asia Minor Current 6h: Ierapetra Gyre (IPG) 6i: Western Cretan Cyclonic Gyre
System 7	7a: Cretan Sea Westward Current (CSWC) 7b: Southward Cyclades Current (SWCC) 7c: North Aegean Anticyclone

Table 1.1: Nomenclature for the surface and intermediate depth circulation structures. Reproduced from Pinardi et al. (2015).

1.1.1 Variability of the Mediterranean circulation

As documented by observations and model simulations, the variability of the Mediterranean circulation peaks at the seasonal and interannual time scales (Pinardi et al., 2015).

Seasonal variability

As Pinardi and Masetti (2000) explain, the seasonal variability is strongly related to the amplitude of the seasonal cycle in the atmospheric forcing thus it is fairly predictable. Aspects of the seasonal variability involve:

- the surface water mass formation cycle (Hecht et al., 1988; Demirov and Pinardi, 2007)
- the seasonal reversal of currents in different portions of the basin (Tziperman and Malanotte-Rizzoli, 1991)
- the strength of the mesoscale flow field (Ayoub et al., 1998)
- the winter deep and intermediate convection sites in the Gulf of Lyon area (Leaman and Shott, 1991), the Adriatic Sea (Artegiani et al., 1997) and the Rhodes Gyre (Lascaratos, 1993)

As already discussed, the wind shows a main westerly component during winter while assuming a stronger northerly component during late summer over the Eastern Mediterranean. Instead, subregional wind regimes are strongly dependent upon the interaction of the Westerlies with the local orography during winter and the land-sea temperature contrast during summer. These different type of interactions give raise to two wind regimes: Mistral westerly jet during winter and Etesian North-easterly jet during the summer.

Interannual variability

Since many mechanisms may contribute strongly, interannual variations are more difficult to explain, also due to the fact that many meteorological anomalies could have a delayed effect on the basin-wide circulation. Interannual fluctuations concern:

- intermediate and deep water mass formation rates (Lascaratos and Nittis, 1998; Castellari et al., 2000)
- the large variations in volume transport between basins at the Straits (Astraldi et al., 1995)
- the sudden switches in the deep water mass formation areas for the Eastern Mediterranean (Roether et al., 1996)

- the changes in the flow direction in several regions (Hecht et al., 1988; Nittis et al., 1993; Artale et al., 1994; Pinardi et al., 1997)
- the abrupt changes in LIW characteristics (Hecht, 1992)

These changes are ascribed to the basin response to interannual fluctuations in winds and buoyancy fluxes, in particular changes in heat fluxes are responsible for water mass formation variability.

Furthermore, another source of interannual fluctuations is the internal nonlinear dynamics as the unstable eddy field, which can alter the dispersal paths of water masses and modify wind driven gyres.

As demonstrated by Pinardi and Masetti (2000) from a coarse model simulation, qualitatively the interannual circulation anomalies are larger in the Eastern than in the Western Mediterranean. This is related to the strong influence of the inflow at Gibraltar on the circulation in the west and the different basin extension which produces large pools of deep mixed layers in the Eastern but not Western Mediterranean area (Korres et al., 2000).

Regarding decadal variability, it is noteworthy the Northern Ionian Reversal phenomenon, which was documented by Poulain et al. (2012) using surface drifters and satellite altimetry, and by Borzelli et al. (2009). It consists in shifts of the Atlantic-Ionian Stream at the surface and a change from cyclonic circulation to anticyclonic motion in the Northern Ionian. Pinardi et al. (2015) suggested that the periodical reversal of the Northern Ionian Gyre is influenced by wind stress curl variability and they managed to obtain for the first time a clear picture of this phenomenon occurred after 1997.

All these mentioned studies agree in setting the time of the surface reversal to 1997: since then, the circulation in the Northern Ionian became cyclonic and AIS started to cross the basin, instead of meandering northward.

1.2 The Mediterranean vertical circulation

The Mediterranean vertical circulation is usually referred to as the overturning circulation and, like the global one, it sets the stratification of the basin as well as supplies the oxygen and other tracers from the surface to the deep layers. In particular, the Mediterranean overturning circulation is key to provide low salinity waters to the Mediterranean as it balances the salt increase associated with the net evaporation inside the basin.

The Mediterranean Sea has been called a miniature ocean for climate studies because it shows an intense deep and intermediate water mass formation which sets a vigorous vertical circulation like the global overturning. This buoyancy driven circulation is made of meridional and zonal cells, which respectively have a multidecadal and decadal timescale.

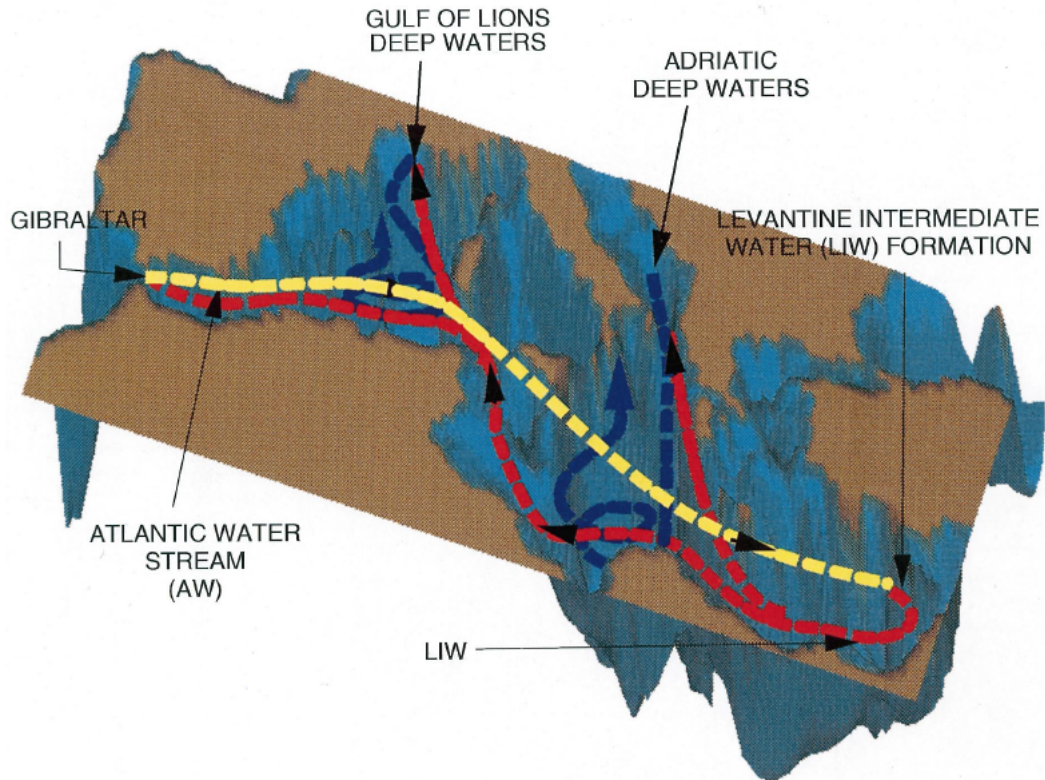


Figure 1.2: The schematic of the thermohaline circulation in the basin with the major conveyor belt systems indicated by dashed lines with different colour. The yellow indicates the AW stream which is the surface manifestation of the zonal conveyor belt of the Mediterranean. The red indicates the mid-depth LIW recirculation branch of the zonal thermohaline circulation. The blue lines indicate the meridional cells induced by deep waters. LIW branching from the zonal conveyor belt connects meridional and zonal conveyor belts. Reproduced from Pinardi and Masetti (2000).

The meridional overturning circulation (MOC) is made of several sub-basin meridional cells due to the shallow Sicily Strait which allows only surface and intermediate waters to be exchanged between the EMED and WMED, confining the deep circulation to sub-basin scale. It is connected to the sites of deep water mass formation which in WMED is in the Gulf of Lyon while for the EMED these areas were considered to be located only in the Adriatic Sea. From 1991, it became clear that another downwelling cell is possible in the Aegean Sea. In fact, from 1987 to 1998, a large climatological event, the so-called Eastern Mediterranean Transient (EMT), affected the deep and intermediate circulation in the EMED. During this period, the engine of the eastern deep thermoaline circulation switched from the Southern Adriatic to the Aegean Sea. The so-formed denser water masses exited from Cretan Arc Straits and spreaded throughout the entire basin and

pushed to the west in the Ionian Sea and to the east in the Levantine basin the less dense water masses from Southern Adriatic origin (Roether et al., 1996).

However, at the moment the degree of impact of the Aegan source on the long term mean meridional conveyor belt is unclear (Pinardi and Masetti, 2000). In fact, there is an ongoing discussion whether the EMT was a single phenomenon that was caused by unique conditions in the EMED during 1987-1992, or whether it is a recurrent event, associated with the natural variability of the EMED (Amitai et al., 2017).

Another denser water formation area was documented by Pinardi et al. (2015) and Hecht and Gertman (2001) in the Rhodes Gyre which is the site of LIW and Levantine Deep Water (LDW) production.

Regarding the zonal overturning circulation (ZOC), it is made of one clockwise cell in the top 600 m which connects the two-layer flow at the Strait of Gibraltar to remote areas of the Eastern Mediterranean basin (Pinardi et al., 2006).

The upper branch is composed of Atlantic Water entering the Gibraltar Strait and then moving eastward to the Levantine basin. Along the way, due to buoyancy fluxes and mixing with surrounding water, it becomes the Modified Atlantic Water (MAW).

Simultaneously, the lower branch corresponds to the east to west path of LIW, which in the Ionian Sea mixes with Cretan Intermediate water, thus modifying partially its properties before exiting the Sicily Strait.

This branch of the basin-wide zonal cell is connected to sub-basin meridional cells, more precisely to areas where deep water formation takes place. In fact, the inflowing LIW in these areas increases the salinity of the local intermediate waters, preconditioning the deep convection of the EMED and WMED cells. Wu and Haines (1996) have demonstrated the key role of LIW in the enhancement of deep convection in Gulf of Lyon and in the Adriatic areas. This result was recently confirmed by Pinardi et al. (2019) who have depicted the connection between the Wüst cell and the meridional cells through the divergence and rotation component of the horizontal velocity field vertically integrated across two layers above 600 m.

This interconnection gives rise to a basin-wide thermoaline circulation, the so-called Mediterranean Conveyor Belt, whose main dispersal pathways are depicted in Fig. 1.1.

1.2.1 Water mass analysis

The vertical circulation is better resolved by means of water masses, that is a body of water that has had its properties set by a single identifiable process (Talley and al., 2011). The imprinted features identify the water mass as it is advected and mixed through the ocean. Usually, a certain water mass is defined by specific value of temperature and salinity as well as potential density.

In order to determine the pathways of the Mediterranean overturning circulation,

several approaches based on tracking specific water masses have been proposed in the past and hereinafter explained.

The first described methods do not supply a quantitative estimate of the transport streamfunction, but only a qualitative scientific description still considered significant. Recently, more quantitative studies have been carried out, showing the strong influence of the mesoscale circulation on both meridional and zonal overturning circulation. The results and the methodology are explained after the qualitative approaches.

Vertical salinity section

Wüst in 1961 for the first time attempted to study the deep and intermediate circulation with the help of the *core method*, that is identify water masses by the intermediate maxima or minima of salinity, oxygen and temperature in order to follow their location and spreading processes.

The vertical distribution of salinity, oxygen and temperature allowed Wüst to outline four different core masses within the Mediterranean whose definitions are still used:

- near-surface Atlantic Water between 0 and 75 m depth
- the intermediate water between 200 and 600 m
- the deep water between 1500 and 3000 m
- the bottom water at depths to 4200 m

His results were handmade figures which are still considered a qualitative representation of the vertical distribution of salt, temperature and oxygen in the Mediterranean.

In particular, some of his figures show longitudinal sections of salinity that were used to infer the zonal and vertical velocities associated with the first characterization of the zonal overturning circulation of the Mediterranean Sea (Pinardi et al., 2019).

Throughout a zonal Mediterranean section of salinity, Wüst inferred the two-layer flow composed by the upper eastward branch of Atlantic Water that crosses the Sicily Strait up to the Levantine basin. The lower returning branch, between 150 and 500m, moves westward to the Gibraltar Strait and it is composed of the Levantine Intermediate Water which is formed in the Rhodes Gyre.

Vertical density distribution

One approach to determine the pathways of the overturning circulation is to examine maps of potential density and the associated velocity field (Talley et al., 2011).

Pinardi et al. (2019) have plot vertical potential density section along a zonal transect and four meridional transects associated to deep water formation areas: the Gulf of Lyon

Gyre in the WMED, the southern Adriatic, the Cretan Sea, and the Rhodes Gyre in the EMED. They used daily mean fields of a reanalysis dataset for over 27 years, from 1987 to 2013, and used σ_0 as potential density referenced to the surface.

In this study, a zonal transect of σ_0 similar to Wust's section is considered and the result is plotted in Fig. 1.3. The Atlantic Water, represented by values $\sigma_0 < 27.3 \text{ kg/m}^3$, enters the Gibraltar Strait, while east of 20°E the outcropping of intermediate isopycnals is evident. The subsurface return flow is along the $28.1/29.1 \text{ kg/m}^3$ isopycnals, crossing the basin east–west at depths between 150 and 400 *m* (Pinardi et al., 2019).

Regarding meridional sections shown in Fig. 1.4, the areas linked to deep water formation processes show an upwelling of the 29.01 kg/m^3 isopycnal up to 200 *m* and the outcropping of isopycnal above that depth. On the other hand, the southern regions are affected by the Atlantic Water flow and below the 300 *m* the deep isopycnals downwell from the open ocean formation areas toward the coasts and upwell on the southern shores, with the exception of the Cretan Passage section.

1.3 Zonal and meridional streamfunction

A recent picture of the Mediterranean vertical circulation is given by Zavatarelli and Mellor (1995) in terms of the Eulerian zonal and meridional transport streamfunction obtained with a coarse-resolution numerical model. In this framework, they describe the water motion in terms of zonal and meridional volume transport defined as the integration from the bottom to a certain level z of the horizontal mean velocity field averaged over a time interval.

Assuming depth as vertical dimension and integrating the continuity equation along the appropriate directions, one obtain:

$$\int_{y_1}^{y_2} \frac{\partial}{\partial x} u(x, y, z, t) dy = - \int_{y_1}^{y_2} \frac{\partial}{\partial z} w(x, y, z, t) dy \quad (1.1)$$

$$\int_{x_1}^{x_2} \frac{\partial}{\partial y} v(x, y, z, t) dx = - \int_{x_1}^{x_2} \frac{\partial}{\partial z} w(x, y, z, t) dx \quad (1.2)$$

where (y_1, y_2) represent the meridional boundaries while (x_1, x_2) the zonal boundaries. By integrating in the vertical direction from the bottom H to a level z and averaging over the considered time interval $T = t_1 - t_0$, it is possible to define the Eulerian zonal and meridional streamfunction:

$$\psi_{zon}(x, z) = -\frac{1}{T} \int_{t_0}^{t_1} \int_{-H}^z \int_{y_1}^{y_2} u(x, y, \tilde{z}, t) dy d\tilde{z} dt \quad (1.3)$$

$$\psi_{mer}(y, z) = -\frac{1}{T} \int_{t_0}^{t_1} \int_{-H}^z \int_{x_1}^{x_2} v(x, y, \tilde{z}, t) dx d\tilde{z} dt \quad (1.4)$$

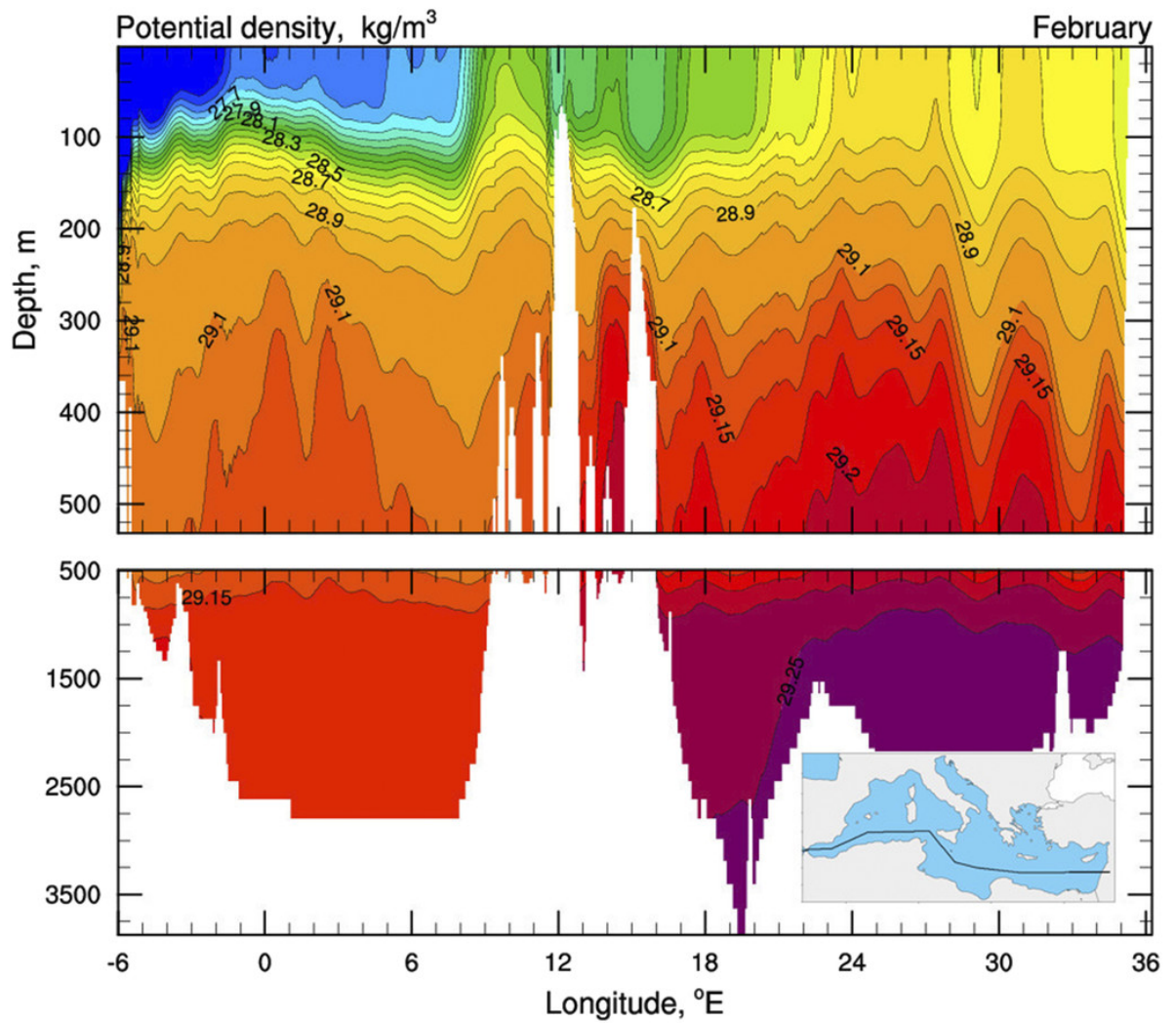


Figure 1.3: Polyline zonal section of the potential density σ_0 for a climatological February average. The location of the section is shown in the inset. Reproduced from Pinardi et al. (2019).

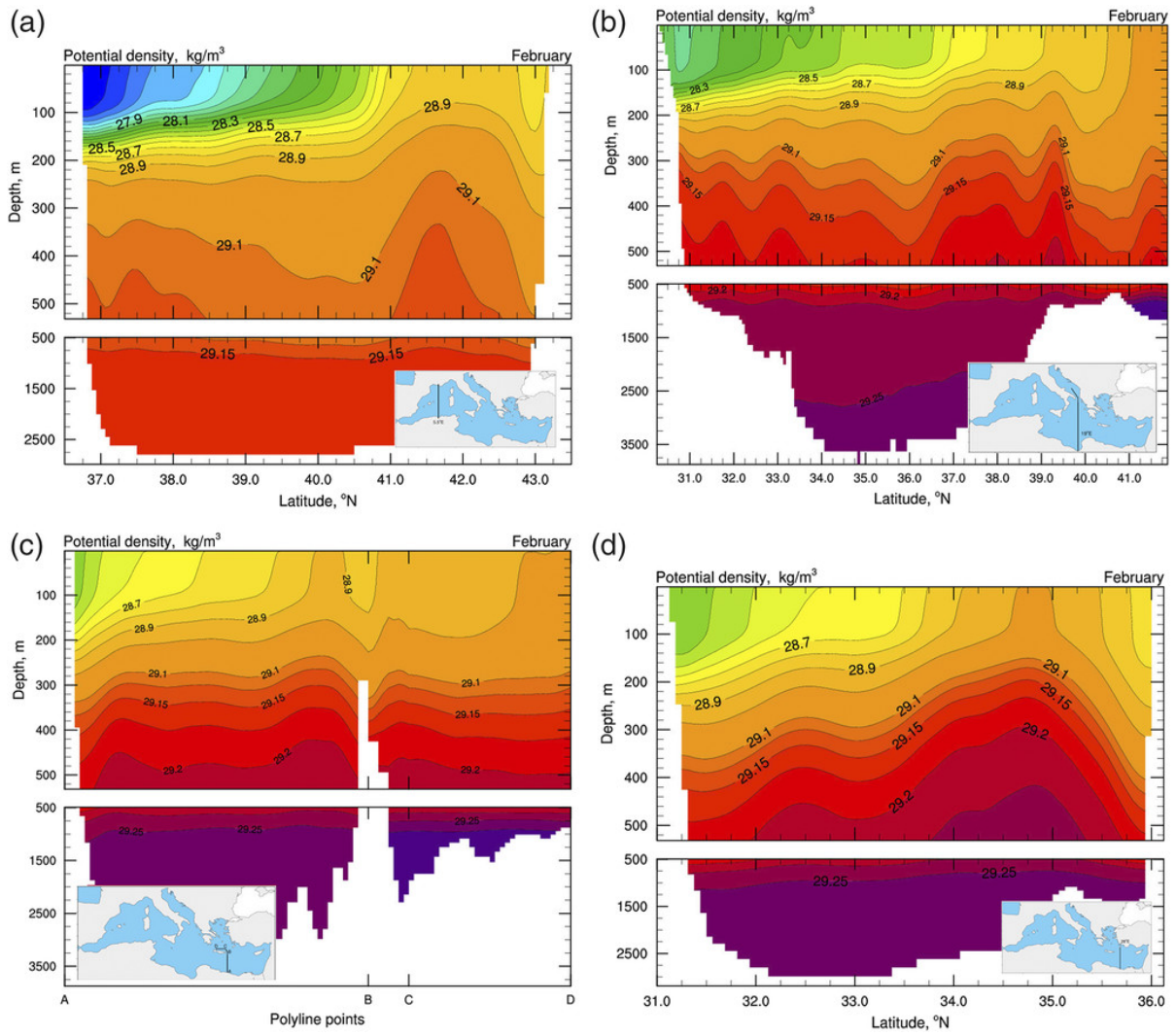


Figure 1.4: Sections of the potential density σ_0 during climatological February along (a) 5.58, (b) 198, (c) 268, and (d) 288 °E. The locations of the sections are shown in the bottom-corner inset of each panel. Reproduced from Pinardi et al. (2019).

Thus, the volume transport is tangent to streamfunction isolines and negative values represent areas of cyclonic motion while positive values describe anticyclonic dynamics.

Nevertheless, this approach neglects all the dynamic processes whose averaged velocity is zero along a certain direction, i.e. the contribution of the eddy field.

To overcome this, recently Pinardi et al. (2019) used the concept of the residual streamfunction to include the transport associated with the contributions from eddies, gyres, and standing waves.

It has been demonstrated that mesoscale eddies are responsible for the isopycnal transport of passive tracers and buoyancy defined as:

$$b = -g \frac{\rho - \rho_0}{\rho_0} \quad (1.5)$$

where ρ_0 is the reference constant density value. In order to analyse the buoyancy fluxes, assuming the gravity acceleration constant with depth, the residual streamfunction is defined by integrating it in potential density space σ , rather than depth. Density is usually a monotonically increasing function in depth, thus it is possible to define a map $\zeta(\sigma)$ to interpolate the σ vertical coordinate to the z coordinate and vice versa. Using the new coordinate, the residual streamfunction results in:

$$\psi_{zon}^*(x, \tilde{\sigma}) = -\frac{1}{T} \int_{t_0}^{t_1} \int_{-H}^0 \int_{y_1}^{y_2} H[\tilde{\sigma} - \sigma(x, y, z, t)] \cdot u(x, y, z, t) dy dz dt \quad (1.6)$$

$$\psi_{mer}^*(y, \tilde{\sigma}) = -\frac{1}{T} \int_{t_0}^{t_1} \int_{-H}^0 \int_{x_1}^{x_2} H[\tilde{\sigma} - \sigma(x, y, z, t)] \cdot v(x, y, z, t) dx dz dt \quad (1.7)$$

Hence, ψ^* is the transport occurring below the isopycnal $\tilde{\sigma}$, which in turn is a function of all three spatial dimensions plus time, and the natural vertical coordinate is $\tilde{\sigma}$.

To compare the Eulerian streamfunction ψ with the residual streamfunction ψ^* previously defined the ψ^* should be remapped onto a depth-like coordinate z , which is the natural coordinate for ψ .

The computation of meridional and zonal residual streamfunctions has been carried out by Pinardi et al. (2019) who used the previously mentioned reanalysis dataset from 1987 to 2003 and the results along with Eulerian streamfunctions are shown in Fig. 1.5, 1.6, 1.7. They averaged over the whole reanalysis dataset and discuss separately the meridional overturning system for the EMED and WMED.

The zonal streamfunction considers a meridional averaging over the entire basin. The streamfunction for the WMED considers a zonal averaging up to a section in the Sicily Strait and the one for the EMED an averaging carried out from the same section up to the Levantine basin coastlines.

1.3.1 Zonal overturning circulation

Both Eulerian and residual streamfunctions are characterized by the presence of the *Wüst cell*, a shallow clockwise cell corresponding to AW flowing eastward and LIW flowing westward and it occupies the first 500 *m* of the water column. In the Eulerian framework, Wüst cell is stronger than in the residual form, supporting the conclusion that the eddy field in the first 300 *m* weakens the zonal transport.

In the WMED deep zonal counterclockwise cell below 700 *m* occupies the regions of the Alboran Sea, the Algerian basin, and the Tyrrhenian Sea, reinforced by the transport of stationary gyres and eddies. Moreover, the residual velocities, tangent to the streamfunction by definition, cross the isopycnals indicating that diapycnal mixing is important for the maintenance of this cell.

Looking at the EMED, the differences between Eulerian and residual streamfunction are more evident. The deep circulation is dominated by a multiple centers clockwise cell which extends to the bottom and it is mainly centered at the longitude of the Aegean deep water outflow, that is 28 °E. Other clockwise cells are present in the Levantine sub-basin, the one connected to denser water formation area in the Rhodes Gyre is centered at approximately 28 °E.

In the residual framework, transport associated to gyres and standing waves weakens the mean circulation. A residual counterclockwise cell emerges at depth and the large Eulerian clockwise cell is splitted into two different cells. The deep overturning associated to Aegan Sea is mainly along isopycnals indicating an adiabatic balance, while the circulation around the secondary maxima located at 28 °E is across isopycnals. Since the reanalysis dataset encompasses the period of the EMT event, the effect of deep water coming from Aegan Sea on the zonal circulation is apparent.

1.3.2 Western Meridional overturning circulation

Considering the Eulerian framework, an anticyclonic cell with several maxima spans from the surface down to 2000 *m*, while below this a deep cyclonic cell is present. The large positive values in the Alboran Sea are associated to the Gibraltar flow. In the residual circulation, the previous mentioned cells are strengthened, suggesting the key role of the mesoscale processes.

In the southern region, a counter-clockwise cell is evident in both frameworks, even though it results empowered in residual circulation. The boundary between the northern clockwise and southern counter-clockwise cell is at approximately 39 °N, that is, the latitude marking the division between the permanent cyclonic gyre of the Gulf of Lyon and the eddy-dominated anticyclonic area of the Algerian current. The northern cell is linked to deep water formation processes that occur in the Gulf of Lyon, approximately at 41-42 °N, while the residual southern abyssal cell has a downwelling branch located

1 – Introduction

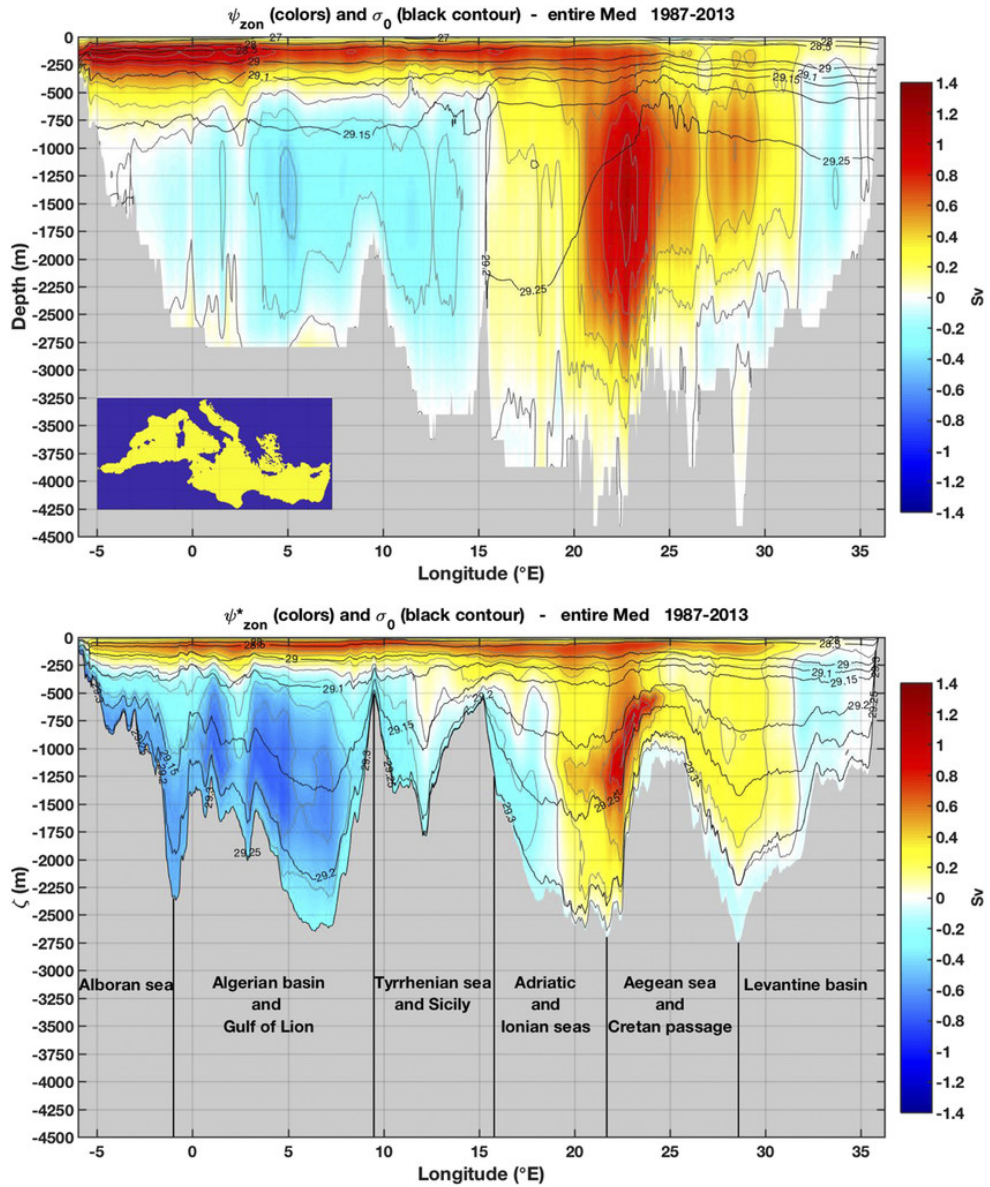


Figure 1.5: (top) Eulerian and (bottom) residual zonal streamfunction, integrated over the latitudinal extension of the basin and averaged in time over the years 1987–2013. The gray contour lines and the colors show streamfunction values at 0.2-Sv intervals. The black contours are isopycnal surfaces of σ (kg m^{-3}). The gray areas mark (top) the deepest bathymetry level and (bottom) calculated from the highest density-layer found over each latitudinal section of the basin. The different regions of the Mediterranean considered in the latitudinal averaging are described over the gray area in the bottom panel. Reproduced from Pinardi et al. (2019).

along the Northern African escarpment.

Since residual transport crosses isopycnals in both cells, the diabatic mixing is essential to Western Meridional overturning circulation.

As documented in several papers and from results of this analysis, Pinardi et al. (2019) state that the western Mediterranean deep water formation and spreading phenomena are eddy dominated processes.

1.3.3 Eastern Meridional overturning circulation

The study of the EMED Meridional overturning takes into account marginal seas where formation of deep waters occur, that are Aegean Sea and Adriatic Sea. The upper 250 m of the water column in southern region are occupied by a counterclockwise cell, which almost disappears in the residual circulation.

Below 250 m, a multicentered clockwise cell is present, whose maxima extend southward of 36.5 °N, which corresponds to the latitude of Sicily Strait, and the other north of it. The northern downwelling branches are linked to deep water formation processes occurring in the Aegean and Adriatic Sea. The transport associated to the latter is weaker than in the Aegean Sea, due to the EMT event which results in smaller southern Adriatic deep water formation rates.

South of Sicily Strait, several clockwise cell are visible, which extend to almost 3000 m. These cells are associated with the Aegean Sea deep water formation area, its outflow during the EMT and the Levantine Deep Water formation processes in the Rhodes Gyre (Pinardi et al., 2019).

In the residual description, the southern circulation is stronger than in the Eulerian counterpart and the cells appears more defined than before.

The one located between 35.5 °N and 36.5 °N, corresponds to the areas where the Aegean Sea dense waters formation occurs, and to the Rhodes Gyre formation area around 36.5 °N. Furthermore, the cell between 33 °N and 35 °N corresponds to the so-called Cretan Passage, where the dense Aegean seawater outflows, and to the southern Rhodes Gyre.

Below 1000 m, north of 35 °N, the mean deep to abyssal circulation is cyclonic and it is larger than its counterpart in the WMED.

Once again the clockwise circulation shows velocities that cross isopycnals, indicating diabatic mixing is important over the whole basin.

1.4 Water mass formation processes

The basin-wide circulation of the Mediterranean is forced by the conversion of lighter Atlantic Water into intermediate, denser and deep water, which sets the stratification of

1 – Introduction

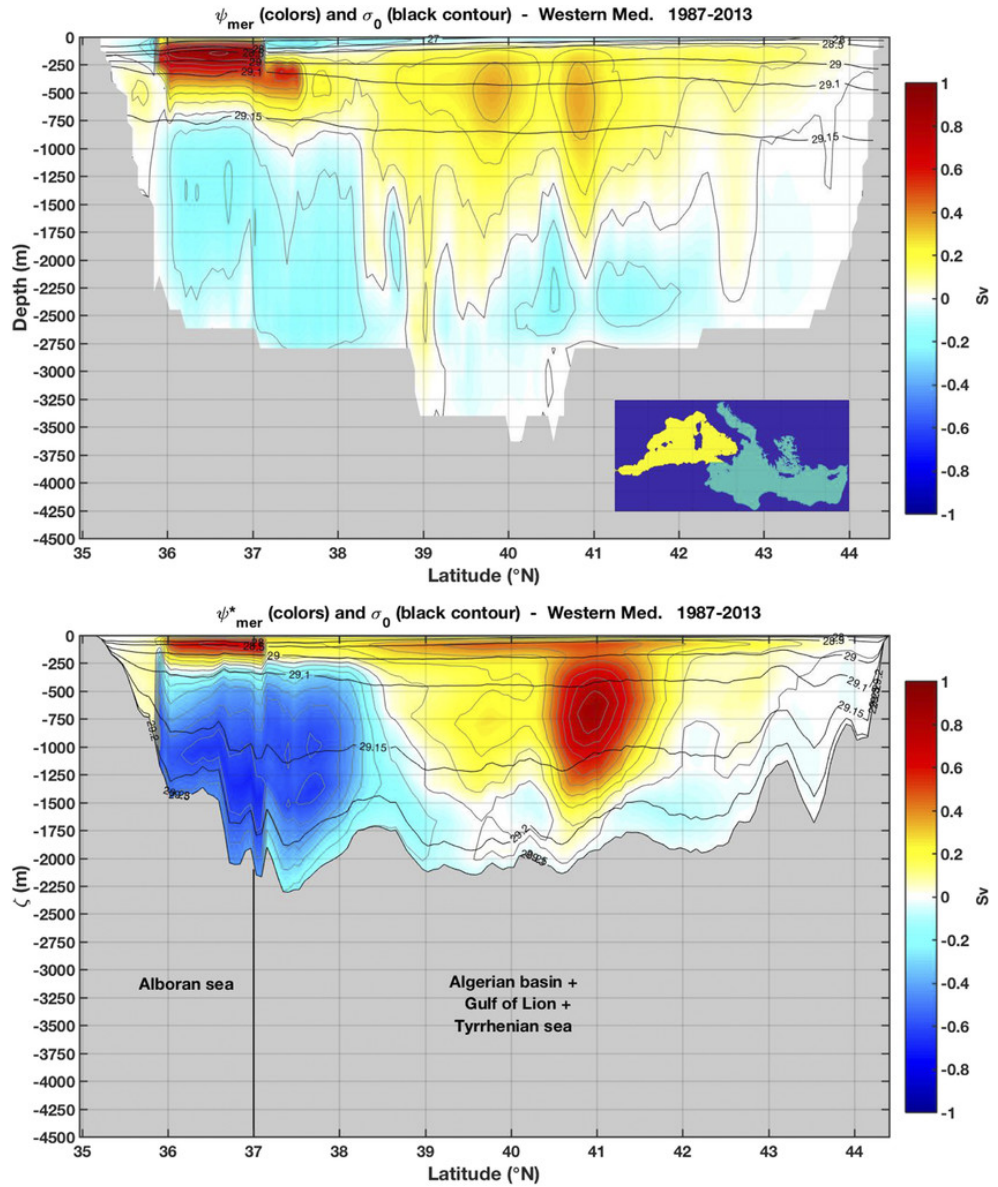


Figure 1.6: (top) Eulerian and (bottom) residual meridional streamfunction for the WMED, integrated in longitude over the yellow region shown in the inset and averaged in time over the years 1987–2013. The gray contour lines and the colors show streamfunction values at 0.1 Sv intervals. The black contours are isopycnal surfaces of σ (kg m^{-3}). The gray areas mark (top) the deepest bathymetry level and (bottom) the highest density-layer depth found over each longitudinal section of the basin. The different regions of the Mediterranean considered in the longitudinal averaging are described over the gray area in the bottom panel. Reproduced from Pinardi et al. (2019).

1.4 – Water mass formation processes

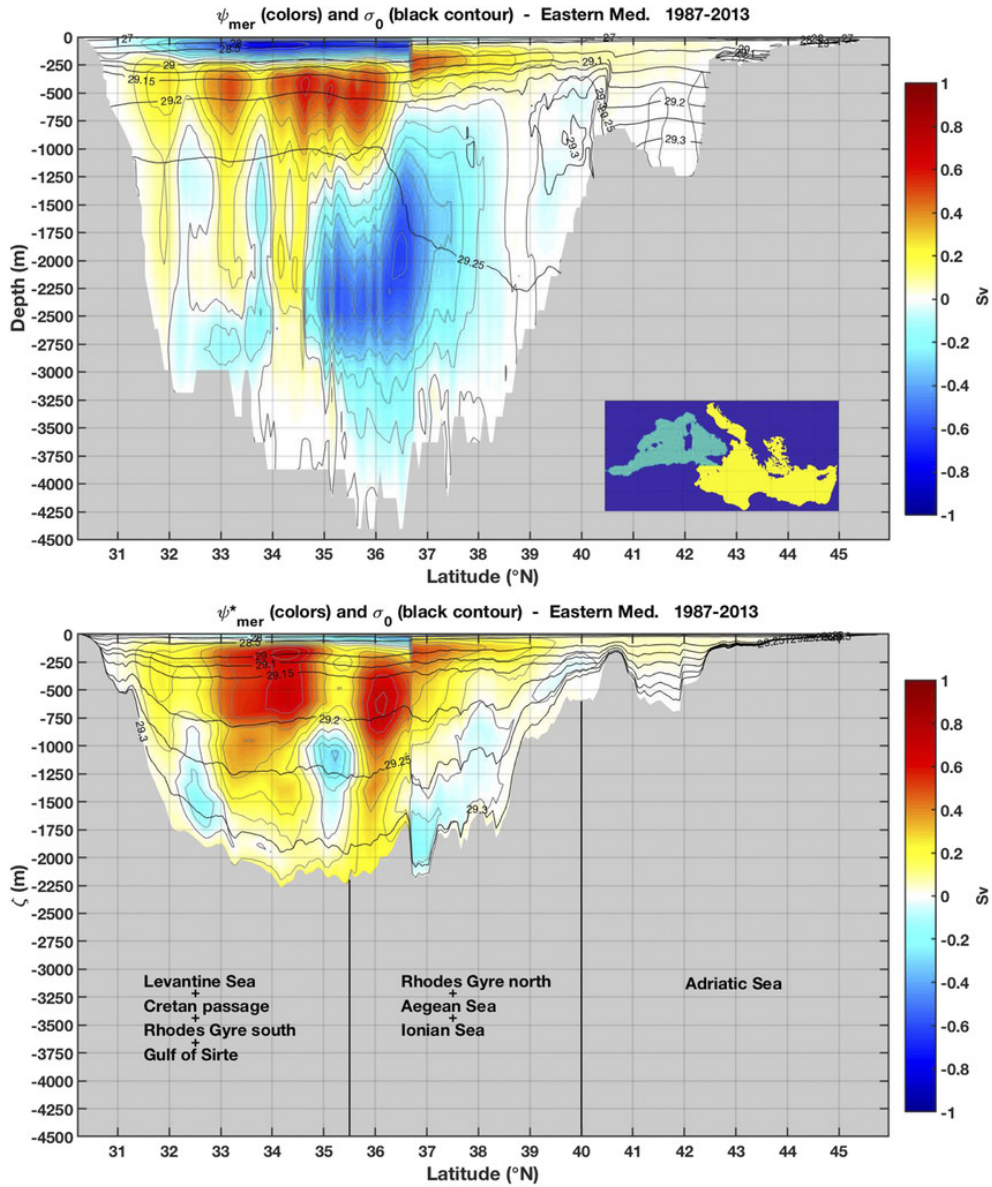


Figure 1.7: (top) Eulerian and (bottom) residual meridional streamfunction of the EMED, integrated in longitude over the yellow region shown in the inset and averaged in time over the years 1987–2013. The gray contour lines and the colors show streamfunction values at 0.1-Sv intervals. The black contours are isopycnal surfaces of σ (kg/m^3). The gray areas mark (top) the deepest bathymetry level and (bottom) the highest density layer depth found over each longitudinal section of the basin. The different regions of the Mediterranean considered in the longitudinal averaging are described over the gray area in the bottom panel. Reproduced from Pinardi et al. (2019).

the basin and transports oxygen and other tracers to intermediate and abyssal layers.

The strong vertical density gradients of the thermocline inhibit the vertical motion between the surface and the abyss, insulating the deep ocean from variations in surface meteorology. However, in a few special regions characterized by weak stratification and, in winter, exposed to intense buoyancy loss to the atmosphere, violent and deep-reaching convection mixes surface waters to great depth. This type of processes, which involves diabatic transformations and mixing, occurs both on open ocean and shelves. The cascading of denser water from shelves can ventilate intermediate or abyssal waters, depending on the specific mixing and spreading mechanisms.

The formation of denser water occurs mainly in few selected northern regions of the basin, because of the more efficiency of the buoyancy fluxes which set deep convective processes.

These areas are reported in Fig. 1.8 while the schematic of the "source" water type in Tab. 1.2. Note that in literature usually the generic term Eastern Mediterranean Deep Water (EMDW) is used with reference to Adriatic Deep Water, Levantine Deep Water, Cretan Deep Water or a combination of them.

Here after the two different theories regarding denser water formation on shelves and on open ocean are presented. Then, both EMED and WMED denser water masses along to their variability are discussed.

1.4.1 Water mass formation variability

The interannual variability of the water mass formation rate is an important parameter to monitor in order to quantify the degree of changes occurring in the thermoaline structure of the basin from year to year (Pinardi and Masetti, 2000).

Pinardi et al. (2015) studied the deep water formation rates and their variability through a part of an eddy-resolving reanalysis dataset, spanning from 1987 to 2007. Several approaches have been suggested to compute the water mass formation rate, but they followed the one proposed by Lascaratos et al. (1993). The method consists of estimating for each year the volume of waters on a specified density interval in the mixed layer of a specific area of interest, and the dividing this volume by one year in seconds (Pinardi et al., 2015). This choice has been dictated by the more accurate estimates of the surface mixed layer properties than the estimates of temperature and salinity profile which are required in the method proposed by Tziperman and Speer (1994).

Since the deep water formation processes occur in winter due to intense buoyancy loss, the upper panel in Fig. 1.9 shows the winter monthly rates averaged over the period 1987-2007. In both panels area 1 represent the Rhodes Gyre where LIW is formed, while area 2 refers to Cretan Deep Water (CDW) formation region. Area 3 takes into account the open ocean deep water formation regions in the Eastern Mediterranean (see Fig. 1.8)

1.4 – Water mass formation processes

Table 1.2: Dense, Deep and Intermediate water mass characteristics in the Mediterranean Sea at the area of formation indicated in Fig. 1.8. Reproduced from Pinardi et al. (2022).

Water Mass Name	Acronym	T-S range	Area of formation	Reference literature
Adriatic Deep Water	AdDW	T=13 S=38.6	4	Artegiani et al., 1997 Gacic et al., 2001 Mantziafou and Lascaratos, 2004 Theocharis et al., 2014 Verri et al., 2018 Manca et al., 2003
Northern Adriatic Dense	NAdDW	T=9-11.3 S=38.3-38.5	6	Artegiani et al., 1997 Orlić et al., 1992 Supić and Vilibić, 2006 Wang et al., 2006 Marini et al., 2010 Theocharis et al., 2014
Mid-Adriatic Dense Water	MAdDW	T=11-12.3 S=38.2-38.6	5	Cushman-Roisin et al., 2001 Artegiani et al., 1997 Marini et al., 2010
Aegean Dense Water	AgDW	T=10 S=38.4	3	Gertman et al., 2006 Zervakis et al., 2000
Cretan Deep Water	CDW	T=14-14.5 S= 38.9-39.1	2	Theocharis et al., 1999 Theocharis et al., 2014 Velaoras et al., 2014 Velaoras et al., 2021
Cretan Intermediate Water	CIW	T=14.5-15.5 S= 38.95-39.1	2	Schlitzer et al., 1991 Theocharis et al., 1999
Levantine Deep Water	LDW	T=13.5-14 S=38.7-38.8	1	Lascaratos, 1993 Gertman et al., 1994 Theocharis et al., 2014
Levantine Intermediate Water	LIW	T=15-16 S=38.95-39.05	1	Wust, 1961 Lascaratos, 1993
Tyrrhenian Intermediate Water	TIW	T=13.2-14 S=38-38.2	7	Napolitano et al., 2019
Western Intermediate Water	WIW	T=13 S=37.7-38.3	9	López-Jurado et al., 1995 Juza et al., 2019 Fuda et al., 2000
Western Mediterranean Deep Water	WMDW	T= 12.7 S=38.4	8	Pinardi et al., 2015 Somot et al, 2018

1 – Introduction

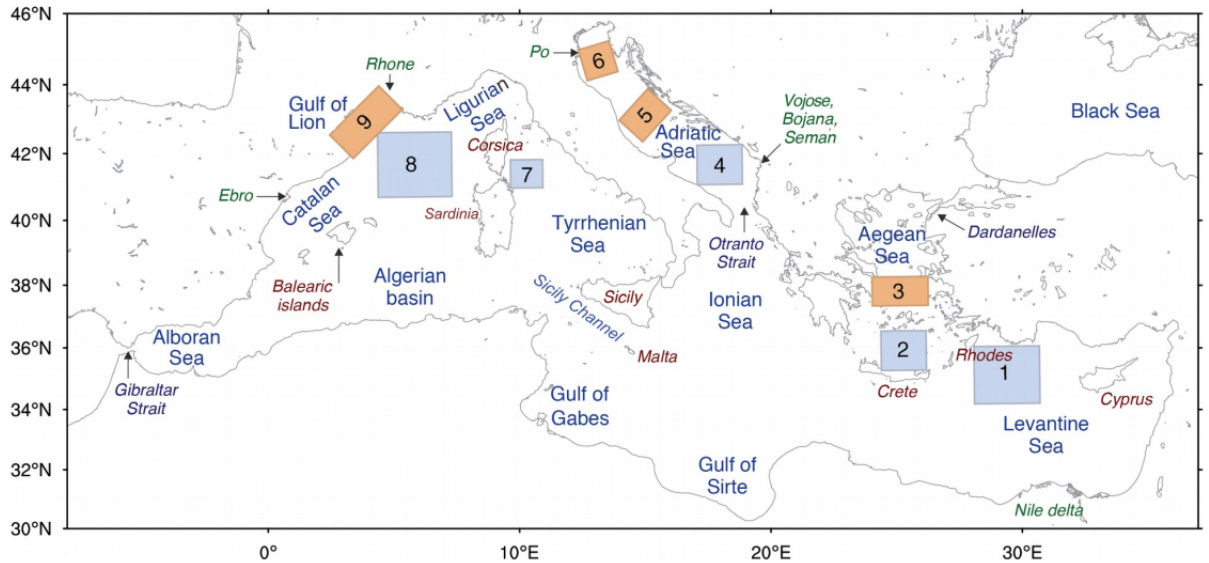


Figure 1.8: The nine areas where dense/deep and intermediate water formation occurs, as documented in observational and modelling studies over the past 40 years. **Area 1** is the Levantine Intermediate (LIW) and Deep Water (LDW) formation area, **Area 2** the Cretan Intermediate (CIW) and Deep Water (CDW) formation area, **Area 3** the Cyclades Plateau where Aegean shelf Dense Water (AgDW) is formed, **Area 4** the DWF area of the Southern Adriatic Sea (AdDW), **Areas 5 and 6** are shelf DWF areas in the Middle (MAdDW) and Northern Adriatic Sea (NAdDW), respectively, **Area 7** is the Tyrrhenian Intermediate Water (TIW) formation area, **Area 8** the Western Mediterranean Deep Water (WMDW) formation area, **Area 9** is the shelf DWF area in the Gulf of Lyon. Western Intermediate Water (WIW) is formed in Areas 8 and 9. Blue boxes indicate open ocean convection areas, red boxes shelf dense cascading areas. Reproduced from Pinardi et al. (2022).

and, finally, area 3 stands for the Gulf of Lyon, where WMDW is formed.

Looking at the upper panel in Fig. 1.9. , the largest rates are reached during February and March with more denser water production in the Gulf of Lyon during February than March.

In the lower panel annual water mass formation rates are compared. Largest deep and intermediate water formation events occur every three to six years, except in the Sea of Crete. Here, between 1992 and 1993 CDW production reached maximum rates, over 1 Sv, but ended abruptly after 1996. Furthermore, a large production of LIW and Levantine Deep Water (LDW) has been documented between 1992 and 1993.

This remarkable CDW production is due to EMT event, which has been captured by the reanalysis dataset. During this period, an additional source from the Aegean Sea

has produced large quantities of dense water that, after overflowing through the Cretan Arc Straits, provided the eastern Mediterranean with water denser than the previously exiting deep and bottom water mass from Adriatic sites.

This event, classified as a transient phenomenon, is thought to be caused by changes in circulation patterns in addition to some important meteorological anomalies that occurred over the eastern Mediterranean. Hereafter the main triggering events are exposed:

- NIR phenomenon: from 1987 to 1996 the anticyclonic gyre diverted Atlantic Water toward the Adriatic Sea, weakening the Adriatic Deep Water formation and enhancing the salt budget in the Levantine basin. After the 1987-96 period, the NIG reversed and the cyclonic gyre returned to advect saline LIW into the Adriatic, empowering deep water mass production.
- Entrance of saltier water in the Aegan Sea: Malanotte-Rizzoli et al., (1999) stated that in 1991 the salty LIW formed in the Northern Levantine was diverted from spreading westwards by the presence of a multi-centered strong anticyclonic region in the Southern Levantine. This induced a substantial LIW recirculation in the Levantine basin itself.

The anticyclonic structure forced also a branch of newly formed CIW, normally spreading eastward into the Ionian interior, to flow again into the Cretan Sea through the Eastern Cretan Arc Straits.

The combined action of these two factors resulted in an increase of the salt budget in intermediate layers, thus in the empowering of deep water formation.

Gertman et al., (2006) confirmed the conclusion of Malanotte-Rizzoli et al. (1999) by analyzing data from two cruises carried out during the late winters of 1988 and 1990. They observed a denser water production in the Northern Aegan due to enhanced lateral advection of salty waters of Levantine origin.

- Lower flux of fresh Black Sea: Gertman et al., (2006) also pointed out that Black Sea Water (BSW) entering into Aegan Sea plays an important role as a regulator of the intensity of water mass formation because of its low salinity.

They observed a large volume of BSW on the Northern Aegan during limited depth convective events, while a smaller volume of BSW was noticed during CDW production.

- Large air-sea fluxes during winters of 1987, 1992 and 1993: using an high resolution model, Stratford and Haines (2002) extended the investigations done by Wu et al., (2000) and Samuel et al., (1999) by analysing the impact of both cooling and changed wind patterns on the Aegan Sea as triggering factors for EMT. They were

able to reproduce the observed trend of temperature in the Cretan Sea with only considering the colder winters of 1992 and 1993.

On the other hand, the role of wind forcing was found to be secondary to that of buoyancy. However, stronger northerly winds for the period 1988-1993 do promote the southward transport of cool north Aegean water as far as the Cretan Sea, and lead to slightly improved water properties in deep eastern basin (Statford and Haines, 2002).

In addition to deep water formation, another intermediate water, the so-called Cretan Intermediate Water (CIW), is usually produced within the Aegean Sea. During EMT period. due to salinity increase in the Aegean Sea, a denser CIW was found to spread into the Ionian interior substituting the LIW.

The weak difference of the CIW properties, reported in Tab. 1.2 from those of LIW may make it difficult to distinguish between them, nevertheless CIW is warmer ($\theta > 15$ °C) and more saline ($S \sim 39.1-39.3$ psu) than LIW (Theocaris et al., 1999).

Results from hydrographic investigations performed in the central regions of the Eastern Mediterranean in 1998 and in 1999 attest that during these years the EMT relaxed (Theocharis et al., 2002), while new developments of the deep dynamics in the Ionian interior were most effective in homogenizing and mixing the new Aegean dense waters with the resident EMDW of Adriatic origin (Manca et al., 2002).

The EMT relaxation led to the peak of deep water formation in Adriatic Sea in 1999. It is probably connected to the redistribution of salinity in intermediate layers, rather than atmospheric conditions, since mild winters have been reported before the peak of deep water formation rate. In fact, since 1996 the reestablished cyclonic NIG started to advect the CIW along the west coast of Greece, prevalently toward the Adriatic Sea, instead of forcing recirculation eastward. Manca et al. (2002) have demonstrated from detailed isopycnal analyses that the CIW spreads over the 29.05 kg/m^3 isopycnal surface and intrudes into the Adriatic Sea, while the LIW/CIW mixture is the dominant water mass in the Ionian interior and spreads prevalently toward the Strait of Sicily. This induced an intrusion of saltier and warmer CIW than LIW into the Adriatic Sea, thus enhancing again the dense water formation in the Southern Adriatic up to ~ 1 Sv in 2000.

Gasparini et al. (2005) studied the hydrographic characteristics in the layer with higher salinity at the Strait of Sicily in order to assess the impact of EMT on the WMED. In order to tracking the behaviour of both intermediate and deep waters, the section near the deep trench in Strait central basin has been considered and the salinity, temperature and density evolution schematics from 1985 to 2004 are shown in Fig. 1.10.

The salinity evolution reported in Fig. 1.10, reveals a dramatic increase starting from 1990 due to the production of CIW, which culminates in a massive presence of salty

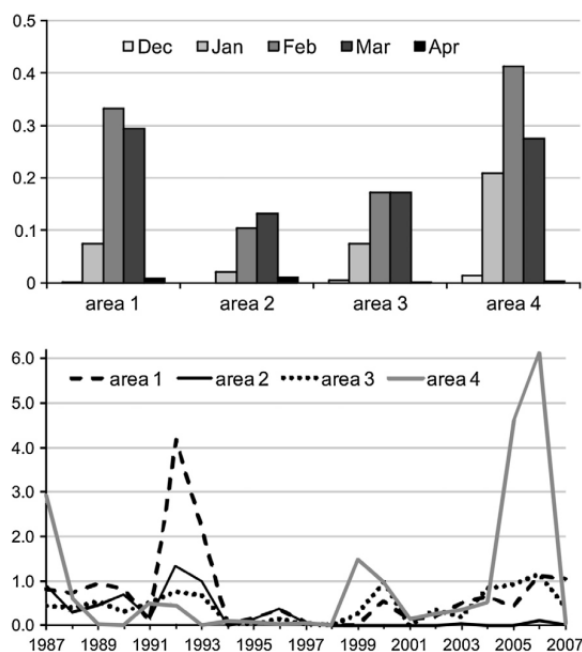


Figure 1.9: Upper panel: WMF rates (Sv) in different months for each of the four areas, average for the 21 years. Lower panel: WMF rates (Sv) for the months of February and March and for the four regions as a function of time. Reproduced from Pinardi et al. (2019).

water in the Strait. Again, the anticyclonic circulation in the Ionian played a crucial role in the advection of CIW towards the Sicily Strait. Then, the salinity and temperature experienced a suddenly decrease until 1997 which resulted in a significant rise of the water density. This was due to the production of the heavy CDW, which sinks, subtracting salt from the LIW layer and generating the uplifting of the resident deep water, inducing into the Strait less salt in the intermediate layer, while a considerable amount of water of Adriatic origin is able to enter the Strait (Gasparini et al., 2005).

Finally, from 1999 with the restoring of deep water source in the Adriatic, a new salty/warm phase with positive salinity and temperature trend has been observed.

Looking again at Fig. 1.9, the largest deep water formation event occurs in 2005 and 2006 in the Gulf of Lyon, concomitant to large deep water formation in the Ligurian Sea (not shown). These unusual convective events occurred along with WMDW production with values of temperature and salinity higher with respect both to the resident deep waters and to the climatological values.

By numerical modelling, Herrmann et al., (2010) were able to reproduce correctly the EMT and the unusual WMDW productions, also performing sensitivity simulations to assess the respective contributions of atmospheric and oceanic conditions to these events. They found out that the EMT was not responsible for the change of WMDW characteristics, but it induced the deepening of the heat and salt maximum in the Northern WMED, potentially leading to double the WMDW volume. Instead, winters of weak atmospheric buoyancy loss since 1988 in the Northern WMED prevented strong convection to occur during the 1990s, enabling heat and salt contents to increase in

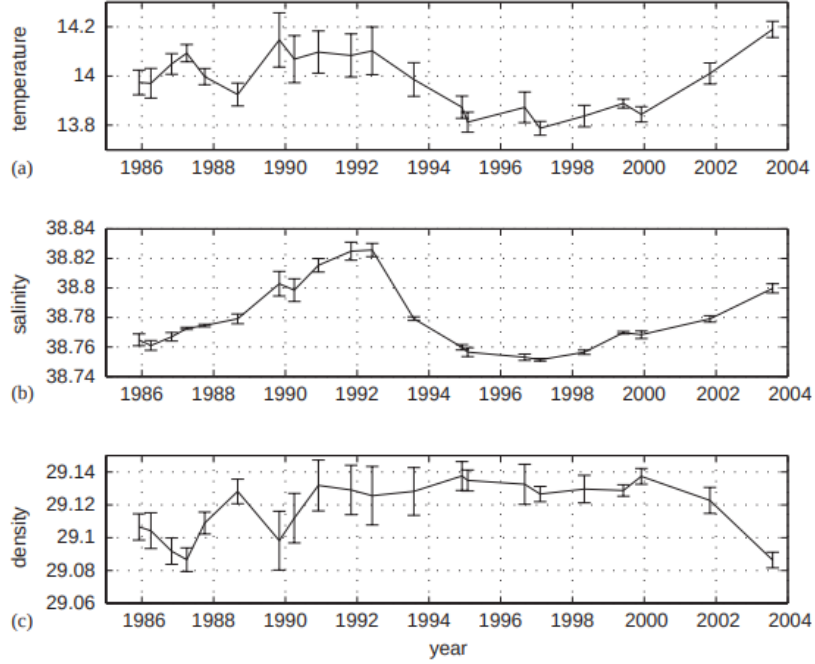


Figure 1.10: Time evolution of (a) potential temperature; (b) salinity; (c) potential density in the central region of the strait using representative stations. Bar indicate the standard deviation. Reproduced from Gasparini et al. (2005).

this region, thus resulting in the change of WMDW characteristics observed in 2005 (Herrmann et al., 2010).

On the other hand, the strong buoyancy loss during winters of 2004 and 2005 increased the volume of newly formed WMDW and allowed convective processes to reach the bottom and covered an area much larger than usually. Thus, the peak of WMDW in 2005 was mostly due to specific atmospheric conditions occurred before and after the large convective event.

1.4.2 Theory of dense and deep water formation

Denser water formation processes are associated with a surface increase of water density, due to diabatic exchanges with the atmosphere. The buoyancy fluxes defined as:

$$B = \frac{g\alpha_T}{\rho_0 C_w} Q_H - \beta_S S_0 g (E - P - R) \quad (1.8)$$

can change the water buoyancy (Eq. 1.5). In Eq. 1.8, g is the reduced gravity, α_T is the coefficient of thermal expansion, C_w specific heat at constant pressure, Q_H is the heat

flux in denser water formation area, β_S is the coefficient of haline contraction. The flux is positive if the heat enters the ocean ($Q_H > 0$) and freshening due to precipitation and runoff exceeds evaporation.

Thus, denser water formation is associated to negative buoyancy fluxes which make water higher than the surrounding, then probably becoming gravitationally unstable.

If only heat exchange is considered and assuming heat flux at the surface is balanced by turbulent diffusivity in a column with height $\Delta z = 100m$, one obtains:

$$K_\nu \frac{\Delta \rho}{\Delta z} = \frac{-\alpha_T}{C_w} Q_H \quad (1.9)$$

where K_ν is the vertical diffusivity, here assumed to be $0.01 \text{ m}^2/\text{s}$, while the considered density difference is $\Delta \rho = 0.2 \text{ kg}/\text{m}^3$. The so-estimated heat loss is of about $-390 \text{ W}/\text{m}$, which is a typical winter values, thus denser waters are "winter" waters, as already confirmed by experimental evidence reported in Fig. 1.9.

Then, the newly formed denser water can reach the bottom through open ocean convection directly at the formation site whether through down-sloping or cascading from the shelf area as bottom currents.

Formation in the open ocean

Theories regarding dense water formation in open ocean regions have been developed through studies conducted in the Northern Western Mediterranean area, however this theory appears to be valid for also the other open ocean areas, i.e areas 4, 2, 1 in Fig. 1.8.

By numerical experiments, Marshall and Schott (1999) defined three main phases of this convective process which are reported in Fig. 1.11.

Preconditioning phase

In this phase, the wind-driven circulation in the northern Mediterranean as well as the bathymetry produces a preconditioning cyclonic gyre with isopycnals outcropping at the center. This gyre is characterized by weak stratification at the centre and by a rim current which later develop a baroclinic instability active during the third phase of the process. The central area of the gyre is referred as *dense water patch* since the net vertical velocity is zero at its centre.

Madec et al. (1996) investigated in detail the preconditioning phase in the Northern WMED using a numerical modelling approach. They found out that in Mediterranean the preconditioning gyre is a wind stress curl forced gyre and the buoyancy forcing has little or no impact on the strenght of it.

Deep convection or violent mixing

The dynamics of deep convection is characterized by downward vertical velocity

with order of magnitude of 10^{-1} *m/s*. The space scale of the convection inside the centre of the gyre is connected to cylindric structures with diameter of 1 km called *plumes*. These are very rapid overturning cells with upward and downward vertical velocities that almost compensate for each other. Jones and Marshall (1993) have estimated the scale of vertical velocity associated to the plumes:

$$w_{plume} = \sqrt{\frac{B}{f}} \quad (1.10)$$

with B the buoyancy flux and f the Coriolis parameter.

The plumes containing dense waters reach the bottom and then collapse under gravity and rotation, giving rise to a geostrophically adjusted well-mixed patch. Then, the dense water formed by convection slump the interface laterally and start moving outwards.

Lateral exchange or spreading phase

The baroclinic rim current, enclosing the patch of dense well-mixed waters, becomes unstable and forms mesoscale eddies, with order of magnitude of 10 km or more, that contain *dense water cones* and spread apart with time. The eddies balance the heat loss during the violent mixing phase by fluxing the heat laterally. Hence, they manage to re-stratifying the cold-water mixed patch in about one week.

Finally, the spreading phase continues for months, as eddies propagate away from the mixed patch. Each region of formation in the Mediterranean Sea has different eddy pathways.

In marginal seas the open ocean convection is a bit different from the one just described. Since marginal seas are bounded in the horizontal direction, the preconditioning cyclonic gyre is constrained by the geometry of the coasts.

Iovino et al. (2008) have investigated the open ocean dense water formation in the Southern Adriatic Sea through numerical modelling forced by the outflow/inflow at the Strait of Otranto and a sill at the entrance.

As a result, they found out that fully open ocean dense/deep convection differs from marginal sea open ocean deep water convection in the last phase of the process, during the lateral exchange and restratification, and during spreading.

Furthermore, Iovino et al. (2008) examined the effect of sill in the marginal sea and found that the temperature of the well-mixed patch of water was lower than without a sill, as the inflow of warm waters by the boundary currents around the basin is affected.

Thus, the greater density of the deep waters of the EMED compared to the WMED (Tab. 1.2) may be due to this, and the deep waters of the Adriatic and Aegean Seas may be denser than the WMDW because they are formed in deep marginal seas with sills.

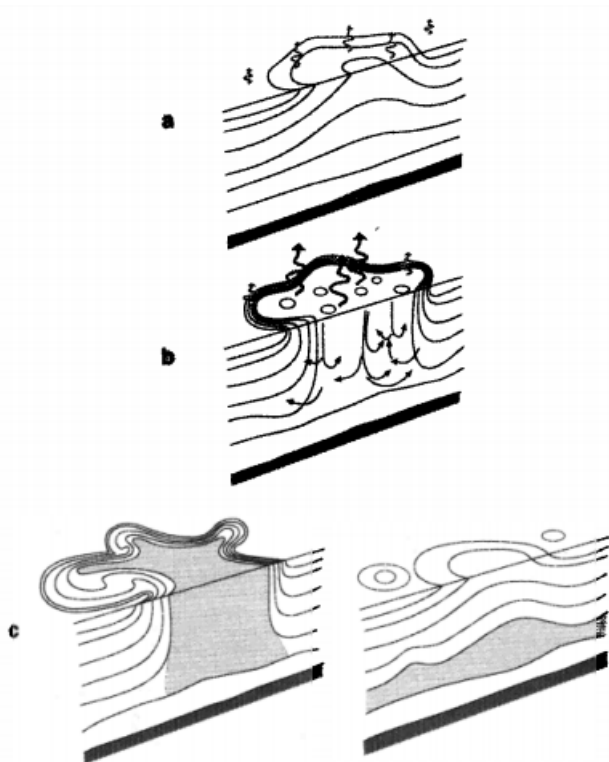


Figure 1.11: Schematic diagram of the three phases of open ocean deep convection: (a) preconditioning, (b) deep convection, and (c) lateral exchange and spreading. Buoyancy flux through the sea surface is represented by curly arrows, and the underlying stratification/outcrops is shown by continuous lines. The volume of fluid mixed by convection is shaded. Reproduced from Marshall and Schott (1999).

Formation on the shelves and cascading

The formation of denser water on shelves as in the open ocean is due to extensive buoyancy losses during winter.

These processes have been documented for areas in the Cyclades Plateau, the Northern and North-Eastern Adriatic and the Gulf of Lyon shelves (areas 3, 5, 6, and 8 in Fig. 1.8).

The preconditioning phase differs from the open ocean one because of vertical geometrical constraints and lateral input of freshwater which can modify the final dense water volume. Thus, the water masses so-formed are cold and have low salinity, due to runoff, and overflows off shelves, a process known as dense shelf water cascading, specific type of buoyancy-driven current.

The cascading can be viewed as a three-stage process, without considering the advection of salinity.

In the first phase, the dense water patch reaches the shelf bottom, because the convection depth is typically greater than the shelf depth. Without considering lateral salinity advection, Shapiro (2003) found that local temperature response to winter cooling is the major driver of the cascade and it leads to a density difference between shelf and

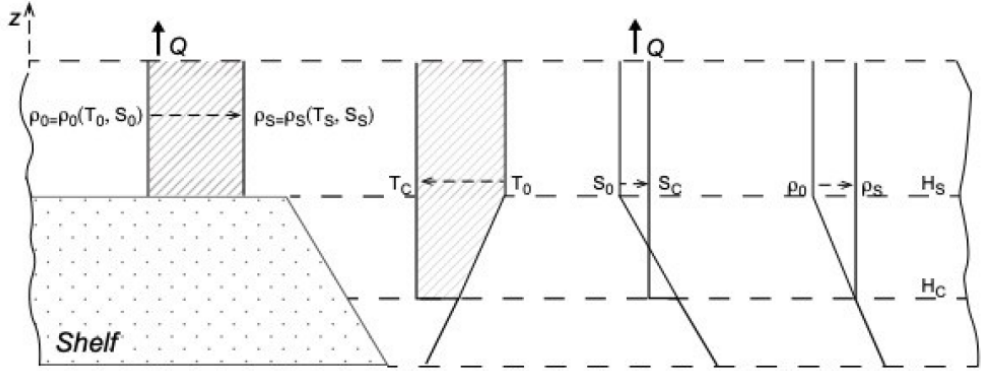


Figure 1.12: Scheme of formation of horizontal density contrast between shelf and slope waters under identical outward heat flux. Subscripts 0, S and C denote the initial state, shelf water and slope water, respectively. Reproduced from Shapiro (2003).

offshore waters:

$$\frac{d\rho}{\rho_0} = \frac{\rho_c - \rho_s}{\rho_0} = \frac{1}{\rho_0} \left(\beta \frac{dS}{dz} - \alpha \frac{dT}{dz} \right) \frac{(H_c - H_s)^2}{2H_s} \quad (1.11)$$

where subscripts s and c correspond to the shelf and offshore convective layers respectively while H_c is the final depth of the offshore mixed layer. The process just described is shown in Fig. 1.12, where the symbols in Eq. 1.11 are explained.

Secondly, Shapiro (2003) considers a bottom boundary layer under a cross-slope density gradient, no along-slope (y) gradients: $u_y = v_y = 0 = p_y$, no lateral diffusion, steady state and negligible cross-slope advection of momentum in the boundary layer. By resolving equation of motion, under suitable boundary conditions, Shapiro (2003) found the steady bottom boundary layer criterion:

$$R_H = \frac{d\rho}{\rho_0} \frac{Sg}{Lf^2} < 1 \quad (1.12)$$

where L is the cross-shelf distance over a slope S and the other terms already specified.

Thus, a non-steady solution is achieved when

$$R_H = \frac{d\rho}{\rho_0} \frac{Sg}{Lf^2} > 1 \quad (1.13)$$

The time-dependent shelf-water cascading process starts only if the above condition is satisfied and hence the association with strong forcing by $d\rho/\rho$ and S together with the weak rotational constraint suggests an accelerating down-slope flow.

The downslope motion can be achieved by several regimes, from plumes dominated by geostrophy to unstable along-slope current, and remnants of these plumes can be found

during the summer because of the long-term cascading process, which is estimated to be 6-7 months.

During cascading, the dense water plume is modified by mixing with ambient water, thus entering the third phase. When it finds its buoyant layer, the plume finally detaches from the bottom, intruding into ambient water.

1.4.3 Intermediate Water

Levantine Intermediate Water

The Levantine Intermediate Water (LIW) can be found either in the EMED and in the WMED, and it constitutes the lower branch of the superficial zonal cell. LIW is also known to be a major contributor to the Mediterranean outflow in Gibraltar.

This ubiquitous water mass is mainly formed in the Rhodes Gyre through open ocean convection.

In winter 1995, the Levantine Intermediate Water Experiment (LIWEX) was carried out and successively the collected dataset during three successive surveys in January, February, and March/April 1995 was examined. The purpose of this study was the monitoring of the convective chimney in the Rhodes Gyre, in which denser waters are formed.

One of the major discoveries was that LIW formation does not follow the MEDOC recipe of the open ocean formation dynamics of denser water. Even in the absence of severe storm events, in fact, wind surface cooling and evaporation are sufficient to produce shallow thermostads of LIW in near-coastal areas (Malanotte-Rizzoli et al., 2003). Since deep convective cells are not involved in LIW production, this water mass is found to be ubiquitous in the Levantine basin because shallow mixed chimneys can occur more frequently in space and time. Then, LIW subducts from the chimneys bottom spreading along isopycnal surfaces and its dispersal pathways are controlled by the upper thermocline circulation.

Moreover, in winter 1995 the LIWEX experiment managed to capture another water mass fresher and colder than LIW, the Levantine Deep Water, (LDW). The production of LDW is not so frequent as LIW because it needs exceptional winter atmospheric conditions. In fact, strong outbreaks of cold, dry winds blowing from the mainland into the northern Levantine started in fall 1994 and they led to a strong total heat loss. Thanks to this triggering event, on February a strong mixing phase within the Rhodes Gyre was noticed, with the convective cell vertically homogeneous to the depth of 900 *m*. Unlike LIW formation, the LDW production has been shown to follow all three phases of open ocean formation process.

Then, mapping of properties on the LDW density horizon reveals that LDW does not spread away from the formation site but remains confined inside the localized Rhodes

Gyre cyclonic circulation, possibly because of topographic effects (Malanotte-Rizzoli et al., 2003).

Thus, the Rhodes Gyre was shown to be the site for multiple, and different, water mass formation processes, depending on atmospheric conditions.

Cretan Intermediate Water

The Cretan Intermediate Water (CIW) mass is formed both on the Aegean continental shelves and by open ocean convective mixing in the Cretan Sea (Velaoras et al., 2021).

This water mass has the typical characteristics of LIW but within the Cretan Sea is generally considered being slightly colder, more saline, and denser. After exiting the Cretan Straits, CIW settles at depths between the LIW horizon and Eastern Mediterranean Deep Water (EMDW) and moves westwards towards the Ionian and Adriatic Sea, providing salt to these basins. During the EMT event, the Aegean Sea produced denser CIW, named dCIW, settling at depths below LIW but not dense enough to penetrate into the deep/bottom layers of the EMED. The density of dCIW ranges in $29.10 < \sigma_\theta < 29.20$ kg/m^3 .

Then, a CIW/dCIW branch moves towards Sicily Strait, mixing with LIW.

Millot (2013) estimated that LIW could represent two-thirds to three-quarters of the intermediate waters found at the Sicily Channel, with CIW responsible for the remainder.

Western Intermediate Water

Western Intermediate Water (WIW) is a cold, low-salinity water mass formed in winter in the WMED and located in the layer between the surface AW and the intermediate LIW/CIW.

Millot (1999) identified two formation mechanisms, one in open sea corresponding to winter winds where the cooling is too weak to trigger deep convection, and the other on the Gulf of Lyon shelf, the Balearic and the Ligurian Sea, which is associated with lower salinities.

The WIW formation is the result of locally MAW cooling during cold wind events, thus it becomes denser and then it reaches the buoyancy equilibrium between the MAW and the LIW layers.

Pinot and Ganachaud (1999) noted the recurrent presence of WIW in mesoscale eddies in the Balearic Sea that strongly affect the general circulation.

WIW was also identified in the Strait of Gibraltar and it is able to penetrate the EMED through the Sicily Channel.

Tyrrhenian Intermediate Water

Napolitano et al. (2019) proposed another denser water formation in the Bonifacio cyclonic gyre. The western intermediate water formed there is called Tyrrhenian Intermediate Water (TIW), it sits above the LIW, in the layer between 100 and 200 m, and it is characterized by a relative minimum of temperature and salinity in the TS diagram (Napolitano et al., 2019). However, evidences are not strong enough to draw conclusions.

In addition, another deep water mass is usually found in the Tyrrhenian Sea in the layer from 700 m to 1500 m deep, between the LIW and the WMDW. The Tyrrhenian Deep Water (TDW) is a local water mass resulting from the mixing of the LIW with resident deep water, and it has temperature and salinity slightly higher (by about 0.2 °C and 0.03 psu) than those of the WMDW.

1.4.4 Deep Water

Adriatic Deep/Dense Water

During winter, the Adriatic is subject to violent northeasterly dry winds (Bora) that produce intense heat loss. Convective mixing involves surface waters and intermediate waters entering from the Otranto Strait as part of the cyclonic circulation of the Adriatic Sea.

Manca et al. (2003) analysed hydrographic and current measurements taken during the period from March 1997 to March 1999 in the Southern Adriatic and in the Otranto Strait. They detected a layer with density in the range of about 29.16–29.17 kg/m^3 corresponding to Adriatic Deep Water (AdDW). Below this, a denser water layer reached 29.34 kg/m^3 , referred to as Northern Adriatic Dense Water (NAdDW).

The formation of very dense waters (Northern Adriatic Dense Water - NAdDW) on the Croatian shelf areas was identified many years ago. It flows as a dense vein along the western Adriatic shelf and escarpment area at a depth of around 50-150 m, cascading in the Middle Adriatic pit, where it rapidly renews old bottom waters.

A mixture of the newly formed AdDW and NAdDW exits the Adriatic through the Otranto Strait as a 200 m thick vein down-sloping in the Ionian Sea as a deep western boundary current and plunging to the bottom of the EMED (Robinson et al., 1992).

The water mass characteristics in the Adriatic Sea appears to be more variable than in the Gulf of Lyon, because of the lateral advection and surface buoyancy forcings. As already discussed, the NIG controls the advection of surface and intermediate water masses into the Adriatic, thus its periodic reversal leads to changes in deep water mass characteristics formed within it.

Another influencing factor is the river runoff. In fact, Kokkini et al. (2020) showed that during a rainy year/season, high river discharges from the North Adriatic and from

the Po can lead to a significant amount of fresher water being advected into the South Adriatic, which prevents dense water formation.

Aegean Deep/Dense Water

The Aegean Sea has been proposed as a possible source of deep waters for the EMED since the 1950s (Pollak, 1951). The Eastern Mediterranean Transient (EMT) event occurred after 1987, which unambiguously defined the Aegean Sea as a source of EMDW.

In fact, in 1989 a massive overflow of deep water, the CDW, was formed in the Cretan Sea and its estimated rate of overflow for the period from 1989 to 1995 was about 1.2 Sv, which is 4 times the estimated typical outflow from the Adriatic Sea (Roether et al., 1996).

As already discussed, this anomaly CDW formation was due to the combined effects of atmospheric conditions and changed circulation in the upper thermocline, which led to an increase of salinity in intermediate layers.

The most plausible areas of CDW formations are indicated to be over the Lemnos–Lesvos Plateau, but the Northern Aegean and the Cyclades plateau DWF processes may also contribute to the bottom waters of the Cretan Sea (Velaoras et al., 2021).

From 1999, the Adriatic source of deep water was reestablished and Manca et al. (2006) estimated that in 2002 the dense water of Adriatic origin again replenished the volume of the deep Ionian basin by more than 50%.

Western Mediterranean Deep Water

The first scientific observations into Mediterranean dense water formation event have been carried out by an international group of oceanographers, whose first experiment is referred to as Mediterranean Ocean Convection experiment (MEDOC Group, 1970). In 1969, they investigated the offshore area of the Gulf of Lyon where open ocean convection occurs and they managed to observe the rapid water column homogenization in terms of temperature and salinity down to approximately 1500 m.

This zone is exposed to the Mistral in the Rhone valley and the Tramontane between the Massif Central and the Pyrenees, intensified by the continental orography. In winter, these winds lead to strong cooling through evaporation, which increases its water density thus producing unstable stratification enabling deep convective mixing. Low stratification of the deep waters characterizes the northern WMED, and thus the erosion of the stratification of surface and intermediate waters by winter storms represents the critical point for deep convection (Anati and Stommel, 1970).

The temperature profiles measured by the MEDOC Group reveal a homogeneous structure in the vertical direction, reflecting the convective process. In the horizontal direction, the mixing affected an area of about 50 km in the north-south direction and

130 km in the west-east direction. Unlike the vertical direction, the properties of the mixed water mass were not homogeneous horizontally within this patch of dense water, because of the nonuniform thickness of the mixing.

Moreover, after the cessation of the wind, they noticed increasing horizontal velocities, with typical values of 15 to 20 cm s^{-1} at the surface, and detect at least three eddies of about 20 km in diameter.

After these early observations, the understanding of the development of open ocean convection and the processes at work increased significantly.

During the second MEDOC experiment in 1987, Acoustic Doppler Current Profilers (ADCP) were positioned on 3 moorings within the center of the convection zone to measure the velocity profile.

These observations confirmed the presence of vertical shear in the horizontal currents, which were organized in a surface-cyclonic circulation. They also revealed the presence of relatively strong barotropic currents (0.4 m s^{-1}) in the mixed patch zone. Regarding vertical velocities, they have been characterized much more systematically than before, with downward velocities of 5-10 cm s^{-1} were recorded, separated by lower upward velocities.

To highlight the vertical velocity structures within the dense water patch, in 2012-2013 a series of campaigns was conducted using glider paths through the convection zone. Thanks to that, Margirier et al. (2017) provided a 3D description of these plumes and a statistical description of their distribution. They have typical vertical velocities of 10-20 cm s^{-1} , a mean radius of 350 m, and are spaced apart about 2 km, covering about 30% of the convection area. The upward velocities are three times lower than the downward velocities and cover the remainder of the area.

They revealed also the presence of different types of Submesoscale Coherent Vortices (SCV, McWilliams, 1985). Some of these SCV are cyclonic and others anticyclonic eddies of 5-8 km in radius and are composed of newly formed water expelled from the convection patch. Their vertical extension can reach that of the entire water column for cyclones (Bosse et al., 2016). These SCV can survive until the following winter and disperse dense water while preserving its characteristics (temperature and salinity). SCV can also encourage local convection the following winter.

Wu and Haines (1996) focused on the impact of LIW on WMDW formation, concluding that three factors determine, in theory, the volume and properties of the deep water formed in the Gulf of Lyon: the weak stratification provided by the wind-driven, large-scale cyclonic gyre, the entrainment of salinity from below supplied by LIW, and the buoyancy loss at the surface due to winter cooling.

Margirier et al. (2020) also documented an interplay between LIW warming and salting trends, and the occurrence of deep ocean convection in the Gulf of Lyon. Annual open ocean DWF events characterized the period between 2009 and 2013, in which the LIW

properties were transferred to the deep layers. During the following years (2014-2018), the lack of convection produced a warming and salinification of the intermediate layers in the convection zone and the deep waters restratified making it increasingly difficult for convection to develop.

As regard formation on shelf and cascading, winters with strong cascading in the Gulf of Lyon are less numerous than those producing deep convection, anyway several years of strong cascading reaching the seafloor have been documented through observations at sea (Durrieu de Madron et al., 2013).

The dense shelf water formation in the Gulf of Lyon appears to be linked to an anticyclonic atmospheric anomaly in the North Atlantic and a cyclonic atmospheric anomaly over the Baltic Sea, which provides particularly favorable conditions for strong, cold, and dry northerly winds over the Gulf of Lyon.

Then, near-bottom gravity currents approaching 1 m s^{-1} have been found on the Cap de Creus Canyon located at the southwestern extremity of the Gulf of Lyon shelf. Although the volume of dense water reaching the open sea is one order of magnitude below that produced by open-sea, cascading can play a more important role in the transfer of matter (carbon, sediment, and pollutants).

1.5 Thesis objectives

Wu and Haines (1996) for the first time have demonstrated the importance of LIW in deep water formation processes in the Gulf of Lyon and Adriatic areas, thus suggesting a connection between zonal and meridional overturning. With probably the same mechanism which connects the Mediterranean salt tongue spreading from Gibraltar Strait to North Atlantic deep water formation areas, the LIW contributes to the salt budget of the newly formed deep waters in Adriatic Sea and in Gulf of Lyon area. Thus, the Eastern and the Western meridional cells are interconnected and they can communicate, even if on longer timescale.

Another evidence of this connection is the outflow at Gibraltar Strait which is mainly made of LIW and WMDW. In the WMED, the LIW coming from the EMED and the dense water masses formed in the Northern WMED undergo dynamical processes which modify their thermohaline properties to eventually mix together before exiting.

The aim of this thesis is to quantify the connection between zonal and meridional cells by computing the main dispersal pathways and transport contributions of water masses composing the Gibraltar outflow.

In order to achieve this, a part of eddy-resolved reanalysis dataset is used, spanning from 2000 to 2012, thus encompassing the peak of WMDW formation.

Through a lagrangian analysis, millions of particles seeded at Gibraltar Strait are tracked backwards in time for 78 years to map the routes of the outflow water. Using

the concept of first passage time, these particles are traced until they reach one of the interception sections, which are located in the Gulf of Lyon, in the Northern Tyrrhenian Sea and at Sicily Strait.

In such a way, we provide for the first time a quantitative description of LIW pathway towards Gibraltar Strait and we present a new route from the Northern Tyrrhenian Sea to Gibraltar.

Chapter 2

Data and methods

The following chapter illustrates the reanalysis product from which the dataset considered in this thesis has been taken. The first section describes how the reanalysis dataset is produced as well as its validation results.

Since the reanalysis products do not include the vertical velocity field, this latter has been calculated from the dataset in order to reduce the computation time during Lagrangian diagnostic and the algorithm is explained at the end of the first section.

Finally, in the second section, the Lagrangian offline analysis is described in great detail as well as the experiments configuration.

2.1 Reanalysis data

Reanalysis products have been used extensively in ocean sciences (Storto et al., 2019) because they supply 4D estimate of ocean circulation by combining observations and model simulations through data assimilation. It improves traditional analysis because it produces more coherent and consistent state of the past ocean, making it a powerful tool in the comprehension of mechanisms responsible for ocean variability.

Ocean reanalyses allow the understanding of processes that cannot be observed completely, like overturning circulation, as in the case of Pinardi et al. (2019), or mesoscale dynamics (Escudier et al., 2016). In addition, they can be used as boundary and initial conditions for regional and subregional models, since regional reanalyses are challenging because of the lack of observational dataset.

For the Mediterranean Sea, several reanalysis datasets are available with observations usually taken either from satellite altimetry (Fu et al., 1994) or in situ data, and only few reanalyses use both datasets (Stammer et al., 2002).

In this thesis, it has been used the reanalysis dataset, hereafter addressed as MED REA, developed by Copernicus Marine Environment Monitoring Service (CMEMS). The

product encompasses both daily mean and monthly mean output of 2D fields of sea surface height and 3D fields of temperature, salinity, meridional and zonal currents, for the time period from 1987 to 2016. Only the dataset that covers daily mean fields on native grid, for the period spanning from 2000 to 2012, is considered.

The MED REA uses the Ocean General Circulation Model (OGCM) based on NEMO (Nucleus for European Modelling of the Ocean). Regarding observational dataset, the reanalyses takes into account in-situ temperature and salinity profiles, and Sea Level Anomaly (SLA) along track satellite data. Then, these data are assimilated in the model by using a variational scheme called OceanVar, set up by Dobricic and Pinardi (2008).

The reanalysis product space domain covers the Mediterranean Basin and also extends into the Atlantic in order to better resolve the exchanges with the Atlantic Ocean at the Strait of Gibraltar. It is defined on the model grid which spans from 18.125 °W to 36.25 °E and from 30.1875 °N to 45.9375 °N.

In the following subsections, the NEMO model which MED REA relies on is described, then an explanation of the assimilation scheme is presented with, eventually, the assessment of the product quality. We mainly reference to MED REA manual for users and to NEMO manual.

2.1.1 Model system description

The OGCM used to produce MED REA is the NEMO-OPA code (Nucleus for European Modelling of the Ocean-Ocean Parallelise), developed and maintained by the NEMO-consortium.

The model solves the primitive equations in spherical coordinates and it has an horizontal resolution of $1/16^\circ$ (ca. 6-7 km) and 72 unevenly spaced vertical layers (Oddo et al., 2009), thus allowing to resolve the eddy-field. The NEMO model is nested in the Atlantic within monthly mean climatological fields computed from ten years of daily output of the global model ($1/4^\circ$) provided by MERCATOR (Drevillon et al., 2008).

Recently, NEMO has been implemented in the Mediterranean at $1/24^\circ$ horizontal resolution and 141 unevenly spaced vertical levels.

The primitive equations are solved by the model under the following assumptions made from scale considerations:

- *Spherical earth approximation*: the geopotential surfaces are assumed to be spheres so that gravity (local vertical) is parallel to the earth's radius.
- *Thin-shell approximation*: the ocean depth is neglected compared to the earth's radius.
- *Turbulent closure hypothesis*: the turbulent fluxes (which represent the effect of small scale processes on the large-scale) are expressed in terms of largescale features.

- *Boussinesq hypothesis*: density variations are neglected except in their contribution to the buoyancy force.
- *Hydrostatic hypothesis*: the vertical momentum equation is reduced to a balance between the vertical pressure gradient and the buoyancy force (this removes convective processes from the initial Navier-Stokes equations and so convective processes must be parameterized instead).
- *Incompressibility hypothesis*: the three dimensional divergence of the velocity vector is assumed to be zero.

First of all, it is useful to define an orthogonal set of unit vectors (i, j, k) linked to the earth such that k is the local upward vector and (i, j) are two vectors orthogonal to k , i.e. tangent to the geopotential surfaces.

By defining $\mathbf{U} = \mathbf{U}_h + w\mathbf{k}$ as the velocity field, T the potential temperature, S the salinity, ρ the in situ density, the vector invariant form of the primitive equations in the (i, j, k) vector system provides the following equations.

Momentum balance:

$$\frac{\partial \mathbf{U}_h}{\partial t} = - \left[(\nabla \times \mathbf{U}) \times \mathbf{U} + \frac{1}{2} \nabla (\mathbf{U}^2) \right] - f\mathbf{k} \times \mathbf{U}_h - \frac{1}{\rho_0} \nabla_h p + \mathbf{D}^{\mathbf{U}} + \mathbf{F}^{\mathbf{U}} \quad (2.1)$$

Hydrostatic equilibrium:

$$\frac{\partial p}{\partial z} = -\rho g \quad (2.2)$$

Incompressibility equation:

$$\nabla \cdot \mathbf{U} = 0 \quad (2.3)$$

Heat conservation equation:

$$\frac{\partial T}{\partial t} = -\nabla \cdot (T \cdot \mathbf{U}) + D^T + F^T \quad (2.4)$$

Salt conservation equation:

$$\frac{\partial S}{\partial t} = -\nabla \cdot (S \cdot \mathbf{U}) + D^S + F^S \quad (2.5)$$

Non-linear equation of state:

$$\rho = \rho(T, S, p) \quad (2.6)$$

2 – Data and methods

where ∇ is the generalised derivative vector operator in (i, j, k) directions, t is the time, z is the vertical coordinate, ρ is the in situ density given by the equation of state (Eq. 2.6), ρ_0 is a reference density, p the pressure, $f = 2\mathbf{\Omega} \cdot \mathbf{k}$ is the Coriolis acceleration (where $\mathbf{\Omega}$ is the Earth's angular velocity vector), and g is the gravitational acceleration. $\mathbf{D}^{\mathbf{U}}$, D^T and D^S are the parameterisations of small-scale physics for momentum, temperature and salinity, and $\mathbf{F}^{\mathbf{U}}$, F^T and F^S surface forcing terms.

Regarding land-ocean interactions, the model considers the no-slip condition both on lateral and vertical boundaries.

The vertical boundary conditions are defined at the bottom, that is the surface $z = -H(i, j)$, and at the free surface $z = \eta(i, j, k, t)$.

The kinematic surface condition plus the mass flux of fresh water $P + R/A - E$, where P is the precipitation, R/A is the river runoff per unit of cell area A and E the evaporation, leads to:

$$w|_{z=\eta} = \frac{\partial \eta}{\partial t} + \mathbf{U}_h|_{z=\eta} \cdot \nabla_h(\eta) + P + R/A - E \quad (2.7)$$

Instead, the dynamic condition ensures the continuity of pressure across the interface $z = \eta$, whereas surface boundary condition on momentum is obtained by equating the stress exerted by the wind with the vertical turbulent momentum flux in the surface water column:

$$A^{vm} \frac{\partial \mathbf{U}_h}{\partial z} |_{z=\eta} = \frac{\tau}{\rho_0} \quad (2.8)$$

where A^{vm} is the vertical eddy viscosity and τ is the wind stress.

The surface boundary equations for heat and salt fluxes are:

$$A^{vT} \frac{\partial T}{\partial z} |_{z=\eta} = \frac{Q}{\rho_0 C_p} \quad (2.9)$$

$$A^{vS} \frac{\partial S}{\partial z} |_{z=\eta} = (E - P - R/A) S |_{z=\eta} \rho_0 \quad (2.10)$$

where C_p is the specific heat capacity at constant pressure, Q is the heat flux at the surface and A^{vT} and A^{vS} are the vertical diffusivity coefficients. The model is forced by momentum, water and heat fluxes interactively computed by bulk formulae using ERAInterim reanalysis fields (Dee et al., 2011) from the European Centre for Medium-Range Weather Forecasts (ECMWF) and the model predicted Sea Surface Temperatures (SST).

The cinematic boundary condition at the bottom are expressed by the following equation:

$$w|_{z=-H} = -\mathbf{U}_h \cdot \nabla_h(H) \quad (2.11)$$

that means the bottom velocity is parallel to solid boundaries.

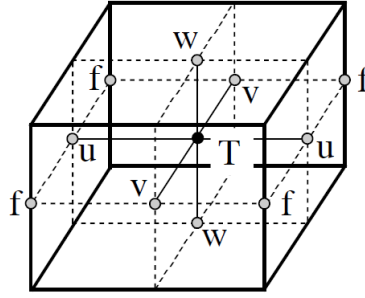


Figure 2.1: Arrangement of variables. T indicates scalar points where temperature, salinity, density, pressure and horizontal divergence are defined. (u, v, w) indicates vector points, and f indicates vorticity points where both relative and planetary vorticities are defined. Reproduced from NEMO v4.3manual.

In addition, momentum transfer occurs at small scales in a boundary layer where bottom friction is parametrised as quadratic, thus the dynamic boundary condition for the momentum becomes:

$$A^{vm} \frac{\partial \mathbf{U}_h}{\partial z} = C_D \sqrt{u_b^2 + v_b^2 + e_b} \cdot \mathbf{U}_h^b \quad (2.12)$$

where C_D is a drag coefficient, e_b a bottom turbulent kinetic energy due to tides, internal waves breaking and other short time scale currents, and $\mathbf{U}_h^b = (u_b, v_b)$ is the near-bottom, horizontal, ocean velocity.

Finally, because heat and salt fluxes through the sea floor are small they are neglected by the model:

$$A^{vT} \frac{\partial T}{\partial z} \Big|_{z=-H} = 0 \quad (2.13)$$

$$A^{vS} \frac{\partial S}{\partial z} \Big|_{z=-H} = 0 \quad (2.14)$$

The model is discretised on a staggered grid, the Arakawa C-type grid (Mesinger and Arakawa, 1976), which set scalar quantities at the center of each grid volume, the so called T point, while vectorial fields are defined at the edges (u, v, w, f points), as illustrated in the Fig. 2.1.

Eventually, the model uses the *partial steps parameterization*, meaning the thickness of the bottom layer is allowed to vary as a function of geographical location in order to allow a better representation of the bathymetry.

2.1.2 Data assimilation scheme

The OceanVar assimilation scheme developed by Dobricic and Pinardi (2008) is used to correct model dynamics fields with observational datasets. This three-dimensional

variational method iteratively finds the minimum of a cost function defined for each model variable.

The vertical covariance matrixs are represented by 20 seasonally and regionally vertical Empirical Orthogonal Functions (EOFs) of surface elevation and vertical profiles of temperature and salinity, estimated from the temporal variability of parameters in a historical model simulation (Dobricic et al., 2005).

The assimilation cycle is daily and both in-situ and satellite data are jointly assimilated to estimate the initial condition for numerical model.

The MED REA uses a comprehensive observational in situ and satellite dataset that includes:

- *Sea Surface Temperature (SST)* observational datasets: they are not assimilated but they are used to correct the surface heat flux by a relaxation of the numerical model surface layer temperature towards the observed SST.
- *in situ temperature and salinity profiles*: they belong from different instrumental data type (CTDs, XBTs, MBTs, bottles, ARGO floats) and they have been collected from different European Marine databases.
- *satellite Sea Level Anomaly (SLA)* from altimetry.

The MED REA has been initialized on the 1st of January 1985 by a temperature and salinity monthly climatology, calculated using the extensive historical in situ dataset from 1900 to 1987. Only observations before 1987 are considered to compute the initial condition thus the climatology cannot be affected by the EMT. The first two years are considered the period of model spin up, making MED REA dataset available from 1987.

2.1.3 Data quality control

The general methodology used to validate reanalysis products consists in an extension of the diagnostics developed by Adani et al. (2011), based on the misfits defined as:

$$m = -[\mathbf{y}_0 - \mathbf{H}(\mathbf{x})] \quad (2.15)$$

In the above equation, \mathbf{y}_0 is the observation vector and \mathbf{H} is the linearized operator used to interpolate the model field \mathbf{x} to the location (in time and space) of the observations \mathbf{y}_0 .

The deviations between the background and the observations are quantified in terms of Root Mean Square Error (RMSE) and BIAS scores, where RMSE provides estimates of the model precision while the BIAS indicates possible systematic errors in the model reanalysis, assuming that the observational dataset is correct.

The quality of MED REA product has been assessed for the whole period of the reanalysis, from 1987 to 2016, by comparing results with observations, climatology and

Temperature (°C)	Bias	RMSE
0 -30 m	0.0 ± 0.29	0.65 ± 0.36
30 -150 m	0.04 ± 0.14	0.46 ± 0.18
150 - 300 m	-0.04 ± 0.08	0.22 ± 0.08
300 - 600 m	-0.06 ± 0.06	0.16 ± 0.06
600 -1000 m	-0.07 ± 0.07	0.12 ± 0.05
Total	-0.02 ± 0.0	0.33 ± 0.02

Table 2.1: Estimated accuracy numbers for temperature computed from misfits of reanalysis product in different layers. Reproduced from MED REA Quality Information document.

literature. Statistics have been computed for temperature and salinity profiles, SST and SLA, within the Mediterranean Sea, without considering the Atlantix box.

The RMSE and BIAS from temperature and salinity misfits are presented as mean value over 5 layers: 0-30 m, 30-150 m, 150-300 m, 300-600 m, 600-1000 m, computed over the entire time period. A deeper layer 1000-3000 m has not been considered because scarce data availability in time and space below 1000 m does not provide enough statistical significance.

Temperature profile

Misfits are calculated by comparing MED REA to observational climatology computed considering observations from 1900 to 2009.

Reported in Tab. 2.1, there are total estimated accuracy numbers over the whole domain, up to 1000 m, for the entire period covered by the MED REA. The reanalysis dataset tends to be warmer than the observational climatology up to 150 m, where the seasonal thermocline evolves, while below 150 m the values are negative. Anomalies show a peak at about 30 m, then decrease with depth.

Salinity profile

The salinity BIAS and RMSE are presented as profiles averaged over the whole domain (up to 1000 m) and over the entire time period, with values showed in Tab. 2.2.

Salinity bias is negative within the first 400 m and positive below. The RMSE reaches maximum value of 0.3 psu at the surface where both the atmospheric and land forcings play a fundamental role.

Salinity (psu)	BIAS	RMSE
0 -30 m	0.02 ± 0.08	0.2 ± 0.1
30 -150 m	-0.03 ± 0.05	0.12 ± 0.05
150 - 300 m	-0.01 ± 0.02	0.06 ± 0.02
300 - 600 m	0.0 ± 0.02	0.04 ± 0.02
600 -1000 m	0.03 ± 0.03	0.05 ± 0.02
Total	0.0 ± 0.003	0.09 ± 0.01

Table 2.2: Estimated accuracy numbers for salinity computed from misfits of reanalysis product in different layers. Reproduced from MED REA Quality Information document.

SST

SST RMSE and BIAS with respect to daily satellite SST maps are presented as horizontal maps averaged over the whole reanalysis period.

The largest RMSE values are located along the Eastern Gulf of Lyon, Western Adriatic coast, the Turkish and Tunisian coasts. The BIAS spatial pattern highlights the areas where atmospheric forcing, numerical model approximations and topography deficiencies are located: Aegean coast and Ierapetra gyre present a cold BIAS, while warm BIAS is located in the Gulf of Taranto, around Cyprus and Rhode Island, South West of Crete and along Libyan coast.

However, the MED REA is able to well reproduce the spatial pattern of satellite observations and the SST quality might be considered of comparable quality of satellite optimally interpolated maps (Marullo et al., 2007).

SLA

SST RMSE and BIAS are computed along track over the reanalysis time period on a daily and monthly basis and the total statistics are included in Tab. 2.3.

The SLA RMSE oscillates from about 3 to 4.5 cm with a mean of ~ 3.6 cm, which is comparable with the RMSE of observations.

It has been noticed that when the number of observations increases, RMSE decreases, while when the number of assimilated observations decreases the RMSE increases.

Parameter	BIAS	RMSE
SLA [cm]	0.08 ± 0.13	3.55 ± 0.59

Table 2.3: Estimated accuracy numbers for SLA computed from misfits. Reproduced from MED REA Quality Information document.

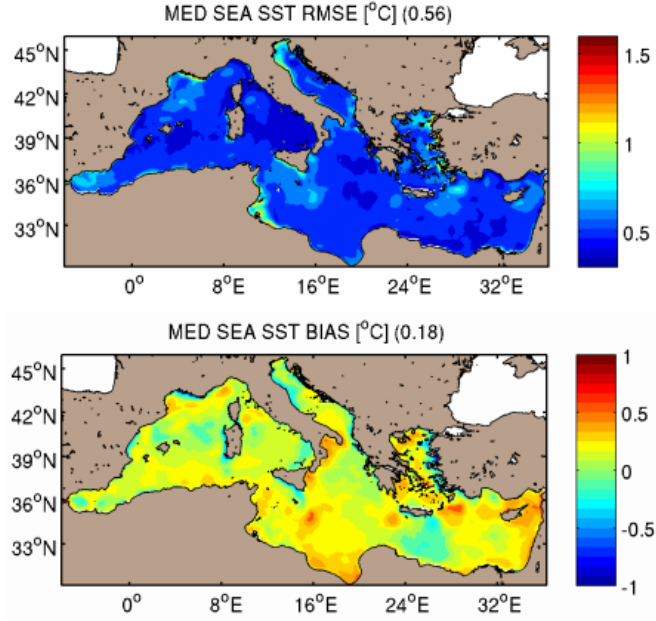


Figure 2.2: SST BIAS and RMSE computed from reanalysis product and satellite observations for the whole reanalysis period (1987-2016). Reproduced from MED REA Quality Information document.

2.1.4 Vertical velocity computation

To reduce drastically the computation time during Lagrangian analysis the vertical velocity field is deduced from the horizontal velocity field produced by MED REA.

The methodology used to calculate vertical velocities follows the one described in the NEMO manual, and it first requires the horizontal divergence field computation:

$$\chi = \frac{1}{e_{1t}e_{2t}e_{3t}}(\partial_i[e_{2u}e_{3u}u] + \partial_j[e_{1v}e_{3v}v]) \quad (2.16)$$

where e_1 , e_2 and e_3 are scale factors at each scalar and velocity grid point, ∂ is the finite difference along the respective dimension (i, j, k) and (u, v) is the horizontal velocity field.

Then, the vertical velocity is computed by an upward integration of the horizontal divergence starting at the bottom, taking into account the change of the thickness of the levels:

$$\begin{cases} w_{k_b} = 0 \\ w_k = w_{k-1} + e_{3t}|_k \chi|_k \end{cases} \quad (2.17)$$

The so computed vertical velocity field differs from the NEMO output mainly at some coastal areas, where the difference reaches the maximum value of 10^9 m/s, as shown in

2 – Data and methods

Fig. 2.3 for the surface level. This discrepancy is present up to ~ 13.5 m deep and then vanishes.

This is due to the fact that NEMO takes into account a non-linear free surface while we have considered a linear free surface, thus we did not add the term related to the variation of the free surface in Eq. 2.17.

The time variations of the free surface affect mainly the first surface layers, explaining why the difference of the two computed velocity field is confined up to ~ 13.5 m.

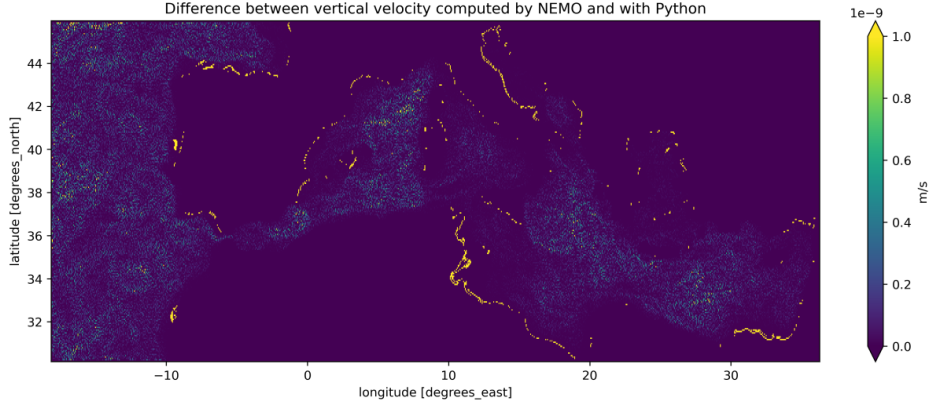


Figure 2.3: Difference at the surface between vertical velocity computed by NEMO and by algorithm exposed above.

2.2 Lagrangian analysis

Lagrangian analysis is a powerful way to evaluate pathways of tracers and water masses at both global and regional scale. Regarding large scale circulation, the Lagrangian approach is widely used to establish the main pathways and the variability of the Global Overturning Circulation, as in Speich et al. (2001) and Rousselet et al. (2021).

The method employs a large set of virtual particles of zero spatial extent whose trajectories are determined by the Eulerian velocity field. In the Lagrangian framework, such particles are considered macroscopically small material fluid volumes, treated as a mathematical continuum and each labelled by their initial coordinates $\mathbf{a} = \mathbf{X}(t = 0)$, where $\mathbf{X}(t)$ is the time evolution of the particle position vector. Thus, the trajectory for each particle is described by $\mathbf{X}(\mathbf{a}, t)$. The velocity of a fluid particle is the time derivative of the trajectory, holding \mathbf{a} fixed. The starting point of the Lagrangian analysis builds on the mathematical connection with the Eulerian description obtained by equating the particle velocity crossing a point in space, $\mathbf{X}(\mathbf{a}, t) = \mathbf{x}$, to the fluid velocity field at that

point:

$$\left(\frac{\partial \mathbf{X}(\mathbf{a}, t)}{\partial t}\right)_{\mathbf{a}} = \mathbf{v}(\mathbf{x}, t) \quad (2.18)$$

Trajectories can be evaluated by a variety of different algorithms starting from Eq. 2.18 and trajectory statistics define particle pathways and their associated time scales.

Lagrangian integration could both occur online and offline. In the first mentioned trajectories are calculated each time step that the Eulerian model is updated. On the other hand, the offline method makes use of stored Eulerian velocity fields and it allows to both backward and forward integrations.

In the first subsection, the Lagrangian tool used to compute trajectories and quantitative statistics of water masses is described as well as the detailed calculations on which it is based. The second subsection is devoted to the explanation of the experiments set up.

2.2.1 Lagrangian offline diagnostic tool

The freely available Ariane utility, developed and maintained at the Laboratoire de Physique des Océans (LPO, Brest, France), has been used to compute Lagrangian diagnostics of intermediate and deep water masses which compose the outflow water exiting at Gibraltar Strait.

This analysis is carried out by integrating multiple trajectories in a volume-conserving velocity field defined on a staggered C-type grid. The algorithm used is based on Blanke and Raynaud (1997) and it allows the exact calculations of three-dimensional streamlines within each box of the three-dimensional mesh. In a stationary field, such streamlines represent trajectories of particles advected by the given velocity field. Nevertheless, this technique can be extended to time dependent velocity fields, as MED REA daily mean product, by assuming the velocity is constant over successive period less or equal to the available sampling.

This so called *step-wise stationary* method has been improved by a *time-dependent* scheme based on de Vries and Döös (2001), which takes into account the field time dependence and it uses a linear interpolation in time and space. Döös et al. (2017) have recently demonstrated that the latter leads to a greater accuracy with only a small increase in computational time respect to the *step-wise stationary* method.

Anyway, Ariane still uses the *step-wise stationary* method and the detailed calculations are provided below.

Trajectories computation

Using the same tensorial formalism of the NEMO OPA model, the divergence of the three dimensional velocity field $U = (U, V, W)$ becomes:

$$\mathbf{V} = \frac{1}{e_1 e_2 e_3} [\partial_i F + \partial_j G + \partial_k H] \quad (2.19)$$

where e_1 , e_2 and e_3 are scale factors at each velocity grid point; $e_1 e_2 e_3$ is the volume of the grid cell defined at the center; ∂ is the finite difference along the respective dimension (i, j, k); $F = e_2 e_3 U$, $G = e_1 e_3 V$ and $H = e_2 e_1 W$ are respectively the zonal, meridional and vertical transport.

Thus, with a non divergence field the Eq. 2.19 becomes:

$$\partial_i F + \partial_j G + \partial_k H = 0 \quad (2.20)$$

Streamlines computation is enabled by assuming a linear variation of velocity components along each corresponding direction. Indeed, it is possible to write analytical trajectory equations along the three axes across the grid cell.

Considering the cell extending from $i = 0$ to $i = 1$, the expression for the zonal transport is:

$$F(r) = F_0 + r \Delta F \quad (2.21)$$

where $r \in [0, 1]$, $F_0 = F(0)$ and $\Delta F = F(1) - F(0)$ is the transport difference between grid cell edges.

The equation which links the position with the velocity $U = dx/dt$ can be written in terms of the new variables $s = t(e_1 e_2 e_3)^{-1}$ and $x = e_1 r$, leading to:

$$\frac{dr}{ds} = F \quad (2.22)$$

Substituting Eq. 2.21 in Eq. 2.22 and with the initial condition $r = 0$ for $s = 0$, the time dependent solution for r can be obtain:

$$r = \frac{F_0}{\Delta F} [e^{\Delta F s} - 1] \quad (2.23)$$

If $\Delta F = 0$, only the limit for Eq.2.23 for $\Delta F \rightarrow 0$ has to be considered:

$$r = F_0 s \quad (2.24)$$

Similar relationships are obtained for each direction.

Since this relationship is valid within an individual grid cell, it is necessary to determine also the time when a particle switches to the next cell. In order to accomplish this, the crossing time in each direction is evaluated independently by imposing as a possible final position each of the six sides of the gridcell.

The solution for the pseudo time s is obtained by rewriting Eq. 2.22:

$$ds = \frac{dr}{F} \quad (2.25)$$

Using Eq. 2.21, the last equation becomes:

$$ds = \frac{dF}{F\Delta F} \quad (2.26)$$

Thus, a crossing time in the zonal direction can be obtained only if $F(1)$ and $F(0)$ have the same sign, i.e. $F \neq 0$ within the grid cell. The non-divergence of the flow ensures that the crossing time is defined in at least one direction.

Assuming this is the case for zonal direction, the solution for Eq. 2.26 is:

$$s = \frac{1}{\Delta F} \ln \left(\frac{F}{F_0} \right) \quad (2.27)$$

and the crossing time corresponds to the moment when the transport reaches the exit face value $F(1)$:

$$\Delta s = \frac{1}{\Delta F} \ln \left(\frac{F_0 + \Delta F}{F_0} \right) \quad (2.28)$$

If $\Delta F = 0$, its limit for $\Delta F \rightarrow 0$ leads to:

$$\Delta s = \frac{1}{F_0} \quad (2.29)$$

The travel time is chosen to be the shortest one between all three computed. Hence, if the particle first reaches the zonal extremity of the cell, its meridional and vertical positions are deduced from the Eq. 2.23 written for the meridional and vertical directions by assuming $s = \Delta s$.

The algorithm used to compute streamlines is fast and accurate, because it calculates positions on the edge of individual grid cells, and it respects fully the local three-dimensional non-divergence of the flow.

Analytic computation of trajectories makes this method flexible too, allowing also backward integrations which are mostly used to track the origin of a given current, insofar calculations do not involve diffusive phenomena (Blanke and Raynaud, 1997).

Quantitative diagnostics

Although Ariane is designed to be run also in the so-called qualitative mode, the most meaningful diagnostics belong to the quantitative one. In the first mentioned, trajectories of particles seeded at a initial selected section are computed in an open domain. Few particles can be initialized because of the high computational cost and their initial coordinates are defined by the user.

Following the technique proposed by Döös (1995), quantitative results are obtained by increasing considerably the number of particles. In fact, by following a water particle, it is,

of course, not possible to say anything about the mass or volume transport. Nevertheless, if several water particles are let in close enough to each other, they should be able to indicate tendencies for different possible water routes (Döös, 1995).

Constant number of particles by grid cell and spatially homogeneous distributions on initial sections are not satisfactory because they may use too few particles to describe regions of weak currents and viceversa.

The best positioning of the particles (over initial sections) is the one that gives the highest accuracy in the computation of the transports associated with the circulation, for a reasonable number of initial positions (Blanke and Raynaud, 1997).

Thus, the approach followed by Ariane is the one proposed by Blanke and Raynaud (1997), who offered a simple formulation where the area of each individual grid cell (with a given transport T_i) is divided into N_i^2 subregions with N_i satisfying:

$$\frac{T_i}{N_i^2} \leq T_0 \quad (2.30)$$

where T_0 is a prescribed maximum transport for any given particle. The total number of particles is the sum of the N_i , and a homogeneous distribution is adopted within each grid cell.

Therefore, in the quantitative mode each particle is tacked with a partial volume transport, whose maximum T_0 is chosen by the user, so that the cumulative transport of all particles released at each time step reflects the total transport crossing the initial section.

Due to water incompressibility, one given particle with an infinitesimal section is to conserve its infinitesimal mass along its trajectory. Thus, the transport of a given water mass can be calculated from its own particles and their associated infinitesimal transport. By defining a closed sub-domain, it is possible to evaluate transport exchanged between the initial section and final interception sections.

Lagrangian transport streamfunctions

To evaluate the major pathways of water masses, the computation of Lagrangian transport streamfunctions has been carried out. This technique was used for the first time by Blanke et al. (1999) and it consists in the sum algebraically of particle associated transport T_i on each junction of two cells of the model, on the velocity grid points of the staggered C-grid. Thus, it has been obtained a three-dimensional transport field that corresponds to the flow of the water mass in study, within the domain of integration of the trajectories.

As one particle entering one model grid cell through one of its six faces has to leave it (by another face), the transport field satisfies the local non-nondivergece expressed by Eq. 2.20.

Then, the transport field is integrated along a specific directions, leading to a two-dimensional and non-divergence field, which can be studied by means of streamfunction.

For a vertically integrated transport field, the streamfunction ψ_h is defined by:

$$\begin{aligned}\frac{\partial\psi_h}{\partial i} &= \sum_k G \\ \frac{\partial\psi_h}{\partial j} &= -\sum_k F\end{aligned}\tag{2.31}$$

while, for a zonally integrated transport field, the streamfunction ψ_{yz} is obtained by:

$$\begin{aligned}\frac{\partial\psi_{yz}}{\partial j} &= \sum_i H \\ \frac{\partial\psi_{yz}}{\partial k} &= -\sum_i G\end{aligned}\tag{2.32}$$

and contours of ψ_h or ψ_{yz} provide an adequate view of the movement in projection onto the selected plane.

In this thesis, the computation of only the horizontal streamfunction has been carried out to reconstruct particle pathways of deep and intermediate water masses.

Negative and positive values represent cyclonic and anticyclonic circulation patterns, respectively. A bundling of streamlines highlights the most prominent pathways, and closed streamlines indicate recirculation patterns (Rühs et al., 2019).

2.2.2 Experiments configuration

Three main experiments with Ariane have been carried out and they are reported in Tab. 2.4. The MED REA dataset covers only 13 years but Ariane allows to integrate trajectories longer than the available time serie by looping on it. However, looping may introduce unphysical jumps in the velocity and tracer fields and, consequently, also in the volume transport pathways and along-track tracer changes (Rühs et al., 2019). These errors in pathways could be reduced by introducing a sufficiently high number of virtual fluid particles and the model drift in the velocity field is not too large, thus quantitative diagnostics can be considerate accurate.

Since transit times of water masses are in the order of decades, quantitative experiments have been carried out by looping six times on the archived dataset, thus integration of trajectories lasts 78 years. The errors introduced by looping should be negligible, since quantitative experiments usually deal with a large number of parcels.

The first two experiments have been run in qualitative mode to roughly evaluate particle pathways at different depths. In fact, this experiment setting does not allow

2 – Data and methods

Experiment name	QUAL-EXP1	QUAL-EXP2	QUAN-EXP1
Type of experiment	qualitative	qualitative	quantitative
# particles	3	~1000	5681201
Time of release	31/12/2012	31/12/2012	every day from 31/12/2012 to 22/06/2005
Simulation length (years)	13 (2000-2012)	13 (2000-2012)	78 (13 · 6 cycles)
Initial section	Gibraltar Strait lat=35.96° lon=-5.5°	Gibraltar Strait lat=[35.75°, 36, 19°] lon=-5.25°	Gibraltar Strait lat and lon reported in Tab. 2.5
Selected position at initial section	55 m, 300 m, 550 m	proportional to grid face transport	proportional to grid face transport

Table 2.4: Table of experiments.

to associate transport to seeded particles, but only to compute trajectories over all the domain, without defining interception sections. Note that longitude and subsequently latitude coordinates differ from QUAL-EXP1 to QUAL-EXP2 and QUAN-EXP1 because initially the reference longitude of Gibraltar Strait section had been chosen in the middle of it. Here, the flux instabilities and nonlinear dynamics give rise to strong mixing processes resulting in a more difficult tracking of water masses outflowing. On this basis, the section has been displaced zonally further towards open sea, exactly at -5.5° .

Because of the high computational time of the qualitative mode, in QUAL-EXP2 Ariane has been forced to run in parallel in order to manage the ~ 1000 particle trajectories.

The most significant experiment has been run in quantitative mode, hereafter addressed as QUAN-EXP1, by seeding virtual fluid parcels every day from 2005 to 2012 at the Strait of Gibraltar whose exact locations are reported in Tab. 2.5 and shown in Fig. 2.4 with a total of $O(10^6)$ particles.

The seeding period should be chosen carefully and it should cover at least one year of particle release in order to take into account seasonal variability. Additional experiments with different seeding periods are required to evaluate interannual variability of Gibraltar outflow.

Subsequently, they are traced backward in time until they reach one of the interception sections to track the origin of the outflowing water masses: the Sicily Strait section identifies the LIW, while the Gulf of Lyon section correspond to WMDW. Since denser

Section	Longitude	Latitude
Gibraltar Strait	-5.25°	[35.69°, 36.31°]
Gulf of Lyon	[3.31°, 8.63°]	42.31°
Sicily Strait		
1 st segment	[11.13°, 12.5°]	36.94°
2 nd segment	12.5°	[36.94°, 37.63°]
Northern Tyrrhenian Sea	[9.5°, 11.56°]	42.31°

Table 2.5: Exact geographic location of control sections set in quantitative analysis.

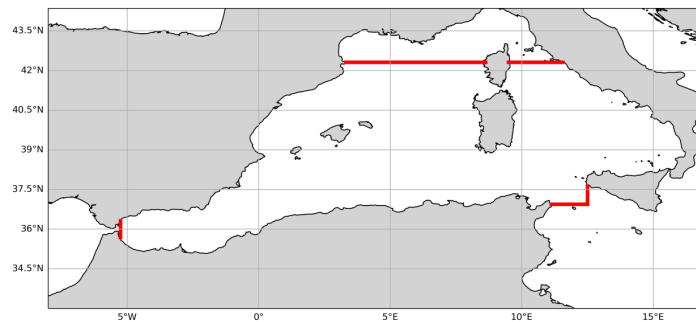


Figure 2.4: Control sections set in quantitative analysis. Exact geographic coordinates are reported in Tab. 2.5.

water formation occurs in the Northern regions of the WMED where buoyancy losses are more efficient, the Northern Tyrrhenian Sea section is designed to encompass any minor routes of denser water formed within the Tyrrhenian or north of it.

Each parcel has been tacked with maximum transport value of 0.001 Sv in order to well represent the current transport at each time step in each grid cell. Once particle has intercepted one of the control section it is no longer considered, while if it is not intercepted within the time allowed will be considered as lost.

Then, the major pathways between section pairs are highlighted by means of vertically integrated horizontal streamfunction, while binned transport-weighted particle frequencies are used to compute diagram for initial and final sections. Particle frequencies are inferred by dividing the cumulative transport of particles occupying a certain bin by the cumulative transport of the whole set of particles initially seeded at Gibraltar (excluding those which remained within the domain, those which evaporate and exit from Gibraltar Strait).

Eventually, transport-weighted transit times quantify faster routes and allows to deduce timescales of water mass anomalies propagation. All the results of Lagrangian quantitative experiments are presented in the common sense, i.e. forward in time.

Chapter 3

The deep water routes

In this chapter the numerical experiment results regarding the deep water mass routes are presented. A first general insight of the dynamics of deep water masses is given by the qualitative experiment which will describe the backward trajectories starting from 550 m depth at Gibraltar for a period of 13 years.

A second section is devoted to the quantitative analysis, allowing to highlight the main routes of deep water masses by the computation of the transport streamfunction, as well as the statistics of the transit times and the T-S diagrams associated with the parcel trajectories. Here "deep water routes" means that we select the intercepting sections of the Tyrrhenian Sea and the Gulf of Lyon where it is known that deep water masses form (see Chapter 1). The quantitative analysis will show then the transports for parcels that are coming from these two sections and then outflow at Gibraltar.

3.1 Qualitative analysis of the parcel trajectories

The qualitative experiments are not capable to completely represent the water mass paths since a very large number of parcels are required to sample the routes with larger probability. Nevertheless, this type of analysis supplies a first general picture of the water mass movement from which the main features of dynamic processes can be speculated.

In QUAL-EXP1, three parcels have been initialized at three different depths to represent the main water masses composing the flow outflowing at Gibraltar. In this experiment, the parcel initially located at 550 m deep is considered to correspond to WMDW that it has been tracked backward in time for 13 years starting from Gibraltar.

To highlight the dynamical processes that the particle undergoes, the values of depth, salinity and temperature at each trajectory position are depicted in Fig. 3.1, Fig. 3.2 and Fig. 3.3 for different time intervals, backward in time: 1-2 years, 3-4 years, 5-8 years and 9-13 years.

3 – The deep water routes

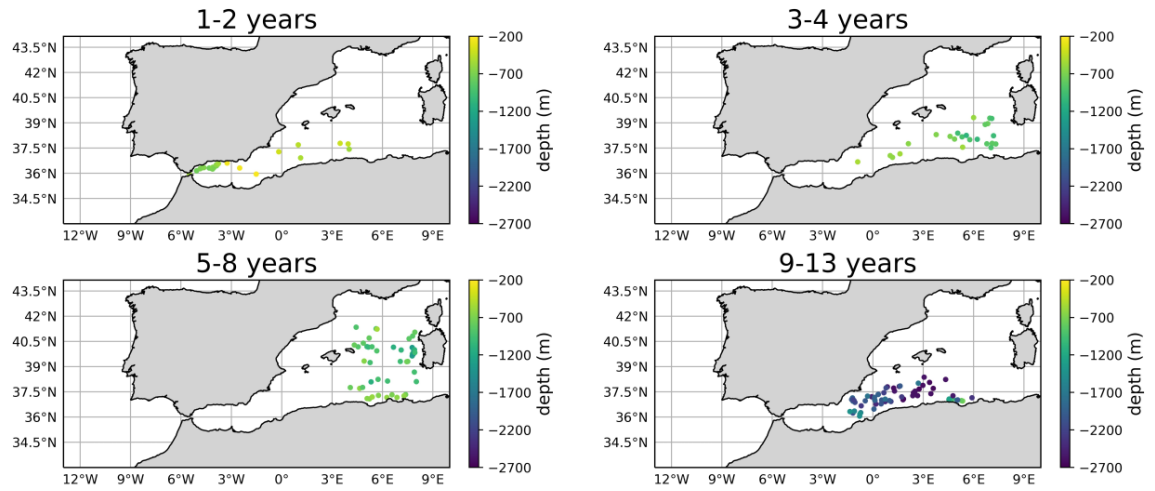


Figure 3.1: Monthly positions calculated over the reanalysis time period (2000-2012) for different backward in time intervals: 1-2 years, 3-4 years, 5-8 years and 9-13 years. Positions refer to the particle seeded on 31/12/2012 at the Gibraltar Strait at 550 m and tracked backward in time until 01/01/2000. The color indicates the computed depth for the particle at each position.

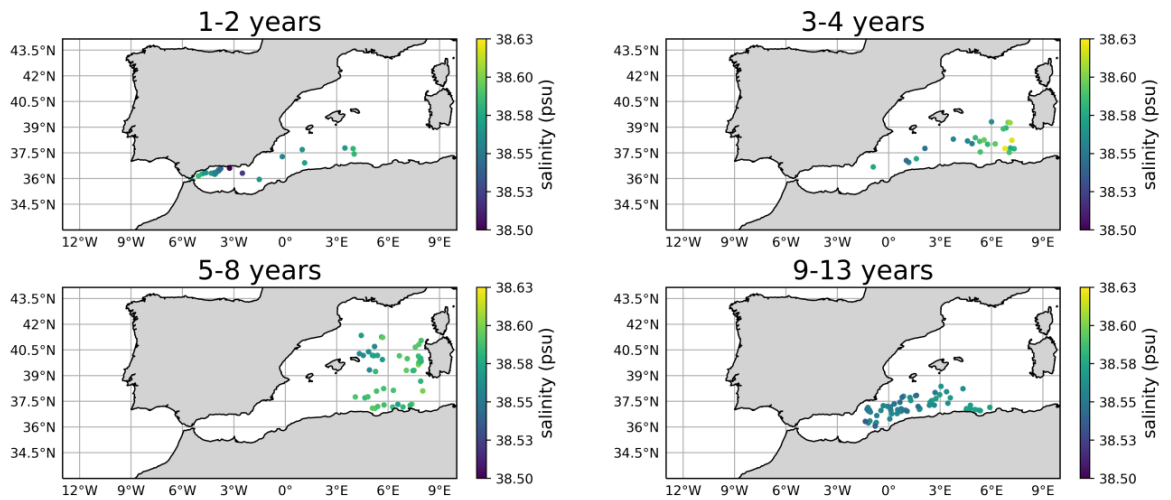


Figure 3.2: Monthly positions calculated over the reanalysis time period (2000-2012) for different backward in time intervals: 1-2 years, 3-4 years, 5-8 years and 9-13 years. Positions refer to the particle seeded on 31/12/2012 at the Gibraltar Strait at 550 m and tracked backward in time until 01/01/2000. The color indicates the computed salinity for the particle at each position.

3.1 – Qualitative analysis of the parcel trajectories

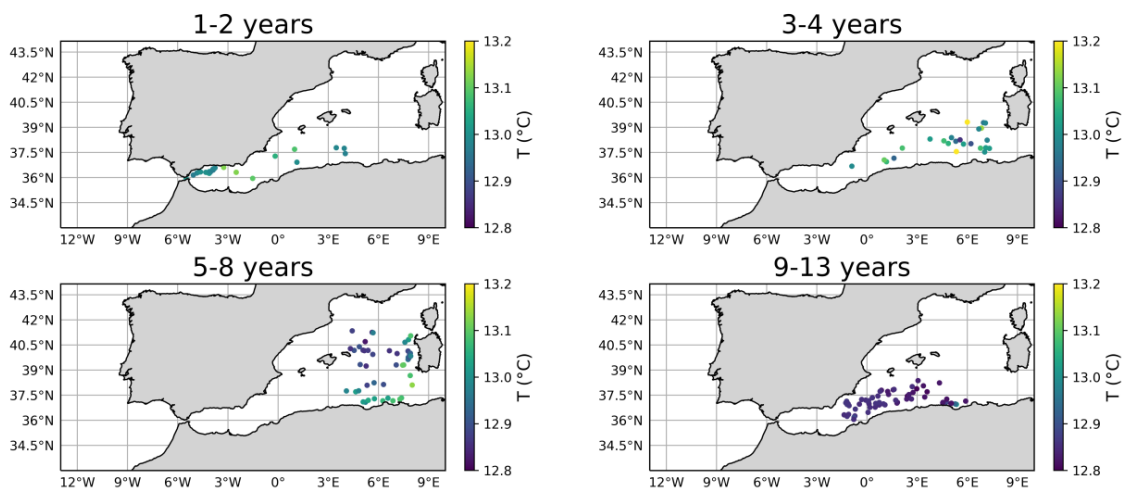


Figure 3.3: Monthly positions calculated over the reanalysis time period (2000-2012) for different backward in time intervals: 1-2 years, 3-4 years, 5-8 years and 9-13 years. Positions refer to the particle seeded on 31/12/2012 at the Gibraltar Strait at 550 m and tracked backward in time until 01/01/2000. The color indicates the computed temperature for the particle at each position.

During these 13 years, the trajectories are confined to the Algerian basin, mainly due to the strong re-circulation patterns which trap the particle for a long period in this region. None of them reach the Gulf of Lyon or the Tyrrhenian Sea. This initial analysis shows the large impact of large scale gyres in the southern WMED.

In the Alboran Sea the particle path is along the Iberian coast; after the Almeria-Oran front (see Chapter 1) the particles leave in the open ocean part of the Algerian basin circulation system (Chapter 1 and Tab. 1.1). In the first 8 years, it tries to move northward (in the backward of time nomenclature) along the Sardinia slope, turning westwards toward the Balearic Islands at approximately 40.5 °N.

Starting from 550 m, the particle reaches the depth of 1400 m in its final position backward in time, approaching also 2700 m during its journey, thus confirming the deep origin of the parcel.

Looking at Fig. 3.1, the particle is first lifted before the Almeria-Oran front, between 1 °W to 6 °E, and then subsides in the Algerian basin where it reaches a stable depth of 700 m for many years (2-8 years backward in time). Between 8-13 years the parcel arrives at its maximum depth of 2700 m in the western part of the Algerian current system.

In the Algeria current system (Tab. 1.1) anticyclonic/cyclonic eddies are formed and are almost stationary for several months up to years. These mesoscale structures are called *Algerian Eddies* (AE) and they play a crucial role in the surface circulation.

Both cyclonic and anticyclonic eddies move eastward toward Sardinia channel, where the topography forces these mesoscale structures to turn northward along the Sardinia slope and detach from it around 40° N moving westward and becoming large open sea eddies, thus describing an overall cyclonic pattern.

Sometimes AEs can extend vertically up to the bottom, thus they are probably influencing the intermediate and deep layer circulation. The deep circulation in the intermediate and deep layers of the Algerian current system, is known to be mainly cyclonic with two main gyres, the *Western Algerian Gyre* and the *Eastern Algerian Gyre* (Testor et al., 2005). Both of them are considered to be permanent features of the Southern WMED circulation, with one centered at 37.5° N and 2.5° E and the other located at 38.5° N and 6° E. These structures show an elliptical shape extending approximately 300 km along the west-east direction.

Testor et al. (2005) argue that these permanent features of intermediate and deep circulation are forced by the boundary currents flowing along Algerian and Sardinia slopes, through lateral fluxes by mesoscale features, thus suggesting surface and deeper circulation coupling. The long persistency of the particle in the Algerian basin indicates a re-circulation pattern due to Algerian Gyres which force the particle to oscillate in the east-west direction before exiting the Gibraltar Strait.

The particle starts with salinity value of 38.57 psu and temperature value of 13.0° C (Fig. 3.2 and Fig. 3.3), reflecting appropriately the outflow at Gibraltar Strait. While the salinity experiences an increase of 0.07 psu, the temperature reaches the value of 12.8° C, which corresponds to the temperature of WMDW found in the bottom layer of the WMED. The simultaneous increase both in temperature and salinity suggests an upwelling along isopycnal because of compensation effects in the density equation.

Low values of temperature are found also between Sardinia and the Balearic Islands, where the particle depth is about 1200 m. Since the particle does not experience any significant vertical displacement in this region, the temperature decrease probably indicates mixing with surrounding colder water masses (WIW).

3.2 The deep routes transports

Here we use the results of the QUAN-EXP1 experiment that integrated the particle trajectories for 78 years (see Tab. 2.4) from the initial release at the Gibraltar Strait.

The mean total transport over the period 2005-2012 of the outflow at Gibraltar Strait is 1.1319 Sv, part of which (0.1416 Sv) is identified as meanders. In this lagrangian framework, meanders refer to particle trajectories which enter and leave the domain through the same section, i.e. the section of Gibraltar Strait. Thus, these particles are considered to belong to upper layer Atlantic Water inflow and they are excluded here. In the 78 years integration time, some particles leave the domain through the surface

while others do not reach the interception sections (the Gulf of Lyon and Tyrrhenian Sea sections); transports attributed to those trajectories are respectively of 0.0001 Sv and 0.0019 Sv. Subtracting these transport contributions from the mean total value yields to the correct 2005-2012 mean transport estimate of 0.9883 Sv outflowing the Gibraltar Strait.

Part of this outflow originates from the Gulf of Lyon, in particular 0.8462 Sv (85.6 %) while the remaining 0.0074 Sv (0.8 %) originates in the Northern Tyrrhenian Sea. The remaining transport (13.6 %) is associated to LIW coming from the EMED and discussed in the Chapter 4.

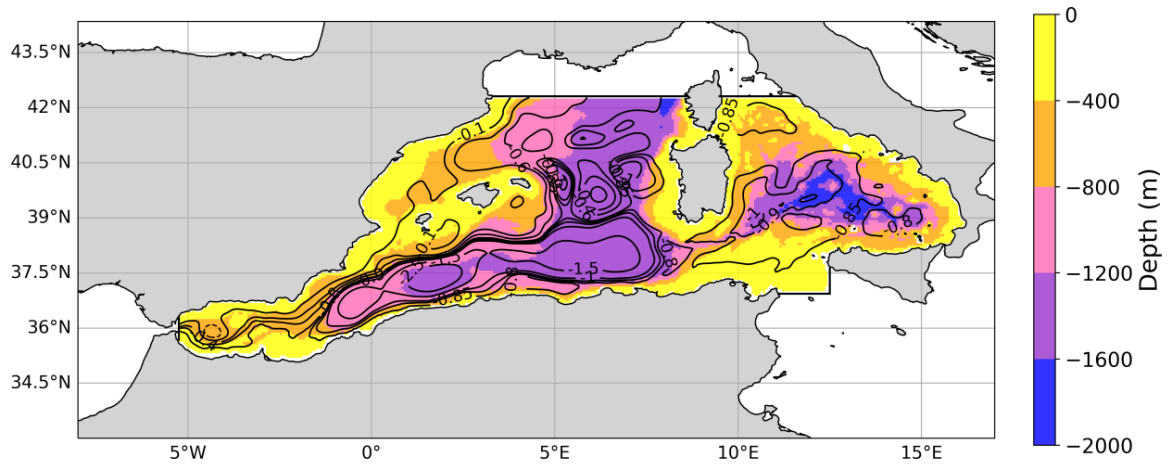
Those values confirm that WMDW is responsible for the majority of the outflowing transport, while a new route that directly link Tyrrhenian Sea to Gibraltar Strait has been detected for the first time. It is probably due to dense water masses formed during strong winter convection events in the Northern Tyrrhenian Sea.

In Fig. 3.4a the well-known routes of WMDW from Gulf of Lyon section are visible: one is the route across the Ibiza Channel and directly going to Gibraltar. The others instead turn eastward around the Balearic islands. Between Balearic Islands and Sardinia, cyclonic and anticyclonic re-circulations trap the particles and give rise to large deep water mass transports at depth greater than 800 m. The anticyclonic transport streamfunction could be interpreted as the eddy-induced mean circulation which is responsible for the spreading of the WMDW from the source region into the interior of the WMED.

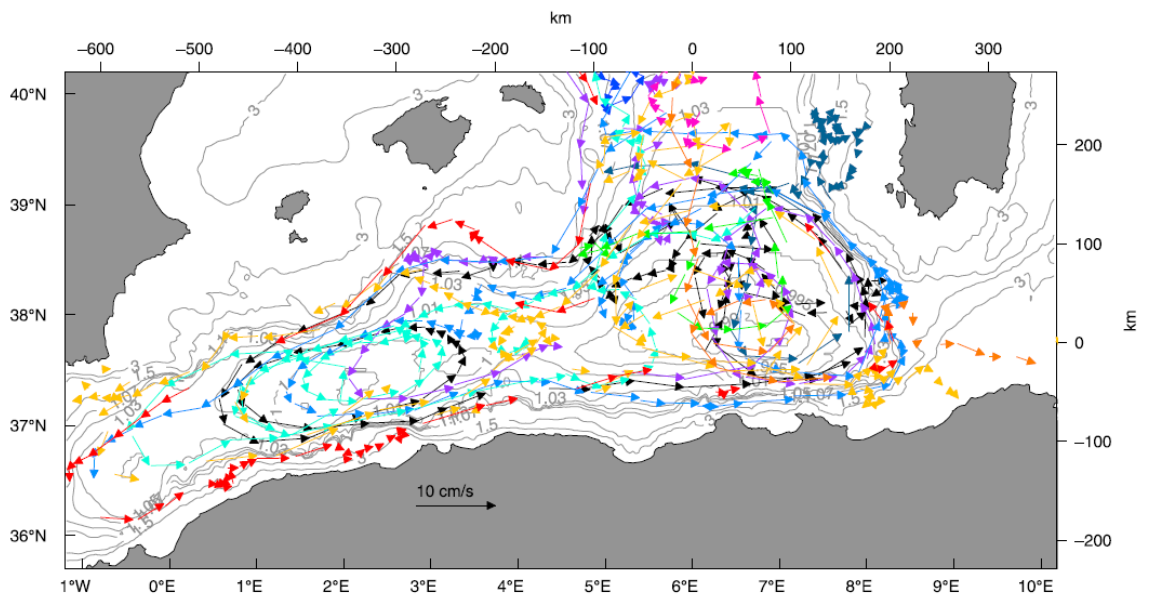
The most prominent feature of WMDW pathways is the strong deep re-circulation between 1200 and 1600 m in the Algerian basin current system, due to Western (2.5 Sv) and Eastern Algerian Gyres (1.5 Sv). Another cyclonic re-circulation centered at 0.5 °W is visible west of Western Algerian Gyre. This deep water mass transport is confined in the layer between 800 m and 1200 m. Testor et al. (2005) have mapped the Algerian Gyres by velocity measurements carried out by profiling and isobaric floats. Since observed velocities closely follow f/H isocontours, where f is the planetary vorticity and H the bathymetry, cyclonic circulation is developed by barotropic potential vorticity balance dominated by the planetary vorticity and topographic effects. In order to compare results of the quantitative analysis with those obtained by Testor et al. (2005), trajectories of profiling floats at 1200 and 2000 metres depth are reproduced in Fig. 3.4b.

According to literature, WMDW flows through the Sardinia channel following the same path of Atlantic water and then turn northwards to Tyrrhenian Sea. This pathway results in a cyclonic re-circulation (0.8 Sv) as depicted in Fig. 3.4a with returning branch along the Sardinia continental slope. Strong anticlockwise re-circulation patterns of 0.9 Sv are present within the closed streamline of 0.85 Sv, indicating an actual spiral motion downward up to 2000 m. In the Tyrrhenian Sea, WMDW coming from the Gulf of Lyon is usually mixed with deep water masses coming from the EMED, LIW and older WMDW present in deep water column portion.

3 – The deep water routes



(a) Lagrangian streamlines representing volume transport from the Gulf of Lyon section towards the Strait of Gibraltar section. Lagrangian streamfunction is inferred from QUAN-EXP1 for which particles were released at the Gibraltar Strait section every day from 31/12/2012 to 22/06/2005 and then traced backwards in time for a maximum of 78 years. Solid lines represent negative values, i.e. cyclonic circulation, while dashed lines indicate positive values, i.e. anticyclonic circulation. Closed streamlines represent re-circulation patterns. In the background, each grid cell is colored according to transport weighted averaged depth.



(b) Trajectories of profiling floats drifting at 1200 and 2000 m depth superimposed on f/H contours normalized by f_0 at $37^{\circ}45' N$ and $H_0 = 2800$ m. One color for each float. Arrows indicate the drift at depth during one cycle (8 days). Reproduced from Testor et al. (2005).

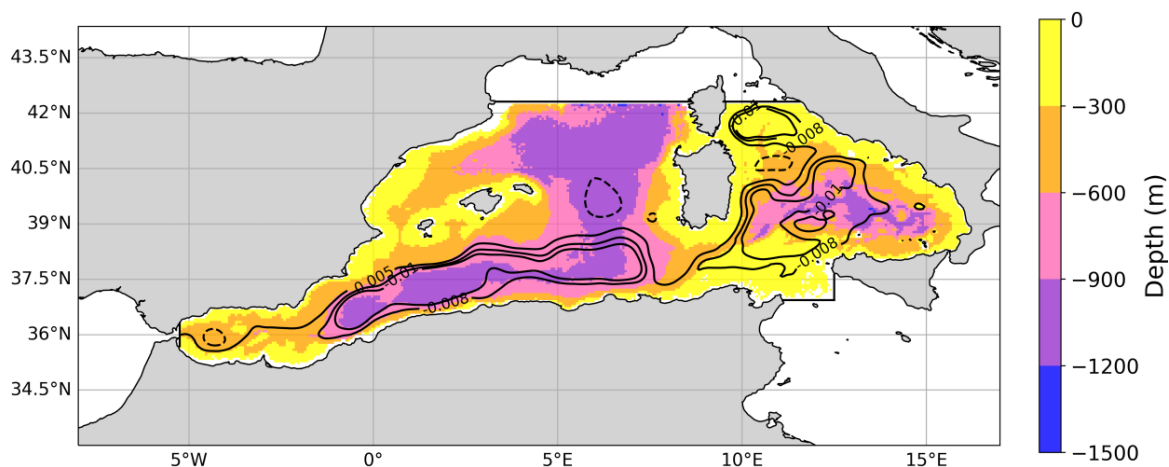


Figure 3.4: Lagrangian streamlines representing volume transport pathways from the Tyrrhenian Sea section towards the Strait of Gibraltar section. Lagrangian streamfunction is inferred from QUAN-EXP1 for which particles were released at the Gibraltar Strait section every day from 31/12/2012 to 22/06/2005 and then traced backwards in time for a maximum of 78 years. Solid lines represent negative values, i.e. cyclonic circulation, while dashed lines indicate positive values, i.e. anticyclonic circulation. Closed streamlines represent re-circulation patterns. In the background, each grid cell is colored according to transport weighted averaged depth.

The deep water mass transports originated in the Northern Tyrrhenian Sea is responsible for the 0.8 % of the mean transport outflow at the Gibraltar Strait and the most significant routes are illustrated in Fig. 3.8. Particles are captured by the Bonifacio dipole, formed by a cyclonic pole to the north (Bonifacio Gyre) and an anticyclonic pole to the south. While flowing through Sardinia channel, part of the volumetric flow is trapped into a cyclonic deep re-circulation. As in the previous case, actual particle trajectories are downwelled toward the abyssal plains.

Also the Tyrrhenian sea deep water routes (Fig. 3.4) encircle the Western and Eastern Algerian Gyres but at lower depths, between 600 m to 1200 m.

Regarding the anticyclonic motion, two re-circulation structures of 0.001 Sv are well-defined in both Tyrrhenian Sea and along the Balearic Islands-Sardinia section of the Algerian basin. The former occupies the intermediate layer, while the other involves the layer between 900 m and 1200 m.

Since the actual integration period accounts only for 13 different years, those gyres could be considered the an "average" eddy field. In fact, the region between Balearic Islands and Sardinia is well-known for the merging of Sardinia Eddies (Testor et al., 2005a), which are formed along the south-western coast of Sardinia at intermediate depths (~ 600

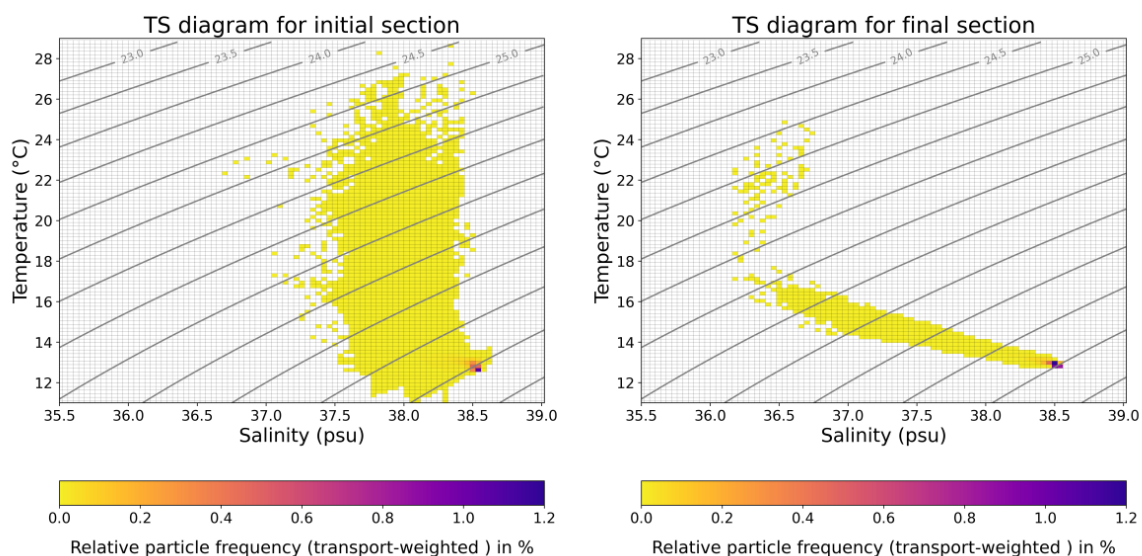


Figure 3.5: Potential temperature and salinity characteristics of water masses at the Gibraltar Strait section (left) and at the Gulf of Lyon section (right) inferred from QUAN-EXP1. Thermoaline properties are represented by means of relative transport-weighted particle frequency per 0.18 °C and 0.04 psu bin in percent. Grey contours represent isopycnals.

m). These eddies stem from instabilities between Western Algerian Gyre and LIW vein flowing northward along Sardinian continental slope and then move towards the open sea where they merge resulting in an averaged anticyclonic circulation.

Both northern water masses are affected by the Western Alboran Gyre and forced to re-circulate at similar depths, thus inducing mixing before exiting at Gibraltar Strait. The Eastern Alboran Gyre effect is not evident, only the Western one, indicating the leading role of the Western Alboran Gyre to mix water masses and determine typical temperature and salinity values to the exiting outflow.

3.2.1 T-S diagrams

The T-S diagrams associated with particles at source (Gulf of Lyon and Tyrrhenian) and exit sections (Gibraltar) are shown in Fig. 3.5 and Fig. 3.6.

Starting with the densest waters, the salinity is approx. 38.5 psu and the temperature approx. 13 °C at Gibraltar and both the Gulf of Lyon (Fig. 3.5) and Tyrrhenian (Fig. 3.6). However, the percentage of Gibraltar outflow transport due to the Gulf of Lyon waters is 1.2%, while only 0.002% from the Tyrrhenian Sea section.

It is interesting to see that at Gibraltar (right panels of Fig. 3.5 and Fig. 3.6) the

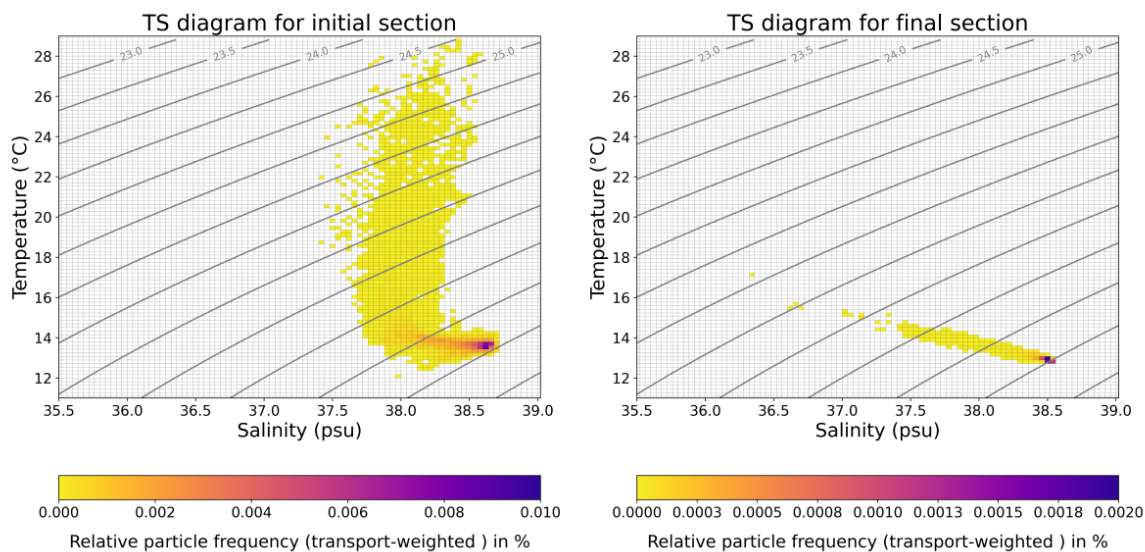


Figure 3.6: Potential temperature and salinity characteristics of water masses at the Gibraltar Strait section (left) and at the Tyrrhenian Sea section (right) inferred from QUAN-EXP1. Thermoaline properties are represented by means of relative transport-weighted particle frequency per $0.18\text{ }^{\circ}\text{C}$ and 0.04 psu bin in percent. Grey contours represent isopycnals.

Tyrrhenian dense water temperature and salinity is higher with respect to the Gulf of Lyon source. The T-S diagram associated to Gulf of Lyon section shows the core shifted to the salinity interval of $38.52\text{--}38.54\text{ psu}$ and temperature interval of $12.5\text{--}12.7\text{ }^{\circ}\text{C}$. Those values clearly identify WMDW. From Fig. 3.5, it is visible also significant transport contributions still associated to WMDW in a higher temperature range, possibly indicating WMDW warming. On the other hand, the deep water mass bulk originated from the Northern Tyrrhenian Sea covers the temperature interval from $13.3\text{ to }13.5\text{ }^{\circ}\text{C}$ and the salinity interval between $38.60\text{ and }38.64\text{ psu}$. If the water mass coming from the Tyrrhenian Sea had been a deep water mass, it should have lied in the isopycnal range $>29.0\text{ kg/m}^3$. Since its density is lower, it probably belongs to intermediate water masses.

Small transport contributions ($<0.1\%$) are associated to a broad range of temperatures and salinities clearly corresponding to intermediate and near surface waters. One common intermediate water mass in the WMED is WIW, that is due to winter cooling of MAW which occurs in several different regions, such as the Gulf of Lion, the Catalan basin and the Ligurian Sea. However, the salinity values which identify WIW should be the typical salinity values of MAW ($<38\text{ psu}$). An intermediate water mass formed in the Northern Tyrrhenian Sea (TIW) has been recently recognized by Napolitano et al. (2019) with characteristic temperature values between $13.2\text{--}14\text{ }^{\circ}\text{C}$, and salinity values in the range

38.00-38.40 psu. The Tyrrhenian Intermediate Water (TIW) is known to form in the Northern region of the Tyrrhenian Sea, whose dynamics is dominated by the Bonifacio dipole, and then reach the buoyancy depth below the MAW and above the LIW stream.

The source water mass reflects the typical temperature values of TIW, while the salinity range is higher than the TIW characteristic one. This can be ascribed to local mixing with the underlying LIW stream, which increase the salt content of TIW. In addition, this could also explain higher average depths reached by particles during their trajectories than the typical averaged depth of TIW (~ 600 m). Napolitano et al. (2019) deduced from profiling ARGO float measurements a robust TIW flow towards Liguro-Provençal basin through Corsica Strait. Maybe, a part of newly formed TIW go through mixing with LIW, which increases its salt content and re-circulates ciclonically in the Tyrrhenian Sea.

In the Algerian basin TIW transport paths (Fig. 3.4) are more similar to WMDW routes than the LIW routes that will be discussed in the next chapter. The strong cyclonic re-circulation undergone by TIW in the Tyrrhenian Sea could induce it to mix with deeper waters. As already pointed out, WMDW experiences violent mixing with LIW. This could be the same pattern followed by TIW, also explaining the greater depths reached by TIW in the sub basin.

3.2.2 Transit times

The distributions of transport-weighted transit times for WMDW routes and TIW routes are shown respectively in Fig. 3.7 and Fig. 3.8. The reanalysis dataset used allows to resolve the eddy field, thus inferred timescales account for the effect of sub-grid-scale physics, broadening transit time distributions.

The median transit time for the particles arriving from the Gulf of Lyon, i.e. WMDW masses, is ~ 5 years and the 90th percentile is ~ 18 years while for the Tyrrhenian particles, i.e. TIW masses, the median transit time is ~ 6 years and the 90th percentile ~ 22 years. However, the transport contribution of TIW to the mean transport outflow accounts for only the 0.8%. The fastest route is also the one that mostly contributes to the outflow volume at Gibraltar. This means that anomalies at the source section can fastly propagate and the interannual variability of the outflow mostly corresponds to the variability of the WMDW contribution.

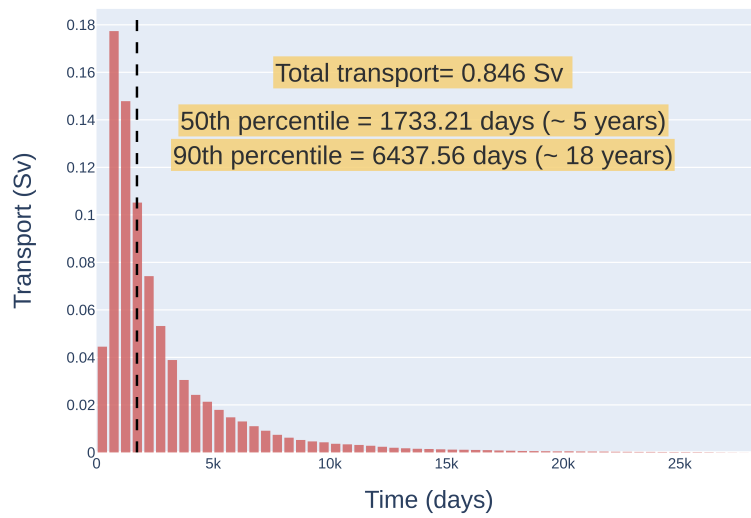


Figure 3.7: Transport-weighted transit time distribution between Gibraltar Strait section and Gulf of Lyon section inferred from QUAN-EXP1. Dashed line indicates the median time displayed on the side along with the 90th percentile.

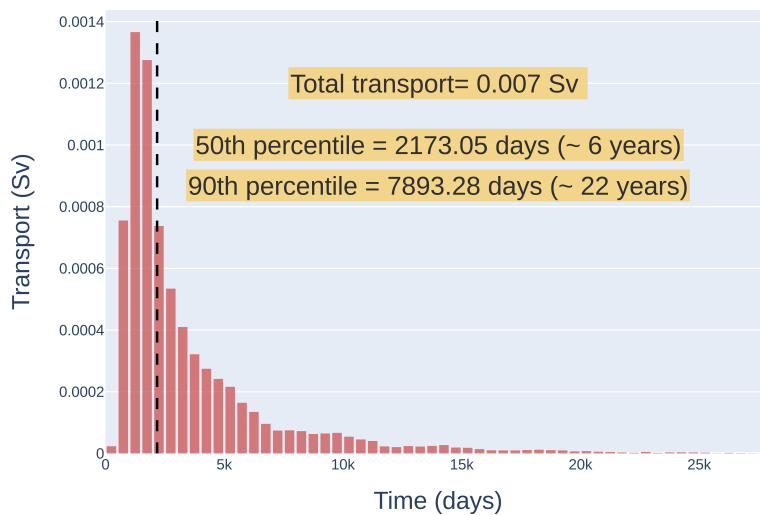


Figure 3.8: Transport-weighted transit time distribution between Gibraltar Strait section and Tyrrhenian Sea section inferred from QUAN-EXP1. Dashed line indicates the median time displayed on the side along with the 90th percentile.

Chapter 4

The intermediate water routes

In this chapter we describe the results of both qualitative and quantitative experiments for parcels inserted at Gibraltar at intermediate depths and for parcels intercepting the Sicily Strait section. This section receives EMED intermediate and deep waters waters that are a mixture of LIW and EMED deep waters. We describe here for the first time the part of LIW or EMED intermediate and deep waters going directly toward the Gibraltar Strait.

4.1 Qualitative analysis of the parcel trajectories

We consider here the parcel initially located at 300 m deep at the Strait of Gibraltar in the QUAL-EXP1 to study the intermediate water mass contribution at the Gibraltar Strait outflow.

Looking at the Fig. 4.1, the particle shows the typical trapping of the trajectory and its re-circulation in the cyclonic Algerian basin current system. As in the deep water mass qualitative discussion, within 5-8 years after the seeding at Gibraltar, the particle seems to experience an uplifting from deeper layers up to the intermediate layer typical of LIW (~ 500 m). Indeed, 13 years before arriving at Gibraltar, the particle occupies for some time the intermediate layer typical of LIW and later it sinks to ~ 2500 m.

During particle uplifting, before 8 years backward in time, salinity and temperature distributions depicted in Fig. 4.3 and Fig. 4.2 show an increase from 12.8 °C to 13.0 °C for temperature and from 38.57 psu to 38.59 psu for salinity. It might be that the particle density is not modified, due to the balancing effects of temperature and salt increase, and thus it is probably moving along isopycnals. The particle raising is likely due to upwelling from deep layers forced by eddies or topographic structures. This isopycnal motion should be further elucidated in the continuation of this work.

During the sinking motion, which occurs within 9-13 years before the outflow at

4 – The intermediate water routes

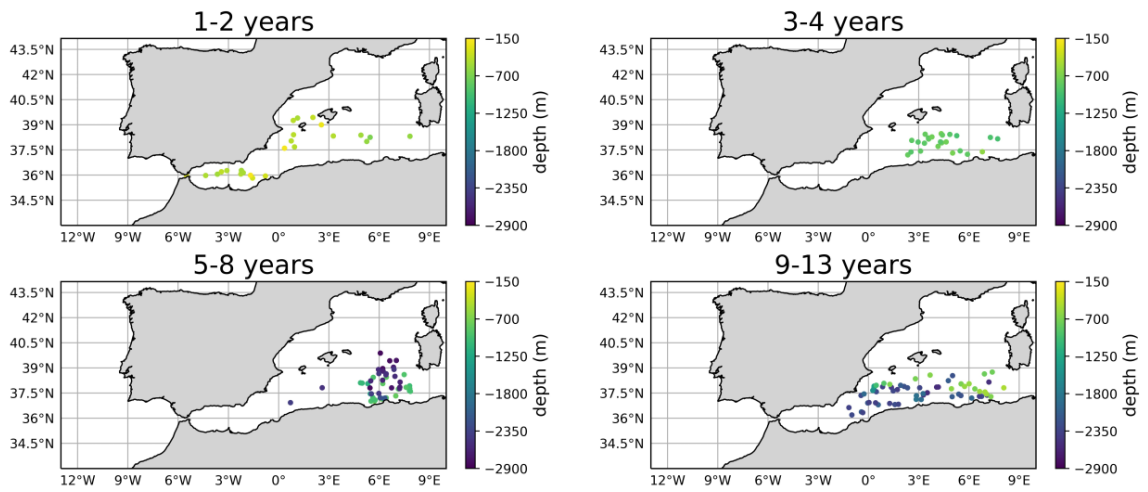


Figure 4.1: Monthly positions calculated over the reanalysis time period (2000-2012) for different backward in time intervals: 1-2 years, 3-4 years, 5-8 years and 9-13 years. Positions refer to the particle seeded on 31/12/2012 at the Gibraltar Strait at 300 m deep and tracked backward in time until 01/01/2000. The color indicates the computed depth for the particle at each position.

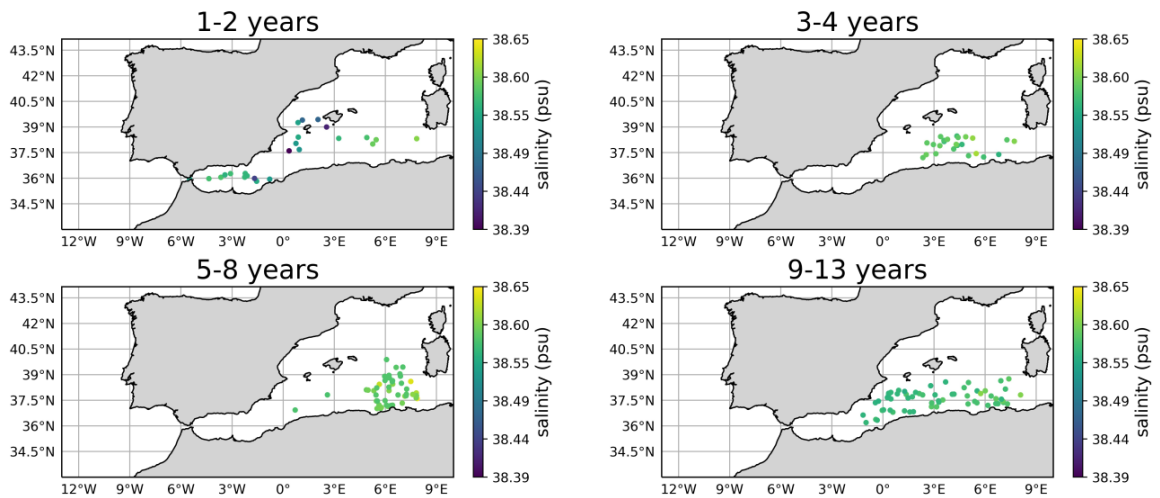


Figure 4.2: Monthly positions calculated over the reanalysis time period (2000-2012) for different backward in time intervals: 1-2 years, 3-4 years, 5-8 years and 9-13 years. Positions refer to the particle seeded on 31/12/2012 at the Gibraltar Strait at 300 m deep and tracked backward in time until 01/01/2000. The color indicates the computed salinity for the particle at each position.

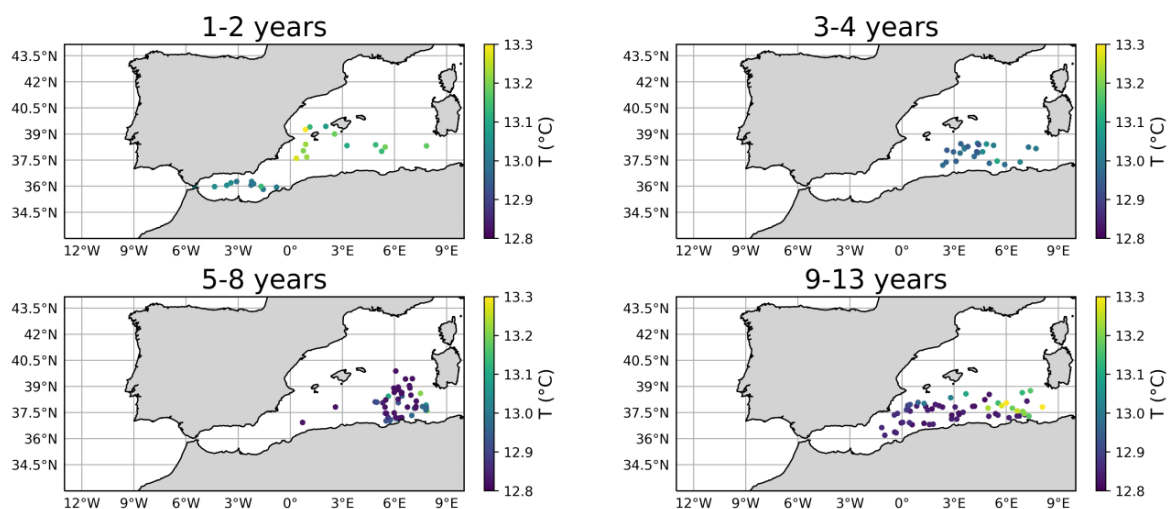


Figure 4.3: Monthly positions calculated over the reanalysis time period (2000-2012) for different backward in time intervals: 1-2 years, 3-4 years, 5-8 years and 9-13 years. Positions refer to the particle seeded on 31/12/2012 at the Gibraltar Strait at 300 m deep and tracked backward in time until 01/01/2000. The color indicates the computed temperature for the particle at each position.

Gibraltar, the particle switches from 13.2 °C to 12.8 °C, changing from typical temperature value of LIW to lower values specific of WMDW layer. Nevertheless, the salinity distribution appears homogeneous, indicating density changes during the sinking are probably due to mixing with surrounding water masses.

In summary, the particle chosen to represent intermediate waters is forced to recirculate within Algerian Gyres while undergoing several sinking and uplifting processes. The upwelling vertical motion seems to not modify the particle density while the sinking process involves mixing with other water masses.

4.2 The intermediate routes transports

The Sicily Strait receives a mixture of intermediate (LIW and CIW) and deep water masses (EMDW) formed in the EMED. However, only a part of this mixture, mostly LIW, contributes to the Gibraltar outflow. The main pathways of water masses coming from Sicily Strait are shown in Fig. 4.4. They account for 0.1347 Sv (13.6%) of the mean outflowing transport over the period 2005-2012.

After having exited the Sicily Strait, EMED water mass spreads northwards flowing along the Sicily northern coast. It circulates cyclonically in the Tyrrhenian Sea, exiting from the Sardinia channel. Looking at Fig. 4.4, the transport weighted average depth

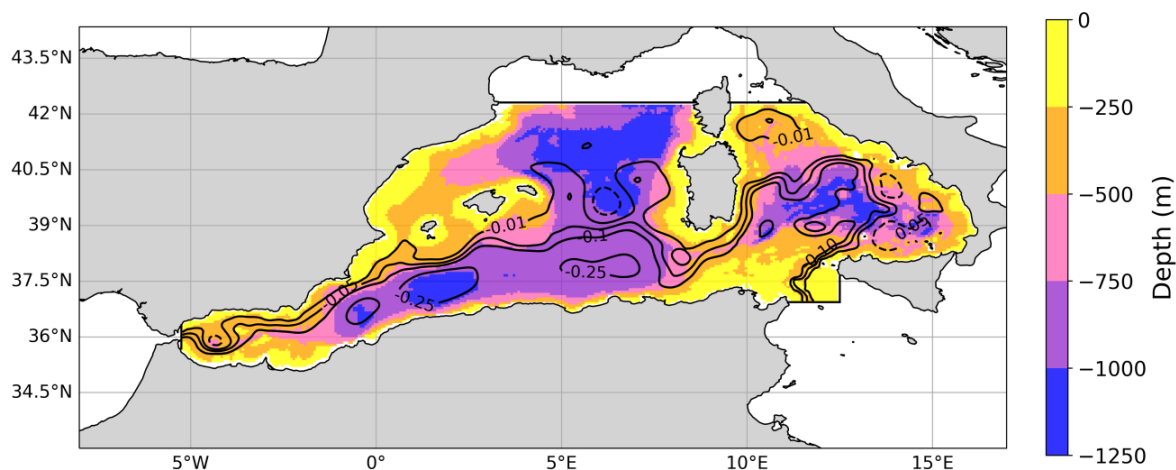


Figure 4.4: Lagrangian streamlines representing volume transport pathways from the Sicily Strait section towards the Strait of Gibraltar section. Lagrangian streamfunction is inferred from QUAN-EXP1 for which particles were released at the Gibraltar Strait section every day from 31/12/2012 to 22/06/2005 and then traced backwards in time for a maximum of 78 years. Solid lines represent negative values, i.e. cyclonic circulation, while dashed lines indicate positive values, i.e. anticyclonic circulation. Closed streamlines represent re-circulation patterns. In the background, each grid cell is colored according to transport weighted averaged depth.

of fluid parcels in the Tyrrhenian Sea (~ 1250 m) confirms the great depths reached by EMED water masses in the basin. Indeed, due to the strong density difference with the resident water in the Tyrrhenian, EMED deep water masses sink along the bottom slope after having entered the Tyrrhenian, while the typical layer of the intermediate ones expands vertically up to ~ 1000 m. Since the average depth does not exceed 1250 m, the EMED water mass mainly accounts for intermediate waters, i.e. LIW and CIW.

In the Tyrrhenian Sea, a fraction of EMED water mass is trapped in cyclonic mesoscale structures, while the south-eastern part of the basin is dominated by anticyclonic re-circulation. Another fraction is forced to re-circulate within the Bonifacio Gyre (0.01 Sv), which promotes the upwelling of intermediate waters to surface layer, indeed the transport weighted average depth of fluid parcels lies within the layer 250-500 m. Note that Bonifacio Gyre induces a minor re-circulation (0.01 Sv) than the southern anticyclonic subgyres (0.05 Sv).

The most significant pathway (0.1 Sv) exits the Sardinia channel mainly flowing along African coast, while 0.01 Sv remain close to the southern Sardinia coast. The signature of eddy field is represented by submesoscale cyclonic re-circulation which traps LIW and transports towards the Gulf of Lyon. The LIW transport mechanisms in the Algerian

basin towards the Gibraltar Strait have been widely discussed and authors agree to state that westward flow of LIW exiting the northern part of the Sardinia channel is mainly due to anticyclonic eddies which deviate the northward LIW vein at Sardinia channel. Our results suggest that the majority of EMED flow exits the southern part of Sardinia channel and then moves eastwards along the northern boundaries of the Algerian Gyres. Cyclonic re-circulations of 0.25 Sv are located in the interior of the gyre at greater depths (~ 1250 m), suggesting that patches of LIW have been trapped. Unlike water masses coming from the Northern WMED, LIW does not show a returning branch along the Algerian coast.

On the other hand, the minor route (0.01 Sv) flows along south-western Sardinia slope and it is more likely to develop instabilities, as the meanders extending north of the Algerian basin current system. Puillat et al. (2006) claimed that LIW transport through Algerian basin is promoted by anticyclonic Algerian Eddies which divert LIW westward instead of flowing northwards. The AE feature is not visible in Fig. 4.4, indicating that LIW has not been trapped by those anticyclonic structures. Nevertheless, an anticyclonic subgyre is well resolved at 6.5 °E and 39.5 °N. Here, the LIW re-circulation (0.05 Sv) extends vertically up to 1250 m. This clockwise re-circulation involves both LIW and TIW, while WMDW describes a cyclonic pattern in the deeper layer, between 1200 and 1600 m.

Once again the Western Alboran Gyre induces a LIW anticyclonic re-circulation, which is a common feature of the all analysed water masses composing the outflow.

4.2.1 T-S diagrams

The binned transport weighted T-S diagrams for the initial section, i.e. Sicily Strait, and for the final section, i.e. Gibraltar Strait, are shown in Fig. 4.5.

The main transport contributions (0.2%) of EMED water masses to the mean outflowing transport at Gibraltar Strait comes from fluid parcels in the salinity interval 38.80-38.88 psu and temperature interval 13.5-14.2 °C. Fluid parcels in the same salinity range but higher temperature (up to 14.5 °C) contribute to a less extent (<0.15%) to the mean outflowing transport. Thus, the main transport contribution comes from the LIW, while the CIW is difficult to recognise because it is slightly warmer and saltier than the LIW. However, the minor transport contributions related to higher temperature values may be due to the CIW which mixes with LIW before exiting the Sicily Strait. Hence, EMED water mass mainly account for LIW.

Fluid parcels coming from Sicily Strait do not cover the same T-S spectra of the previous water masses. Indeed, EMED contributions result saltier than TIW and WMDW, reaching the maximum of 39.00 psu, but also extending to lower values of salinity (the majority of the transport do not exceed the lower limit of 37.00 psu). Instead, the

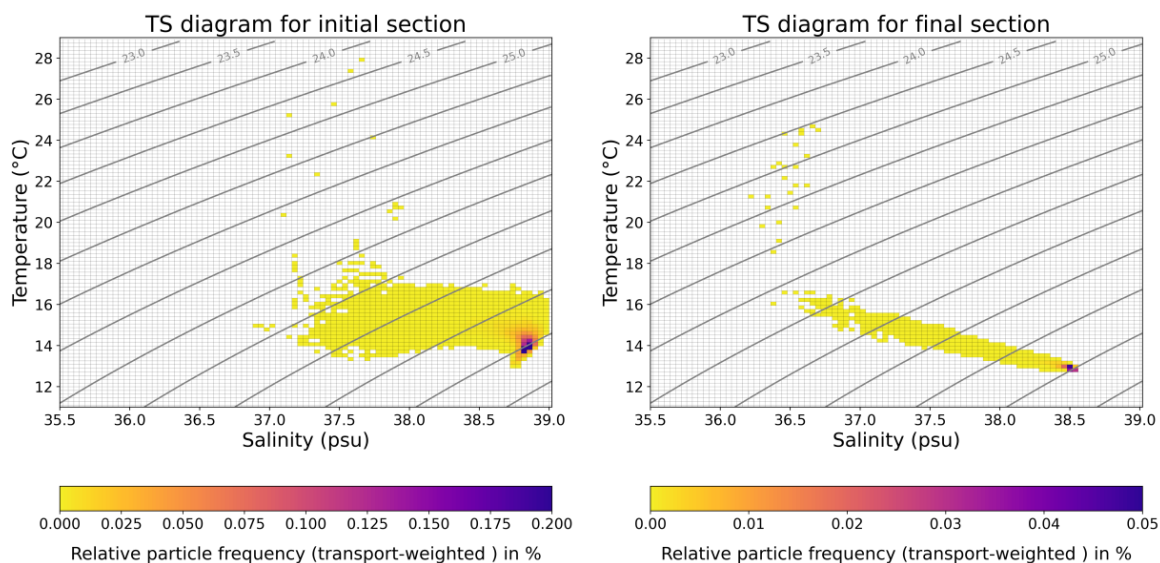


Figure 4.5: Potential temperature and salinity characteristics of water masses at the Gibraltar Strait section (left) and at the Tyrrhenian Sea section (right) inferred from QUAN-EXP1. Thermoaline properties are represented by means of relative transport-weighted particle frequency per 0.18 °C and 0.04 psu bin in percent. Grey contours represent isopycnals.

temperature spectrum covers a narrower range and significant transport contributions come from temperature lower than 17 °C. This could be related to the different origins of water masses, thus fluid parcels at Sicily Strait reflects the wide salinity range resulted by the mixing of salty water masses coming from the EMED and surface Atlantic Water.

LIW undergo significant thermohaline properties modifications during the transit through WMED, which decrease its salt content and its temperature. However, LIW does not experience any resulting density transformations, since the water mass bulk lies on the 29.0 kg/m^3 at both Sicily Strait and Gibraltar Strait.

4.2.2 Transit times

The inferred advective timescale from the simulated volume transport trajectories of LIW from Sicily Strait to Gibraltar Strait is reported in Fig. 4.6. The 50% of the LIW transport coming from Sicily Strait reaches the Gibraltar section within the first 8 years and also the 90th percentile (~ 28 years) is well captured by trajectories integration. Thus, the connecting pathways of LIW are longer than water masses formed in the Northern WMED. Generally, deep water masses move slower than intermediate and surface water masses. In addition, WMDW routes cover greater distance, re-circulating also in the Tyrrhenian Sea. Anyway, the LIW takes longer than WMDW to reach Gibraltar Strait.

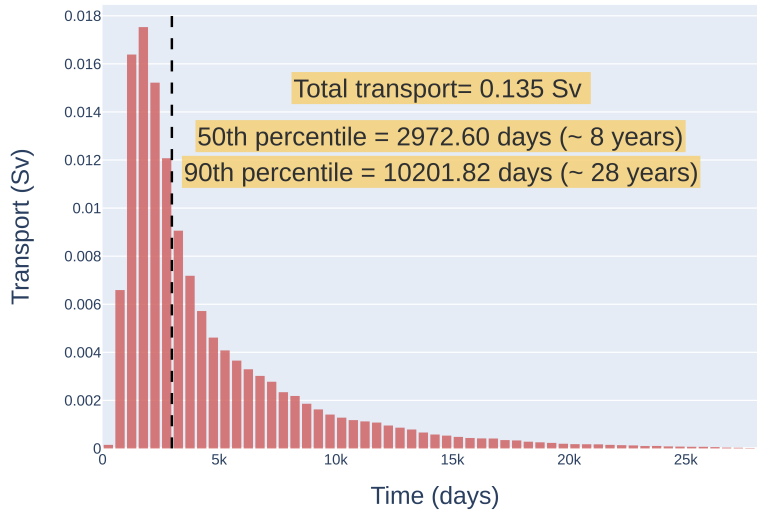


Figure 4.6: Transport-weighted transit time distribution between Gibraltar Strait section and Sicily Strait section inferred from QUAN-EXP1. Dashed line indicates the median time displayed on the side along with the 90th percentile.

This could be apparently related to the higher WMDW contribution compared to LIW to the mean outflow at Gibraltar Strait. Since the time integration starts on the 31st December 2012, the 2005-2012 mean outflow partially accounts for the high deep water formation rate documented in the Gulf of Lyon between 2004 and 2007 with a peak in the 2005. The large volume of newly formed WMDW may have made the spreading mechanisms dominated by mesoscale eddies more efficient.

Chapter 5

Conclusions and outlooks

In this thesis the eddy-resolving reanalysis dataset produced by the Copernicus Marine Environment Monitoring Service and spanning from 2000 to 2012 has been used to develop a lagrangian description of water masses routes composing the mean outflow at the Gibraltar Strait. The main aim is to understand the time scales and pathways of waters composing the Mediterranean outflow.

An overview of the circulation pattern of the outflow water masses in the Algerian basin current system is inferred from the qualitative experiment initialised with three particles at different depths. It shows the strong influence of Algerian Gyres and eddies which control the intermediate and deep circulation and force the particle to move in the east-west direction before exiting. During this re-circulation, deep and intermediate water masses experience uplifting and sinking processes during which diapycnal mixing occurs. This result confirms the presence of a counter-clockwise meridional overturning cell extending from 300 *m* to the bottom, located in the Southern WMED and described in Pinardi et al. (2019) by means of the residual transport streamfunction.

In the lagrangian framework, the quantitative analysis performed allows to infer significant statistics and main routes transports of water masses between source sections, the Northern Tyrrhenian Sea, the Gulf of Lyon and the Sicily Strait, and exit section, the Gibraltar Strait. The resulting main contributors to the Gibraltar outflow are LIW and WMDW, which are responsible for respectively the 13.6% and 85.6% of the mean outflow over the period 2005-2012. In addition, the TIW has been recognised in the outflow bulk, however its transport contribution over the indicated period is almost negligible (0.8%).

As already documented by Demirov and Pinardi (2007) and Send and Testor (2017), the WMDW spreading from the Gulf of Lyon to the Algerian basin is an eddy dominated process evidenced by several cyclonic mesoscale and submesoscale deep re-circulations. Before exiting the Gibraltar Strait, both WMDW and TIW are forced to re-circulate in the Tyrrhenian basin following general cyclonic patterns. Due to the strong density difference with the Tyrrhenian resident waters, mixing processes occur and promote the

sinking to greater depths of both water masses coming from the Sardinia channel. In the Algerian basin current system, TIW and WMDW are affected by the strong recirculation of Algerian Gyres, as already found out in the qualitative analysis.

For the first time, a description of LIW pathway towards the Gibraltar Strait is presented. After the Sicily Strait, the LIW turns northwards, spreading into the Tyrrhenian interior. As demonstrated for the WMED water masses, the LIW experiences a sinking process up to 1250 *m*. In the Algerian basin current system, the majority of LIW transport occur along the northern boundary of the Algerian Gyres, while a small fraction detaches from this boundary current to develop meanders northwards. Although LIW does not show a returning branch along the African coast, it is forced to re-circulate in the interior of the Algerian Gyres at great depths.

In contrast to deep water mass, the intermediate ones are trapped in a clockwise re-circulation between Balearic Islands and Sardinia. The resulting circulation could be the signature of the merging surface eddies, typically anticyclonic in this part of the WMED.

In the Tyrrhenian Sea, both EMED and WMED water masses are forced to re-circulate within the Bonifacio Gyre, which promotes upwelling processes. Another common feature of the water masses circulation is the presence of the Western Alboran Gyre. This anticyclonic re-circulation is a persistent component of the Alboran Sea and it plays a key role in ventilating WMDW before exiting the Gibraltar Strait.

This thesis has shown the importance of both reanalysis as the basic information to study ocean dynamics and the Lagrangian methods to understand water mass pathways that compose the climate circulation of the Mediterranean Sea.

Several issues remain to be discussed in the future. In this thesis only the mean outflow transport over the period 2005-2012 has been taken into account, while it would be interesting to examine the interannual variability of water mass transport. Secondly it would be important to extend the analysis to the EMED where different deep and intermediate water mass formation processes occur and influence the outflow at Gibraltar and then the global ocean circulation.

Acknowledgements

This thesis would not have been possible without the help of many people. First of all, I would like to thank my supervisor, Prof. Nadia Pinardi, who guided me through this experience and shared her knowledge with me. Many thanks also to Prof. Paola Cessi who provided me with valuable advice and teachings on lagrangian diagnostics.

I am grateful to Dr. Francesco Trotta for having dedicated much of his time to solving doubts and technical problems. I would also like to thank Dr. Louise Rousselet for her precious help with the Ariane software.

I am indebted to Dr. Federica Borile for having shared with me her master thesis work, thus helping me to develop my codes.

A special thought to Mirko for always being there and believing in me. Thank you for teaching me everything I know about programming and thank you for being the best friend anyone could wish for.

Immense gratitude to Luca for teaching me what love is, always being by my side even in the most difficult moments.

Thanks also to Sara for having solved all my linguistic doubts and for always being so supportive.

Thanks to my friends, Beniamino and Federico: with their laughter and long conversations they have managed to make this period the best of my life.

Last but not least, a heartfelt thanks to my whole family, especially to my mum who, despite ups and downs, has always been on my side.

Bibliography

- Adani, M., Dobricic, S., and Pinardi, N. (2011). “Quality Assessment of a 1985-2007 Mediterranean Sea Reanalysis”. In: *Journal of Atmospheric and Oceanic Technology - J ATMOS OCEAN TECHNOL* 28, pp. 569–589. DOI: 10.1175/2010JTECH0798.1.
- Amitai, Y., Ashkenazy, Y., and Gildor, H. (2017). “Multiple equilibria and overturning variability of the Aegean-Adriatic Seas”. In: *Global and Planetary Change* 151, pp. 49–59. DOI: 10.1016/j.gloplacha.2016.05.004.
- Anati, D. and Stommel, H. (1970). “The initial phase of deep-water formation in the North-west Mediterranean, during Medoc '69”. In: *Cahiers Océanographiques* 22, pp. 347–351.
- Artale, V., Astraldi, M., Buffoni, G., and Gasparini, G. P. (1994). “Seasonal variability of gyre-scale circulation in the northern Tyrrhenian Sea”. In: *Journal of Geophysical Research: Oceans* 99.C7, pp. 14127–14137. DOI: <https://doi.org/10.1029/94JC00284>.
- Artegiani, A., Bregant, D., Paschini, E., Pinardi, N., Raicich, F., and Russo, A. (1997). “The Adriatic Sea General Circulation. Part I: Air–Sea Interactions and Water Mass Structure”. In: *Journal of Physical Oceanography* 27, pp. 1492–1514. DOI: 10.1175/1520-0485(1997)027<1492:TASGCP>2.0.CO;2.
- Astraldi, M., Bianchi, C. N., Gasparini, G. P., and Morri, C. (1995). “Climatic fluctuations, current variability and marine species distribution - a case-study in the Ligurian sea (north-west Mediterranean)”. In: *Oceanologica Acta* 18, pp. 139–149.
- Ayoub, N., Le Traon, P.-Y., and De Mey, P. (1998). “A description of the Mediterranean surface variable circulation from combined ERS-1 and TOPEX/POSEIDON altimetric data”. In: *Journal of Marine Systems* 18.1, pp. 3–40. ISSN: 0924-7963. DOI: [https://doi.org/10.1016/S0924-7963\(98\)80004-3](https://doi.org/10.1016/S0924-7963(98)80004-3). URL: <https://www.sciencedirect.com/science/article/pii/S0924796398800043>.
- Blanke, B., Arhan, M., Madec, G., and Roche, S. (1999). “Warm Water Paths in the Equatorial Atlantic as Diagnosed with a General Circulation Model”. In: *Journal*

BIBLIOGRAPHY

- of Physical Oceanography* 29.11, pp. 2753–2768. DOI: 10.1175/1520-0485(1999)029<2753:WWPITE>2.0.CO;2.
- Blanke, B. and Grima, N. (2019). *Ariane*. URL: <http://stockage.univ-brest.fr/~grima/Ariane/>.
- Blanke, B. and Raynaud, S. (1997). “Kinematics of the Pacific Equatorial Undercurrent: An Eulerian and Lagrangian Approach from GCM Results”. In: *Journal of Physical Oceanography* 27. DOI: 10.1175/1520-0485(1997)027<1038:KOTPEU>2.0.CO;2.
- Borzelli, G. L. E., Gacic, M., Cardin, V., and Civitarese, G. (2009). “Eastern Mediterranean Transient and reversal of the Ionian Sea circulation”. In: *Geophysical Research Letters - GEOPHYS RES LETT* 36. DOI: 10.1029/2009GL039261.
- Bosse, A., Testor, P., Houpert, L., Damien, P., Prieur, L., Hayes, D., Taillandier, V., Durrieu de Madron, X., d’Ortenzio, F., Coppola, L., Karstensen, J., and Mortier, L. (2016). “Scales and dynamics of Submesoscale Coherent Vortices formed by deep convection in the northwestern Mediterranean Sea”. In: *Journal of Geophysical Research: Oceans* 121.10, pp. 7716–7742. DOI: <https://doi.org/10.1002/2016JC012144>.
- Bryden, H. L. and Stommel, H. (1982). “Origin of The Mediterranean Outflow”. In: *J. MAR. RES.* 40, pp. 55–71. ISSN: 0022-2402.
- Castellari, S., Pinardi, N., and Leaman, K. (2000). “Simulation of water mass formation processes in the Mediterranean Sea: Influence of the time frequency of the atmospheric forcing”. In: 105, pp. 24, 157–24, 181.
- Castellari, S., Pinardi, N., and Leaman, K. (1998). “A model study of air sea interactions in the Mediterranean Sea”. In: *Journal of Marine Systems* 18.1, pp. 89–114. DOI: 10.1016/S0924-7963(98)90007-0.
- Cessi, P., Pinardi, N., and Lyubartsev, V. (2014). “Energetics of Semienclosed Basins with Two-Layer Flows at the Strait”. In: *Journal of Physical Oceanography* 44. DOI: 10.1175/JPO-D-13-0129.1.
- Cushman-Roisin, B., Gacic, M., Poulain, P.-M., and Artegiani, A. (2001). *Physical Oceanography of the Adriatic Sea: Past, Present and Future*. ISBN: 978-90-481-5921-5. DOI: 10.1007/978-94-015-9819-4.
- Dee, D. P., Uppala, S., Simmons, A., Berrisford, P., Poli, P., Kobayashi, S., Andrae, U., Balmaseda, M., Balsamo, G., Bauer, P., Bechtold, P., Beljaars, Berg, L. van de, Bidlot, J., Bormann, N., Delsol, C., Dragani, R., Fuentes, M., and Vitart, F. (2011). “The ERA-Interim reanalysis: Configuration and performance of the data assimilation system”. In: *Quarterly Journal of the Royal Meteorological Society* 137, pp. 553–597. DOI: 10.1002/qj.828.
- Demirov, E. and Pinardi, N. (2007). “On the relationship between the water mass pathways and eddy variability in the Western Mediterranean Sea”. In: *Journal of Geophysical Research* 112. DOI: 10.1029/2005JC003174.
- Dobricic, S., Pinardi, N., Adani, M., Bonazzi, A., Fratianni, C., and Tonani, M. (2005). “Mediterranean Forecasting System: An improved assimilation scheme for sea-level

- anomaly and its validation”. In: *Quarterly Journal of the Royal Meteorological Society* 131.613, pp. 3627–3642.
- Dobricic, S. and Pinardi, N. (2008). “An oceanographic three-dimensional variational data assimilation scheme”. In: *Ocean Modelling* 22, pp. 89–105. DOI: 10.1016/j.ocemod.2008.01.004.
- Döös, K., Jönsson, B., and Kjellsson, J. (2017). “Evaluation of oceanic and atmospheric trajectory schemes in the TRACMASS trajectory model v6.0”. In: *Geoscientific Model Development* 10.4, pp. 1733–1749. DOI: 10.5194/gmd-10-1733-2017. URL: <https://gmd.copernicus.org/articles/10/1733/2017/>.
- Döös, Kristofer (1995). “Interocean exchange of water masses”. In: *Journal of Geophysical Research: Oceans* 100.C7, pp. 13499–13514. DOI: <https://doi.org/10.1029/95JC00337>.
- Drevillon, M., Bourdalle-Badie, R., Derval, C., Drillet, Y., Lellouche, J., Remy, E., Tranchant, B., Mounir, B., Greiner, E., Guinehut, S., Verbrugge, N., Garric, G., Testut, C., Laborie, M., Nouel, L., Bahurel, P., Bricaud, C., Crosnier, L., Dombrowsky, E., and Parent, L. (2008). “The GODAE/Mercator-Ocean global ocean forecasting system: results, applications and prospects”. In: *Journal of Operational Oceanography* 1, pp. 51–57. DOI: 10.1080/1755876X.2008.11020095.
- Durrieu de Madron, X., Houpert, L., Puig, P., Sanchez-Vidal, A., Testor, P., Bosse, A., Estournel, C., Somot, S., Bourrin, F., Bouin, M.-N., Beauverger, M., Beguery, L., Calafat, A., Canals, M., Coppola, L., Dausse, D., D’Ortenzio, F., Font, J., Heussner, S., and Raimbault, P. (2013). “Interaction of dense shelf water cascading and open-sea convection in the Northwestern Mediterranean during winter 2012”. In: *Geophysical Research Letters* 40. DOI: 10.1002/grl.50331.
- Escudier, R., Renault, L., Pascual, A., Brasseur, P., Chelton, D., and Beuvier, J. (2016). “Eddy properties in the Western Mediterranean Sea from satellite altimetry and a numerical simulation”. In: *Journal of Geophysical Research: Oceans* 121.6, pp. 3990–4006. DOI: <https://doi.org/10.1002/2015JC011371>.
- Fu, L.-L., Christensen, E. J., Yamarone Jr., C. A., Lefebvre, M., Ménard, Y., Dorrer, M., and Escudier, P. (1994). “TOPEX/POSEIDON mission overview”. In: *Journal of Geophysical Research: Oceans* 99.C12, pp. 24369–24381. DOI: <https://doi.org/10.1029/94JC01761>.
- Fuda, J., Millot, C., Taupier-Letage, I., Send, U., and Bocognano, J. (2000). “XBT monitoring of a meridian section across the western Mediterranean Sea”. In: *Deep Sea Research Part I: Oceanographic Research Papers* 47.11, pp. 2191–2218. ISSN: 0967-0637. DOI: [https://doi.org/10.1016/S0967-0637\(00\)00018-2](https://doi.org/10.1016/S0967-0637(00)00018-2).
- Gacic, M., Lascaratos, A., Manca, B., and Mantziafou, A. (2001). “Adriatic Deep Water and Interaction with the Eastern Mediterranean Sea”. In: pp. 111–142. ISBN: 978-90-481-5921-5. DOI: 10.1007/978-94-015-9819-4_4.

BIBLIOGRAPHY

- Garrett, C., Outerbridge, R., and Thompson, K. (1993). “Interannual Variability in Mediterranean Heat and Buoyancy Fluxes”. In: *Journal of Climate* 6.5, pp. 900–910. ISSN: 08948755, 15200442. URL: <http://www.jstor.org/stable/26197277> (visited on 09/22/2022).
- Gasparini, G., Ortona, A., Budillon, G., Astraldi, M., and Sansone, E. (2005). “The effect of the Eastern Mediterranean Transient on the hydrographic characteristics in the Strait of Sicily and in the Tyrrhenian Sea”. In: *Deep Sea Research Part I: Oceanographic Research Papers* 52.6, pp. 915–935. ISSN: 0967-0637. DOI: <https://doi.org/10.1016/j.dsr.2005.01.001>.
- Gertman, I., Ovchinnikov, I., and Popov, Y. (1994). “Deep convection in the eastern basin of the Mediterranean Sea”. In: *Oceanology* 34, pp. 19–25.
- Gertman, I., Pinardi, N., Popov, Y., and Hecht, A. (2006). “Aegean Sea Water Masses during the Early Stages of the Eastern Mediterranean Climatic Transient (1988–90)”. In: *Journal of Physical Oceanography - J PHYS OCEANOGR* 36. DOI: [10.1175/JPO2940.1](https://doi.org/10.1175/JPO2940.1).
- Hecht, A. (1992). “Abrupt changes in the characteristics of Atlantic and Levantine intermediate waters in the Southeastern Levantine Basin”. In: *Oceanologica Acta* 15, pp. 25–42.
- Hecht, A. and Gertman, I. (2001). “Physical features of the eastern Mediterranean resulting from the integration of POEM data with Russian Mediterranean Cruises”. In: *Deep Sea Research Part I: Oceanographic Research Papers* 48, pp. 1847–1876. DOI: [10.1016/S0967-0637\(00\)00113-8](https://doi.org/10.1016/S0967-0637(00)00113-8).
- Hecht, A., Pinardi, N., and Robinson, A. R. (1988). “Currents, Water Masses, Eddies and Jets in the Mediterranean Levantine Basin”. In: *Journal of Physical Oceanography* 18.10, pp. 1320–1353. DOI: [10.1175/1520-0485\(1988\)018<1320:CWMEAJ>2.0.CO;2](https://doi.org/10.1175/1520-0485(1988)018<1320:CWMEAJ>2.0.CO;2).
- Herrmann, M., Sevault, F., Beuquier, J., and Somot, S. (2010). “What induced the exceptional 2005 convection event in the northwestern Mediterranean basin? Answers from a modeling study”. In: *Journal of Geophysical Research: Oceans* 115.C12. DOI: <https://doi.org/10.1029/2010JC006162>.
- Iovino, D., Straneo, F., and Spall, M. (May 2008). “On the effect of a sill on dense water formation in a marginal sea”. In: *Journal of Marine Research* 66. DOI: [10.1357/002224008786176016](https://doi.org/10.1357/002224008786176016).
- Jones, H. and Marshall, J. (1993). “Convection with Rotation in a Neutral Ocean: A Study of Open-Ocean Deep Convection”. In: *Journal of Physical Oceanography* 23.6, pp. 1009–1039. DOI: [10.1175/1520-0485\(1993\)023<1009:CWRIAN>2.0.CO;2](https://doi.org/10.1175/1520-0485(1993)023<1009:CWRIAN>2.0.CO;2).
- Juza, M., Escudier, R., Vargas-Yáñez, M., Mourre, B., Heslop, E., Allen, J., and Tintoré, J. (2019). “Characterization of changes in Western Intermediate Water properties enabled by an innovative geometry-based detection approach”. In: *Journal of Marine Systems* 191, pp. 1–12. DOI: [10.1016/j.jmarsys.2018.11.003](https://doi.org/10.1016/j.jmarsys.2018.11.003).

- Kokkini, Z., Mauri, E., Gerin, R., Poulain, P., Simoncelli, S., and Notarstefano, G. (2020). “On the salinity structure in the South Adriatic as derived from float and glider observations in 2013–2016”. In: *Deep Sea Research Part II: Topical Studies in Oceanography* 171. Revisiting the Eastern Mediterranean: Recent knowledge on the physical, biogeochemical and ecosystemic states and trends (Volume II), p. 104625. ISSN: 0967-0645. DOI: <https://doi.org/10.1016/j.dsr2.2019.07.013>.
- Korres, G., Pinardi, N., and Lascaratos, A. (2000). “The Ocean Response to Low-Frequency Interannual Atmospheric Variability in the Mediterranean Sea. Part I: Sensitivity Experiments and Energy Analysis”. In: *Journal of Climate - J CLIMATE* 13, pp. 705–731. DOI: 10.1175/1520-0442(2000)013<0705:TORTLF>2.0.CO;2.
- Lascaratos, A. (1993). “Estimation of deep and intermediate water mass formation rates in the Mediterranean Sea”. In: *Deep Sea Research Part II: Topical Studies in Oceanography* 40.6, pp. 1327–1332. ISSN: 0967-0645. DOI: [https://doi.org/10.1016/0967-0645\(93\)90072-U](https://doi.org/10.1016/0967-0645(93)90072-U).
- Lascaratos, A. and Nittis, K. (1998). “A high-resolution three-dimensional numerical study of intermediate water formation in the Levantine Sea”. In: *Journal of Geophysical Research: Oceans* 103.C9, pp. 18497–18511. DOI: <https://doi.org/10.1029/98JC01196>.
- Leaman, K. D. and Schott, F. A. (1991). “Hydrographic Structure of the Convection Regime in the Gulf of Lions: Winter 1987”. In: *Journal of Physical Oceanography* 21.4, pp. 575–598. DOI: 10.1175/1520-0485(1991)021<0575:HSOTCR>2.0.CO;2.
- Legates, D. R. and Willmott, C. J. (1990). “Mean seasonal and spatial variability in gauge-corrected, global precipitation”. In: *International Journal of Climatology* 10, pp. 111–127.
- López-Jurado, J., Lafuente, J. and Cano, L. (1995). “Hydrographic conditions of the Ibiza Channel during November 1990, March 1991 and July 1992”. In: *Oceanologica acta* 18, pp. 235–243.
- Madec, G., Delecluse, P., Crépon, M., and Lott, F. (1996). “Large-Scale Preconditioning of Deep-Water Formation in the Northwestern Mediterranean Sea”. In: *Journal of Physical Oceanography* 26.8, pp. 1393–1408. DOI: 10.1175/1520-0485(1996)026<1393:LSPODW>2.0.CO;2.
- Madec, G. et al. (2022). *NEMO ocean engine*. Version v4.2. DOI: 10.5281/zenodo.6334656. URL: <https://doi.org/10.5281/zenodo.6334656>.
- Malanotte-Rizzoli, P., Manca, B., Marullo, S., Ribera d’Alcala, M., Roether, W., Theocharis, A., Bergamasco, A., Budillon, G., Sansone, E., Civitarese, G., Conversano, F., Gertman, I., Hernt, B., Kress, N., Kioroglou, S., Kontoyiannis, H., Nittis, K., Klein, B., Lascaratos, A., and Kovacevic, V. (2003). “The Levantine Intermediate Water Experiment (LIWEX) Group: Levantine basin - A laboratory for multiple water mass formation processes”. In: *Journal of Geophysical Research* 108, p. 8101. DOI: 10.1029/2002JC001643, .

BIBLIOGRAPHY

- Malanotte-Rizzoli, P., Manca, B. B., d'Alcala, M. R., Theocharis, A., Brenner, S., Budillon, G., and Ozsoy, E. (1999). "The Eastern Mediterranean in the 80s and in the 90s: the big transition in the intermediate and deep circulations". In: *Dynamics of Atmospheres and Oceans* 29.2, pp. 365–395. ISSN: 0377-0265. DOI: [https://doi.org/10.1016/S0377-0265\(99\)00011-1](https://doi.org/10.1016/S0377-0265(99)00011-1). URL: <https://www.sciencedirect.com/science/article/pii/S0377026599000111>.
- Manca, B., Budillon, G., Scarazzato, P., and Ursella, L. (2003). "Evolution of dynamics in the eastern Mediterranean affecting water mass structures and properties in the Ionian and Adriatic Seas". In: *J. Geophys. Res.* 108. DOI: 10.1029/2002JC001664.
- Manca, B., Ibello, V., Pacciaroni, M., Scarazzato, P., and Giorgetti, A. (2006). "Ventilation of deep waters in the Adriatic and Ionian Seas following changes in thermohaline circulation of the Eastern Mediterranean". In: *Climate Research - CLIMATE RES* 31, pp. 239–256. DOI: 10.3354/cr031239.
- Manca, Beniamino and Kovačević, V. and Gačić, M. and Viezzoli, Dino (2002). "Dense water formation in the Southern Adriatic Sea and spreading into the Ionian Sea in the period 1997–1999". In: *Journal of Marine Systems* 33, pp. 133–154. DOI: 10.1016/S0924-7963(02)00056-8.
- Mantziafou, A. and Lascaratos, A. (2004). "An eddy resolving numerical study of the general circulation and deep-water formation in the Adriatic Sea". In: *Deep Sea Research Part I: Oceanographic Research Papers* 51.7, pp. 921–952. ISSN: 0967-0637. DOI: <https://doi.org/10.1016/j.dsr.2004.03.006>.
- Margirier, F., Bosse, A., Testor, P., L'Heveder, B., Mortier, L., and Smeed, D. (2017). "Characterization of Convective Plumes Associated With Oceanic Deep Convection in the Northwestern Mediterranean From High Resolution In-Situ Data Collected by Gliders". In: *Journal of Geophysical Research: Oceans* 122. DOI: 10.1002/2016jc012633.
- Margirier, F., Testor, P., Heslop, E., Mallil, K., Bosse, A., Houpert, L., Mortier, L., Bouin, M.-N., Coppola, L., D'Ortenzio, F., Durrieu de Madron, X., Mourre, B., Prieur, L., Raimbault, P., and Taillandier, V. (2020). "Abrupt warming and salinification of intermediate waters interplays with decline of deep convection in the Northwestern Mediterranean Sea". In: *Scientific Reports* 10. DOI: 10.1038/s41598-020-77859-5.
- Marini, M., Grilli, F., Guarnieri, A., Jones, B. H., Klajic, Z., Pinardi, N., and Sanxhaku, M. (2010). "Is the southeastern Adriatic Sea coastal strip an eutrophic area?" In: *Estuarine, Coastal and Shelf Science* 88.3, pp. 395–406. ISSN: 0272-7714. DOI: <https://doi.org/10.1016/j.ecss.2010.04.020>.
- Marshall, J. and Schott, F. (1999). "Open-ocean convection: Observations, theory, and models". In: *Reviews of Geophysics* 37.1, pp. 1–64. DOI: <https://doi.org/10.1029/98RG02739>.
- Marullo, S., Nardelli, B. B., Guarracino, M., and Santoleri, R. (2007). "Observing the Mediterranean Sea from space: 21 years of Pathfinder-AVHRR sea surface temperatures (1985 to 2005): Re-analysis and validation". In: *Ocean Sci.* 3, pp. 299–310.

- McWilliams, J. C. (1985). “Submesoscale, coherent vortices in the ocean”. In: *Reviews of Geophysics* 23.2, pp. 165–182. DOI: <https://doi.org/10.1029/RG023i002p00165>.
- MEDOC Group (1970). “Observations of formation of deep-water in the Mediterranean Sea”. In: *Nature* 227, pp. 1037–1040. DOI: <https://doi.org/10.1038/2271037a0>.
- Mesinger, F. and Arakawa, A. (1976). “Numerical Methods Used In Atmospheric Models”. In: *GARP Public Ser.* 1.
- Millot, C. (1999). “Circulation in the Western Mediterranean Sea. Journal of Marine System”. In: *Journal of Marine Systems* 20, pp. 423–442. DOI: 10.1016/S0924-7963(98)00078-5.
- Millot, C. (2013). “Levantine Intermediate Water characteristics: An astounding general misunderstanding”. In: *Scientia Marina* 78. DOI: 10.3989/scimar.04045.30H.
- Napolitano, E., Iacono, R., Ciuffardi, T., Reseghetti, F., Poulain, P.-M., and Notarstefano, G. (2019). “The Tyrrhenian Intermediate Water (TIW): Characterization and formation mechanisms”. In: *Progress in Oceanography* 170, pp. 53–68. ISSN: 0079-6611. DOI: <https://doi.org/10.1016/j.pocean.2018.10.017>.
- Nittis, K., Pinardi, N., and Lascaratos, A. (1993). “Characteristics of the summer 1987 flow field in the Ionian Sea”. In: *Journal of Geophysical Research* 981, pp. 10171–10184. DOI: 10.1029/93JC00451.
- Orlić, M., Gacić, M., and Laviolette, P. (1992). “The currents and circulation of the Adriatic Sea”. In: *Oceanologica Acta* 15, pp. 109–124.
- Pinardi, N. and Navarra, A. (1993). “Baroclinic wind adjustment processes in the Mediterranean Sea”. In: *Deep-Sea Research II* 40.6, pp. 1299–1326.
- Pinardi, N., Arneri, E., Crise, A., Ravaioli, M., and Zavatarelli, M. (2006). “The physical, sedimentary and ecological structure and variability of shelf areas in the Mediterranean Sea”. In: *The Sea-Ideas and Observations on Progress in the Study of the Seas* 14B, pp. 1243–1330.
- Pinardi, N., Cessi, P., Borile, F., and Wolfe, C. L. P. (2019). “The Mediterranean Sea Overturning Circulation”. In: *Journal of Physical Oceanography* 49.7, pp. 1699–1721. DOI: 10.1175/JPO-D-18-0254.1.
- Pinardi, N., Gerasimos, K., A.Lascaratos, Roussenov, V., and Stanev, E. (1997). “On the interannual variability of the Mediterranean Sea upper ocean circulation”. In: *Geophysical Research Letters*.
- Pinardi, N. and Masetti, E. (2000). “Variability of the large scale general circulation of the Mediterranean Sea from observations and modelling: A review”. In: *Palaeogeography, Palaeoclimatology, Palaeoecology* 158, pp. 153–173. DOI: 10.1016/S0031-0182(00)00048-1.
- Pinardi, N., Zavatarelli, M., Adani, M., Coppini, G., Fratianni, C., Oddo, P., Simoncelli, S., Tonani, M., Lyubartsev, V., Dobricic, S., and Bonaduce, A. (2015). “Mediterranean Sea large-scale low-frequency ocean variability and water mass formation rates from 1987 to 2007: A retrospective analysis”. In: *Progress in Oceanography* 132. Oceanography

BIBLIOGRAPHY

- of the Arctic and North Atlantic Basins, pp. 318–332. ISSN: 0079-6611. DOI: <https://doi.org/10.1016/j.pocean.2013.11.003>.
- Pinardi, N. et al. (2022). “Dense and deep water formation processes and Mediterranean overturning circulation”. In: *Mediterranean Sea Oceanography*. Elsevier.
- Pinot, J. and Ganachaud, A. (1999). “The role of winter intermediate waters in the spring-summer circulation of the Balearic Sea: 1. Hydrography and inverse box modeling”. In: *J. Geophys. Res.*, pp. 29843–29864. DOI: [doi:10.1029/1999JC900202](https://doi.org/10.1029/1999JC900202).
- Pollak, M. (Jan. 1951). “The sources of deep water of the eastern Mediterranean Sea”. In: *J. Mar. Res.* 10, pp. 128–152.
- Poulain, P., Menna, M., and Mauri, E. (2012). “Surface Geostrophic Circulation of the Mediterranean Sea Derived from Drifter and Satellite Altimeter Data”. In: *Journal of Physical Oceanography* 42.6, pp. 973–990. DOI: [10.1175/JPO-D-11-0159.1](https://doi.org/10.1175/JPO-D-11-0159.1).
- Puillat, I., Sorgente, R., Ribotti, A., Natale, S., and Echevin, V. (2006). “Westward branching of LIW induced by Algerian anticyclonic eddies close to the Sardinian slope”. In: *Chemistry and Ecology* 22, S293–S305. DOI: [10.1080/02757540600670760](https://doi.org/10.1080/02757540600670760).
- Robinson, A. et al. (1992). “General circulation of the Eastern Mediterranean”. In: *Earth-Science Reviews* 32.4, pp. 285–309. ISSN: 0012-8252. DOI: [https://doi.org/10.1016/0012-8252\(92\)90002-B](https://doi.org/10.1016/0012-8252(92)90002-B).
- Roether, W., Manca, B. B., Klein, B., Bregant, D., Georgopoulos, D., Beitzel, V., and Luchetta, V. K. A. (1996). “Recent Changes in Eastern Mediterranean Deep Waters”. In: *Science* 271.5247, pp. 333–335. DOI: [10.1126/science.271.5247.333](https://doi.org/10.1126/science.271.5247.333).
- Rousselet, L., Cessi, P., and Forget, G. (2021). “Coupling of the mid-depth and abyssal components of the global overturning circulation according to a state estimate”. In: *Science Advances* 7.21, eabf5478. DOI: [10.1126/sciadv.abf5478](https://doi.org/10.1126/sciadv.abf5478).
- Rühs, S., Schwarzkopf, F. U., Speich, S., and Biastoch, A. (2019). “Cold vs. warm water route – sources for the upper limb of the Atlantic Meridional Overturning Circulation revisited in a high-resolution ocean model”. In: *Ocean Science* 15.3, pp. 489–512. DOI: [10.5194/os-15-489-2019](https://doi.org/10.5194/os-15-489-2019). URL: <https://os.copernicus.org/articles/15/489/2019/>.
- Samuel, S., Haines, K., Josey, S., and Myers, P. G. (1999). “Response of the Mediterranean Sea thermohaline circulation to observed changes in the winter wind stress field in the period 1980–1993”. In: *Journal of Geophysical Research: Oceans* 104.C4, pp. 7771–7784. DOI: <https://doi.org/10.1029/1998JC900130>.
- Schlitzer, R., Roether, W., Oster, H., Junghans, H.-G., Hausmann, M., Johannsen, H., and Michelato, A. (1991). “Chlorofluoromethane and oxygen in the Eastern Mediterranean”. In: *Deep Sea Research Part A. Oceanographic Research Papers* 38.12, pp. 1531–1551. ISSN: 0198-0149. DOI: [https://doi.org/10.1016/0198-0149\(91\)90088-W](https://doi.org/10.1016/0198-0149(91)90088-W).
- Shapiro, G. I., Huthnance, J. M., and Ivanov, V. V. (2003). “Dense water cascading off the continental shelf”. In: *Journal of Geophysical Research: Oceans* 108.C12. DOI: <https://doi.org/10.1029/2002JC001610>.

- Simoncelli, S., Fratianni, C., Pinardi, N., Grandi, A., Drudi, M., Oddo, P., and Dobricic, S. (2019). “Mediterranean Sea Physical Reanalysis (CMEMS MED-Physics) (Version 1) [Data set]”. In: *Copernicus Monitoring Environment Marine Service (CMEMS)*. DOI: https://doi.org/10.25423/MEDSEA_REANALYSIS_PHYS_006_004.
- Somot, S., Houpert, L., Sevault, F., Testor, P., Bosse, A., Taupier-Letage, I., Bouin, M.-N., Waldman, R., Cassou, C., Sanchez-Gomez, E., Durrieu de Madron, X., Adloff, F., Nabat, P., and Herrmann, M. (2018). “Characterizing, modelling and understanding the climate variability of the deep water formation in the North-Western Mediterranean Sea”. In: *Climate Dynamics* 51. DOI: 10.1007/s00382-016-3295-0.
- Speich, S., Blanke, B., and Madec, G. (2001). “Warm and cold water routes of an O.G.C.M. thermohaline conveyor belt”. In: *Geophysical Research Letters* 28.2, pp. 311–314. DOI: <https://doi.org/10.1029/2000GL011748>.
- Stammer, D., Wunsch, C., Giering, R., Eckert, C., Heimbach, P., Marotzke, J., Adcroft, A., Hill, C. N., and Marshall, J. (2002). “Global ocean circulation during 1992–1997, estimated from ocean observations and a general circulation model”. In: *Journal of Geophysical Research: Oceans* 107.C9, pp. 1-1-1–27. DOI: <https://doi.org/10.1029/2001JC000888>.
- Storto, A., Alvera-Azcárate, A., Balmaseda, M., Barth, A., Chevallier, M., Counillon, F., Domingues, C., Drevillon, M., Drillet, Y., Forget, G., Garric, G., Haines, K., Hernandez, F., Iovino, D., Jackson, L., Lellouche, J.-M., Masina, S., Mayer, M., Oke, P., and Zuo, H. (2019). “Ocean Reanalyses: Recent Advances and Unsolved Challenges”. In: *Frontiers in Marine Science* 6, p. 418. DOI: 10.3389/fmars.2019.00418.
- Stratford, K. and Haines, K. (Feb. 2002). “Modelling nutrient cycling during the Eastern Mediterranean Transient event 1987–1995 and beyond”. In: *Geophysical Research Letters - GEOPHYS RES LETT* 29, pp. 5–1. DOI: 10.1029/2001GL013559.
- Supić, N. and Vilibić, I. (2006). “Dense water characteristics in the northern Adriatic in the 1967-2000 interval with respect to surface fluxes and Po river discharge rates”. In: *Estuarine, Coastal and Shelf Science* 66.3, pp. 580–593. ISSN: 0272-7714. DOI: <https://doi.org/10.1016/j.ecss.2005.11.003>.
- Talley, L. D., Pickard, G. L., Emery, W. J., and Swift, J. H. (2011). “Chapter 4 - Typical Distributions of Water Characteristics”. In: *Descriptive Physical Oceanography (Sixth Edition)*. Ed. by L. D. Talley, G. L. Pickard, W. J. Emery, and J. H. Swift. Sixth Edition. Boston: Academic Press, pp. 67–110. ISBN: 978-0-7506-4552-2. DOI: <https://doi.org/10.1016/B978-0-7506-4552-2.10004-6>.
- Testor, P., Béranger, K., and Mortier, L. (2005). “Modeling the deep eddy field in the southwestern Mediterranean: The life cycle of Sardinian eddies”. In: *Geophysical Research Letters* 32.13. DOI: <https://doi.org/10.1029/2004GL022283>.
- Testor, P., Send, U., Gascard, J.-C., Millot, C., Taupier-Letage, I., and Béranger, K. (2005). “The mean circulation of the southwestern Mediterranean Sea: Algerian Gyres”.

BIBLIOGRAPHY

- In: *Journal of Geophysical Research: Oceans* 110.C11. DOI: <https://doi.org/10.1029/2004JC002861>.
- Theocharis, A., Klein, B., Nittis, K., and Roether, W. (2002). “Evolution and status of the Eastern Mediterranean Transient (1997–1999)”. In: *Journal of Marine Systems* 33-34. MATER: MAAss Transfer and Ecosystem Response, pp. 91–116. ISSN: 0924-7963. DOI: [https://doi.org/10.1016/S0924-7963\(02\)00054-4](https://doi.org/10.1016/S0924-7963(02)00054-4).
- Theocharis, A., Krokos, G., Velaoras, D., and Korres, G. (2014). “An Internal Mechanism Driving the Alternation of the Eastern Mediterranean Dense/Deep Water Sources”. In: *The Mediterranean Sea*. American Geophysical Union (AGU). Chap. 8, pp. 113–137. ISBN: 9781118847572. DOI: <https://doi.org/10.1002/9781118847572.ch8>.
- Theocharis, A., Nittis, K., Kontoyiannis, H., Papageorgiou, E., and Balopoulos, E. (1999). “Climatic changes in the Aegean Sea influence the Eastern Mediterranean thermohaline circulation(1986-1997)”. In: *Geophysical Research Letters* 20, pp. 1617–1620. DOI: 10.1029/1999GL900320.
- Tziperman, E. and Malanotte-Rizzoli, P. (1991). “The Climatological Seasonal Circulation of the Mediterranean Sea”. In: *Journal of Marine Research* 49. DOI: 10.1357/002224091784995783.
- Tziperman, E. and Speer, K. (1994). “A study of water mass transformation in the Mediterranean Sea: analysis of climatological data and a simple three-box model”. In: *Dynamics of Atmospheres and Oceans* 21.2, pp. 53–82. ISSN: 0377-0265. DOI: [https://doi.org/10.1016/0377-0265\(94\)90004-3](https://doi.org/10.1016/0377-0265(94)90004-3).
- Velaoras, D., Krokos, G., Nittis, K., and Theocharis, A. (2014). “Dense intermediate water outflow from the Cretan Sea: A salinity-driven, recurrent phenomenon, connected to thermohaline circulation changes”. In: *Journal of Geophysical Research: Oceans* 119, pp. 4797–4820. DOI: 10.1002/2014JC009937.
- Velaoras, D., Zervakis, V., and Theocharis, A. (2021). “The Physical Characteristics and Dynamics of the Aegean Water Masses”. In: DOI: 10.1007/698_2020_730.
- Velez-Belchi, P., Vargas-Yáñez, M., and Tintoré, J. (2005). “Observation of a western Alborán gyre migration event”. In: *Progress In Oceanography* 66, pp. 190–210. DOI: 10.1016/j.pocean.2004.09.006.
- Verri, G., Pinardi, N., Oddo, P., Ciliberti, S., and Coppini, G. (2018). “River runoff influences on the Central Mediterranean overturning circulation”. In: *Climate Dynamics* 50, pp. 1–29. DOI: 10.1007/s00382-017-3715-9.
- Vries, P. and Döös, K. (2001). “Calculating Lagrangian Trajectories Using Time-Dependent Velocity Fields”. In: *Journal of Atmospheric and Oceanic Technology - J ATMOS OCEAN TECHNOL* 18, pp. 1092–1101. DOI: 10.1175/1520-0426(2001)018<1092:CLTUTD>2.0.CO;2.
- Wang, X., Oddo, P., and Pinardi, N. (2006). “On the bottom density plume on coastal zone off Gargano (Italy) in the southern Adriatic Sea and its interannual variability”. In: *Journal of Geophysical Research* 112. DOI: 10.1029/2005JC003110.

- Wu, P. and Haines, K. (1996). “Modeling the dispersal of Levantine Intermediate Water and its role in Mediterranean deep water formation”. In: *Journal of Geophysical Research: Oceans* 101.C3, pp. 6591–6607. DOI: <https://doi.org/10.1029/95JC03555>.
- Wu, P., Haines, K., and Pinardi, N. (2000). “Toward an Understanding of Deep-Water Renewal in the Eastern Mediterranean”. In: *Journal of Physical Oceanography* 30.2, pp. 443–458. DOI: 10.1175/1520-0485(2000)030<0443:TAUODW>2.0.CO;2.
- Wüst, G. (1961). “On the vertical circulation of the Mediterranean Sea”. In: *Journal of Geophysical Research (1896-1977)* 66.10, pp. 3261–3271. DOI: <https://doi.org/10.1029/JZ066i010p03261>.
- Zavatarelli, M. and Mellor, G. L. (1995). “A Numerical Study of the Mediterranean Sea Circulation”. In: *Journal of Physical Oceanography* 25.6, pp. 1384–1414. DOI: 10.1175/1520-0485(1995)025<1384:ANSOTM>2.0.CO;2.
- Zervakis, V., Georgopoulos, D., and Drakopoulos, P. (2000). “The role of the north Aegean in triggering the recent Eastern Mediterranean Transient”. In: *Journal of Geophysical Research C: Oceans* 105, pp. 26103–26116. DOI: 10.1029/2000JC900131.